Republic of Iraq
Ministry of Higher Education
and Scientific Research
University of Babylon
College of Science for Women

Investigation of Morphological and Optical Properties (linear and nonlinear) of Nanoparticles as Optical Limiting

A dissertation

Submitted to the Council of the College of Sciences for Women,
University of Babylon
In Partial Fulfillment of the Requirements for Degree of Doctor of Philosophy in Laser Physics and its Applications

By

Hayder Hussein Hummood Alaaraji

B.Sc. in Physics 1994
M.Sc. in electro-optics 2002

Supervisor

Asst. Prof. Dr. Qussay Mohammed Salman

2022 A.D. **1443 A.H.**

بسم الله الرحمن الرحيم

أَوْ كَظُلُمَاتٍ فِي بَحْرٍ لُجِّيٍّ يَغْشَاهُ مَوْجٌ مِنْ فَوْقِهِ مَوْجٌ مِنْ فَوْقِهِ سَحَابٌ ۚ ظُلُمَاتٌ
بَعْضُهَا فَوْقَ بَعْضٍ إِذَا أَخْرَجَ يَدَهُ لَمْ يَكَدْ يَرَاهَا ۗ وَمَنْ لَمْ يَجْعَلِ اللَّهُ لَهُ نُورًا فَمَا لَهُ
مِنْ نُورٍ

صدق الله العلي العظيم

سورة النور ﴿٤٠﴾

Supervisor Certification

I certify this dissertation entitled (**Investigation of Morphological and Optical Properties (linear and nonlinear) of Nanoparticles as Optical Limiting**), was prepared by **Hayder Hussein Hummood Alaaraji** under my supervision, at laser physics department, college of sciences for women, University of Babylon as a partial of fulfillment of the requirements for degree of doctor of philosophy in laser physics and its applications.

Signature:

Name: **Dr. Qussay Mohammed Salman**

Title: Assistant Professor

Address: Dept. of laser physics, College of sciences for Women, University of Babylon

Date: / / 2022

In view of the available recommendations, I forward this thesis for debate by the examination committee.

Signature:

Name: **Ass. Prof. Dr. Jinan Ali Abd**

Title: Head of the department

Address: Dept. of laser physics, College of sciences for Women, University of Babylon

Date: / / 2022

Dedication

First: Upon the holy Prophet Muhammad, peace and blessings of Allah be upon him and his immaculate progeny.

Second: Upon the one who leaves an unfathomable hiatus in the heart of my soul and almost always urges me vehemently to purse my PhD; it is my uncle, ever venerated, JABER, may Allah grant him tranquil slumber and a great niche in paradise …...

Third: Upon my Family.

I bestow such a modest effort.

Acknowledgment

First of all, I would like to thank **ALLAH** Almighty for giving me this blessing, which is knowledge seeking, then, I would like to commit my thanks and gratitude to my supervisor Asst. Prof. Dr. Qussay Mohammed Salman for his valuable contribution, unwavering help encouragement, motivation and his precious time that he gave to me during the research period.

Many thanks and gratitude to all the distinguished professors for providing us with their knowledge and spared no effort but to give us useful knowledge during the semesters of the preparatory year for doctoral studies.

Many thanks to our professor, head of the Photonics Group, Professor Dr. Jassim Muhammed Jassim, for his relentless support and backing.

I can only express my sincere thanks of praise and gratitude to the one who helped us with his sound advice, and who does not skimp on scientific information or technical advice, my respected brother Dr. Ahmed Baqer Sharba, Allah guide him, direct his steps and grant him the highest ranks and degrees in this life and the hereafter.

Thank you very much to the two chairs whom respectively headed the Department of Laser Physics. Assistant Professor Dr. Sadiq Hassan Al-Zurqani and Assistant Professor Dr. Janan Ali Abd, who spares not any effort to help and support graduate students during her management of the affairs of graduate students or during her headship of the department, so she has all success from Allah.

Many thanks and praise to the Department of Physics at the University of Basra, especially my brother and friend, Professor Dr. Mazen Awni Mahdi, for his assistance in conducting some laboratory measurements, wishing him continued success and prosperity.

Recognition and thanks for all the kinds of cooperation to the all the staff in the Department of Laser Physics and especially to the staff of advanced laboratory.

Thanks and appreciation to my colleagues in PhD students for the academic year 2018-2019, wishing them continued success and prosperity.

Thank you very much to everyone who supports and boosting morale me in my studies, even with a word or a prayer.

Hayder

Abstract:

This study aims to investigate the morphological properties, linear and nonlinear optical properties of metallic nanoparticles and one of the metal oxides to be used as an optical limiter in addition to making mixtures of these materials to enhance optical limiting properties. The materials that were used in this study are (spherical silver nanoparticles (Ag NPs), silver nanowires (Ag NWs), spherical gold nanoparticles (Au NPs), spherical copper nanoparticles (Cu NPs), copper nanowires (Cu NWs), and iron oxide Nano fragments (Fe_2O_3 Nano fragments).

The morphological properties were studied for determining the shape and size of the particles under study for all prepared samples and prepared mixtures by analyzing the images obtained from (SEM). The results of (Ag NPs) were that they are spherical in shape with a predominant size of (70) nm. (Ag NWs) are of three diameters (50, 100, 200) nm and one length, all of which ranges from (5-50) microns. The results of (Au NPs) were that they are spherical in shape with three dominant sizes (4, 6 and 8) nm. The (Cu NPs), they were also spherical in shape with two dominant sizes. The first (50) nm and the second (90-99) nm. As for the (Cu NWs), they were (50) nm in diameter and (50) micron in length. The results of (Fe_2O_3) nanoparticles were that they are nanoscale in the form of fragments and with a predominant size of (65) nm. As for the results of the mixtures, which were four mixtures, the first was (Ag NWs D200 + Cu2) with volume ratio (1:1) in absolute ethanol. The mixing was done by using ultrasonic waves. The results of (SEM) images showed, that the occurrence of surface adhesion between the spherical copper nanoparticles and the silver nanowires. The second mixture was (Cu NWs D50 + Ag NPS) in the same volume proportions as the first mixture and same method of preparation. The results also showed, that the occurrence of superficial adhesion between the two materials. The third mixture was (Fe_2O_3 Nano fragments + Ag NPs) with volume ratio (1:3) of their suspensions in absolute ethanol with concentration (0.12) mg/ml. The mixing process was done by two different ways (pulsed laser and the ultrasonic waves). The results showed, that the occurrence of a new structure between them, which is the structure of the core-shell. As for the fourth mixture (Fe_2O_3 Nano fragments + Cu1), it was in the same volume proportions as the third mixture and in the same mixing methods for the third mixture, the results were the same as for the third mixture.

The optical absorption properties of prepared samples and mixtures in absolute ethanol at three concentrations (0.04, 0.08 and 0.12) mg/ml were studied. The linear absorption coefficient (α) and transmittance were calculated for all prepared samples, and the absorption bandwidth and peak were determined for each suspension of material. The results showed low linear absorption rates for all materials. All samples except the Fe_2O_3 Nano fragments showed a good absorption bandwidth within the visible region of the electromagnetic spectrum. All samples have a low linear absorbance and high transmittance. In addition, the linear refractive index was measured for all suspensions of materials and mixtures.

The nonlinear optical properties of all materials and mixtures at all concentrations were studied by using the Z-scan technique with using four wavelengths (405, 473, 532 and 650) nm of continuous semiconductor laser (CW). The results showed that all materials have a negative (n_2) resulting from the self-defocusing process. The results showed that there was no nonlinear absorption for all materials and mixtures. The ($Re\ \chi^{(3)}$) was calculated for all prepared samples and mixtures. The highest values of the n_2 and the $Re\chi^{(3)}$ of Cu2 nanoparticles suspension in absolute ethanol for the three concentrations used were recorded at the wavelength of (473 nm) and the intensity of (4.98 Mw/m^2) and their values were (1.13795×10^{-10}, 1.23016×10^{-10} and 1.32163×10^{-10}) m^2/W and (5.32×10^{-5}, 5.75×10^{-5} and 6.18×10^{-5}) esu respectively. The lowest values of the n_2 and the $Re\chi^{(3)}$ were recorded for the suspension of Fe_2O_3 Nano fragments in absolute ethanol with a concentration of (0.04 mg/ml) at a wavelength of (405 nm) and an intensity of (13.5 Mw/m^2) and their values were (1.94×10^{-12} m^2/W) and (9.12×10^{-7} esu) respectively.

The optical limiting properties of all suspensions and mixtures were studied by using two wavelengths (405 and 532) nm. The results showed that all materials have optical limiting properties at the two wavelengths used, except for spherical gold nanoparticles, which did not have optical limiting properties at (532) nm for the two concentrations (0.04 and 0.08) mg/ml, as well as iron oxide Nano fragments for the same wavelength and for all concentrations. The results showed that the values of the threshold power and the limiting power for all materials decreased with increasing concentration and wavelength. The results of the optical limiting for the mixtures which they mixed by ultrasonic method, showed the appearance of a two-stage optical limiter at the wavelength (405) nm.

Table of contents

List of Symbols

Symbol	Description	Unit
α_o	Linear absorption coefficient	cm^{-1}
T	Transmittance	-
l	Thickness of medium	cm
n_o	Linear refractive index	-
P	Electric Polarization	C/m^2
χ	First order linear optical susceptibility	-
E	Electric field	V/m
χ^2	Second order nonlinear optical susceptibility	cm/v
χ^3	Third order nonlinear optical susceptibility	cm^2/v^2
n_2	Nonlinear refractive index	cm^2/w
γ	absorption coefficient of an ordered photon (n + 1)	cm^{-1}
β	Nonlinear absorption coefficient	cm/w
I	Intensity of the laser	w/cm^2
r_a^2	Square of aperture radius	mm^2
w_a^2	Square of laser beam radius at the aperture	mm^2
ω_0^2	Square of laser beam radius at the focus point	m^2
L_{eff}	Effective length of sample	m
k	Wave number	nm^{-1}
K	Extinction coefficient	-
S	Aperture linear transmittance	-
L	Propagation length (Cuvette thikness)	mm
I_0	Incident pulse intensity	Mw/cm^2
σ_1	Ground Cross section	-
σ_2	Exited Cross section	-
σ	Total (electron + hole) FCA cross section	-
N	Number of electron-hole pairs	-

I_T	Intensities of the Transmitted	mw/cm^2
I_A	Intensities of the Absorbed	mw/cm^2
I_R	Intensities of the Reflected	mw/cm^2
t	Thickness of sample	cm
$\boldsymbol{P}$	Power	W
c	Speed of light in the vacuum	m/s
ε_0	Electric permittivity of vacuity	F/m
j	Energy flux density	$W \cdot m^{-2}$
$\Delta\Phi_o$	Nonlinear phase shift	-
$\boldsymbol{\Delta T_{p-v}}$	Change in normalized transmittance between peak and valley	-
$\boldsymbol{\lambda}$	Wavelength of the beam	nm
$\boldsymbol{\Delta T}$	Transmittance on one peak or one valley at the open aperture Z-scan curve	-
w	Spot size of beam	mm
$R_{(z)}$	Radius of curving of the beam	mm
θ_o	Deviation of a Gaussian beam	rad
Z_o	Rayleigh length	mm
r	Spot width at the focal point,	mm
f	Focal length of a lens	mm
Ψ	Amplitude rate	-
$\Delta\lambda$	Bandwidth	nm
E_c	Clamping energy	J

List of Abbreviation

Abbreviation	Description
UV	Ultra violet
Vis	Visible
MIR	mid-infrared
NIR	Near-infrared
CW	Continuous wave
Q-Switching	Quality Factor Switching
SHG	Second harmonic generation
LSPR	Local surface plasmon resonance
SPR	Surface plasmon resonance
SVEA	Slowly varying envelope approximation
NRM	Negative-refractive index material
NRMs	Negative-refractive index materials
TE- polarized	Transverse electric polarized
TPA	Two photon Absorption
MPA	Multiple photon absorptions
ESA	Excited state absorption
SA	Saturable Absorption
RSA	Reverse Saturable Absorption
OL	Optical limiting
FCA	Free-carrier Absorption
LA	Linear absorption
DFWM	Degenerate Four Wave Mixing
THG	Third Harmonic Generation
TCSPS	Time Correlated Single Photon Counting
TEM_{00}	Transverse electromagnetic mode (Gaussian mode)
NP	Nanoparticle
NPs	Nanoparticles
NW	Nanowire
NWs	Nanowires
SEM	Scan electron microscope
P_{th}	Threshold power
P_L	Limiting power
Ag NPs	Silver spherical nanoparticles of a size (70) nm
Ag NWs D50	Silver Nano wires of a diameter (50) nm
Ag NWs D100	Silver Nano wires of a diameter (100) nm
Ag NWs D200	Silver Nano wires of a diameter (200) nm
Cu1	Copper spherical nanoparticles of a size (50) nm
Cu2	Copper spherical nanoparticles of a size (99) nm

Cu NWs D50	Copper Nano wires of a diameter (50) nm
Au1	Gold spherical nanoparticles of a size (4) nm
Au2	Gold spherical nanoparticles of a size (6) nm
Au3	Gold spherical nanoparticles of a size (8) nm
Fe_2O_3 Nano fragments	Iron trioxide Nano fragments

List of Tables

List of Figures

Chapter 1

Introduction

CHAPTER 1 Introduction

1.1 Introduction

The laser beam was used in various applications immediately after the first laser was turned on, as the beam was used to treat eye and skin diseases. Since its design thirty years ago, the laser has found uses in many fields as a device that is now used in medicine, astronomy, metrology, chemistry, biology, spectroscopy, holography and power engineering in various processes in engineering as well as in communications technology, automation and remote control, in military technology [1].

The field of nonlinear optics was born in 1875 AD, through a study that observed the change of the refractive index of Cs2 by the effect of a quadrupole electric field. Kerr [2] presented this study, and then the research followed. In 1893 AD, the change in the refractive index of quartz was monitored, but by the effect of a linear electric field, which was later known as the Pockels effect [2]. And upon the invention of the laser in Ham 1960 AD, as mentioned above, studies and observations followed that noticed the second harmonic generation (SHG) by Fianken et al. In quartzites [3]. In 1965 Rentzepis and Pao [4] recorded the first observation of SHG in organic matter. The discoveries continued to reach in 1981 to Bloemberge and his colleagues, where they explored the full nonlinear response of systems of materials and they were awarded the Noble Prize. Buckingham and his colleagues followed them in exploring the nonlinear processes in atoms and molecules [3]. We can define nonlinear optics as a branch of optics that describes the behavior of electromagnetic waves in nonlinear mediums, which are media in which polarization responds nonlinearly to the electric field (E) of the

electromagnetic wave. This nonlinear characteristic is observed only at high intensities of light such as those available with lasers, where the principle of superposition does not apply in this phenomenon. Nonlinear optics is a phenomenon that studies changes in the optical properties of a material due to interaction with high-intensity light. The laser beam alone has sufficient intensity to change the optical properties of the material, which enables the study of nonlinear processes at very high levels. Whereas, nonlinearity occurs when the response to the optical field that is focused on is nonlinearly dependent on the intensity of the optical field [5].

Nonlinear optical materials can change the characteristics of the light scattered through them, that is, the light can be controlled by light, and thus can be used in photonic applications. To choose a nonlinear optical material in photonic applications or in a particular application, it must have some properties or characteristics for that application such as fast response, large nonlinear optical coefficients, low threshold limit (Law Threshold), and threshold limit with High Laser Damage Threshold [6 &7].

The nonlinear behavior can be occurred with high intensity laser beams. Moreover, each nonlinear optical process may consist of two parts [5]:

(i) Firstly, the intense light can induce a nonlinear response in a medium.

(ii) Secondly, the medium tends to modify the optical field in nonlinear way.

The development of nonlinear optical materials was the result of the need for them in technological applications, as the development of techniques requires materials that achieve this development. All this led to an increase in researchers' interest in the science of nonlinear optical materials to include organic and inorganic crystals, semiconductors, metal nanostructures, thin films of polymers, and so on [8

& 9]. With the growing interest in nanostructures of materials in the 1990s, many nanomaterials were developed for use in the fields of photonics, chemical and biological detection. Among the nanomaterials, metallic nanomaterials stood out due to their surface plasmon properties, which made them an important material in nonlinear optics. A paper on this topic was reported in 1974 AD about the diffusion of surface plasmon polaritons on the surface of silver films [10].

The incident light is absorbed by the metal nanoparticles when the free electrons in them are pushed by the electric field of the beam falling on them to collectively oscillate at a certain frequency. The oscillation of free electrons in metallic nanoparticles is limited to a finite size that depends on the dimensions of the nanoparticle. If the surface plasmon are confined to a nanostructure whose size is much smaller than the wavelength of the incident rays, they are localized and do not propagate and show a limited frequency known as local surface plasmon resonance (LSPR). The width and frequency of the surface plasmon absorption will depend on the size and shape of the metallic nanoparticles, the dielectric constant of the metal and the surrounding host [11].

The process of rapid development in the field of lasers lead to a transformative revolution in various scientific and technological fields. The high powers of the laser were not limited to the use of them only in the research and academic fields, but also in various industrial and military applications. The manufacture of portable, compact and efficient lasers such as semiconductor lasers and solid-state lasers has facilitated work in a variety of applications. With the increasing capabilities of the lasers used, it was necessary to find a way to protect the optical detectors used with them, the human eye of the user and the optical components from damage due to these high energies. Under these challenges, optical limiters had an important role in providing

this protection and preventing damage, as they reduce transmittance at high intensities (power per unit area) and fluence (power per unit area), so the optical limiters have received great attention by researchers [12].

1.2 Nanomaterials

Nanomaterials have unique physical and chemical properties that drawn the attention of scientific researchers to delve into their specifications and properties. Research has shown that it plays an important and growing role in the future development of science and technology. With increasing research, metallic nanomaterials have been used in many fields such as photoelectric information storage, unique catalyst and nano-enhanced catalysis [13]. Materials with metallic nanostructures, especially those that include noble metals (Au, Ag, ... etc.), show unique photoelectric properties, low bio toxicity, and good stability. That is why they have received wide interest from researchers working in the fields of spectroscopy, photonics, electro-optics, medical fields and other fields. For applications that contain metallic nanoparticles, surface plasmon resonance (SPR) will play an important role in influencing their linear and nonlinear optical properties. The addition of metallic nanoparticles (NPs) to other materials led to the emergence of new classes of materials that changed the course of electro-optics applications. Colloidal media or suspensions containing metallic nanoparticles are very promising for the improvements in nonlinear absorption and refraction in these media [14].

Interest in exploring the important role that metallic nanoparticles play in the photothermal response has increased as gold nanoparticles (Au NPs) have been used in processes involving heat transfer of a composite medium. The thermal-optical

behavior (dn/dT) of solid materials containing (Au NPs) has been studied theoretically and experimentally [15]. Thermo-optical effects are very important for optical applications that require a continuous running (CW) or pulsed laser. Because of the thermal conductivity, the nonlinear thermal response can be used to investigate many non-local nonlinear phenomena such as spatial soliton (*a quantum or quasiparticle propagated as a traveling non dissipative wave that is neither preceded nor followed by another such disturbance*) propagation and shock waves. Colloidal solutions or suspensions indicate that thermal nonlinearity enhances colloidal optical absorption [120].

Silver (Ag), have attracted a lot of attention in the electronics, chemistry, physics, biology and medicine fields because of their unique properties that depend strongly on the composition, size, shape of metal nanostructure [17]. The ability to control the size and shape of metal nanostructures provides a great opportunity to check the electrical and optical properties of these materials and opens up prospects for use in different applications as the optical limiting systems [18]. (Ag) has a highest thermal and electrical conductivity among the metals. It also has unique optical properties, and this is evident in its major role in photography. The (Ag NPs) advantages over other noble metals in relation to its physical and chemical properties are: stability at ambient conditions, low cost than other noble metals such as gold and platinum, broad absorption band in the visible region of the electromagnetic spectrum, chemical stability, and non-linear optical behavior [19]. Silver nanowires (Ag NWs) are a cheap and flexible component of transparent conductive layers, pressure sensors, temperature sensors, surface-enhanced Raman spectroscopy substrates, and conductivity layers in solar water splitting photo-electrodes, not to mention their high electrical conductivity and low optical extinction in the visible

part of the electromagnetic spectrum [20]. Silver nanowire suspensions have a very high optical density and are used in a variety of electro-optical applications from (photovoltaic) stimulation to batteries, color dyes, drug delivery and sensing [21].

Copper nanoparticles (Cu NPs) have also received great attention due to their high electrical conductivity, linear and nonlinear optical properties, low electrochemical transmission behavior, high melting point, excellent weldability and low material cost [22]. (Cu NPs) have been used as a substitute for other noble metals in many applications such as jet-printing, thermal conductivity and photonics because their cost is low compared to other noble metals [23]. Copper nanowires (Cu NWs) have unique properties such as thermal conductivity, electrical conductivity and tribological properties [24]. These properties made it important in many applications such as photonics, solar cells, electronic optics, optical limiters, chemical sensors, and genetic engineering [25].

Placing the semiconducting materials, including Nano iron oxide (Fe_2O_3) as a suspension in an organic solvent, showed a quantum confinement of charge carriers that significantly affected the linear and nonlinear properties of the solvent. The linear and nonlinear changes that occurred are caused by heat and these changes are useful in optical and photonic applications [26]. When the suspended solution of the semiconducting material is excited by an external radiation source such as laser, the trapping states between the holes and electrons will become more effective for the excited states and lead to many non-radiative (thermal) transfers. These thermal transfers lead to a change in the refractive index of the medium, which in turn leads to the material (Fe_2O_3) being promising in the field of optical applications, including optical determinants, where the suspended (Fe_2O_3) showed a very large thermally induced nonlinearity [27].

1.3 Historical Survey of the Literature

Undoubtedly, tens or even hundreds of scientific papers dealing with the study of nonlinear optical properties of materials and applications. In particular the optical limiter application. In order for the historical review of the previous literature to be objective and simulate the work presented in this dissertation, we have touched upon the articles in which the same materials that were used in this dissertation were used. We have included in this review the articles that used CW lasers in the study as we did in this dissertation, as well as the articles that used pulsed lasers to show the wide range of use of these metallic nanomaterials as well as their improvement of the properties of other materials when used with them.

In 1999, Ya-Ping Sun *et. al.* studied the strong optical limiting of silver-containing nanocrystalline particles in a stable suspension. It was stabilized using PVP polymer in ethanol. Its optical limiter properties were studied using a nanosecond pulsed laser at (532) nm. The threshold fluence value was (0.37) J/cm^2 and the intensity limit was (0.18) J/cm^2. These results showed superiority over the standard substances such as chloroaluminum phthalocyanine and fullerene in the solutions [28].

In 2001 R. A., Ganeev *et. al.* studied the refractive indexes, absorption coefficients and nonlinear susceptibility of the Au, Pt, Ag and Cu colloids. Using lasers pulsed in picoseconds and nanoseconds at (1064) nm and (532) nm, these properties were studied. The nonlinear refractive index of the materials showed a negative value, except for gold at the wavelength of (1064) nm and the same thing at the wavelength of (532) nm, except that copper became positive as well. It has shown good properties for use as an optical limiter for ultra short pulse lasers [29].

In 2002, Renjis T. Tom *et. al.* prepared the structures for the core-shell of the Au@TiO2, Au@ZrO2, Ag@TiO2 and Ag@ZrO2 nanoparticles. The results of the nonlinear optical properties and the results of the optical limiter showed that these structures work well for picosecond and nanosecond lasers with a high damage threshold [30].

In 2003, R. A. Ganeev *et. al.* studied the nonlinear absorption of two types of glass doped with Cu nanoparticles by ion implantation method. The types of glass were silicate glas and soda-lime glas, and after doping, they were denoted by SG: Cu and SLSG: Cu, respectively. Using Z-Scan technology and a picosecond pulsed laser with a wavelength of (1064) nm, the properties of nonlinear absorption and optical limiter properties of the two types of glass were studied. The results showed an increase in the nonlinear absorption of the SG:Cu type over the other type, as well as the two types showed good optical definition compared to the unblemished glass, but the Cu:SG type had a (15) times higher optical definition than the second type [31].

In 2004, P. Prem Kiran *et. al.,* studied the enrichment of the optical limiting of Ag-Cu co-doped in SiO_2 sol-gel films depending on the nonlinear optical properties and the role of surface plasmon resonance (SPR). The study was carried out using high-powered picosecond and nanosecond pulsed lasers. Films made from these materials showed a self-defocusing nonlinearity of both lasers. The nonlinear refractive index decreases with decreasing particle size. As for the nonlinear absorption, it increases with increasing Cu concentration. The excitation near the surface plasmon resonance of Cu affected the behavior of the optical limiter in contrast to the excitation near the surface plasmon resonance of Ag. It also appeared that the contribution of scattering is much less than that of nonlinear absorption in affecting the optical

limiting. The values of the nonlinear refractive index (n_2) were recorded in the range of ((1.66 - 3.12) $\times 10^{-9}$ cm^2/W) and the third-order susceptibility (X_r^3) about ((0.89-1.68)$\times 10^{-7}$ esu) [32].

In 2006, Hui Pan *et. al.* studied the properties of the optical limiting of metallic nanowires of Cu, Ni, Co, Pd, Ag, and Pt. It was studied using a pulsed laser with a repetition rate of (10 Hz) with wavelengths of (1064 and 532) nm. The results showed that the optical limiting of some metallic nanowires is much better than the results of carbon nanotubes, except for (Cu and Co) nanowires, for the two wavelengths used. It also has a broadband optical limiter. The dimensions of the studied wires were (diameter = 50 nm, length = 30 microns). It appears that the dominant mechanism for nonlinear limiting of metallic nanowires is nonlinear scattering [33].

In 2007, Yachen Gao *et. al.* studied the effect of the size of the Au nanoparticles on the optical limiting. The sizes (15, 25, 50 and 70) nm were studied using a nanosecond pulsed laser at a wavelength of (532) nm. The results showed that the optical limiter depends on the size of the nanoparticles and that it does not increase monotonously with the increase in size. It turns out that the best size is (25) nm [34].

In 2008, R. Sreeja *et. al.* studied the effect of the size of Au nanoparticles suspended in deionized water and as films in (PVP) polymer on their nonlinear optical properties. The size of the Au nanoparticles was (4 and 6) nm. The study was carried out using a pulsed Nd:YAG laser operating at a repetition rate of (10) Hz. The results showed that the values of the nonlinear refractive index and the real and imaginary of third-order susceptibility values are negative and increase with decreasing particle size, and they are better for the polymer suspension than for the water suspension.

The reason is that the mechanism of influence in the two hosts, is the interband transitions of nanoparticles, but the effect of the thermal lens in the polymer is added to it due to self-defocusing. It appears that the optical limiter increases with decreasing particle size [35].

In 2009, Qiguang Yang *et. al.* studied the effect of morphology-controlled on linear and nonlinear optical properties by using the Z-Scan technique for Au-SiO2 coposite film and the degeneration four-wave mixing technique. The predominant size of Au nanoparticles was (15) nm and (2.5) nm width. A nanosecond pulsed laser with a wavelength of (532) nm was used. The results showed that the dominant mechanism is the reverse saturated absorption by influencing the nonlinear properties. The optical limiting results showed that it works efficiently at large sizes of Au nanoparticles for short pulses laser, but this efficiency is lacking at 2.5 nm size because large particles cause high scattering [36].

In 2010, J. Zamir Anvari *et. al.* studied the thermo-optical properties and the nonlinear responses of copper nanoparticles in polysiloxane oil. A CW laser source with a wavelength of (532) nm was used. The results showed a low-power optical limiter for a low limitation threshold resulting from thermal solf-defocusing and self-focusing. The nonlinear optical response was studied by measuring the intensity dependent on the refractive index in the medium using the Z-Scan technique. The value of the nonlinear refractive index was negative, about (-1.5 2×10^{-7}) cm^2/w. The study showed that the values of the optical limiting changed according to the change in the engineering design of the system (the distance of the sample from the focus, the distance of the detector from the sample and the diameter of the detector aperture). The study showed that the non-local thermal nonlinear refractive index

plays a major role in the development of photonic applications based on metallic nanoparticle suspensions [37].

In 2011, Yaping Han *et. al.* studied the optical limiting properties of silver nanowires Ag NWs. Using a 30 picosecond pulsed laser with a wavelength of (532) nm and Z-Scan technic. The results showed that the silver nanowires Ag NWs had a strong optical limitation, and that the greatest mechanism prevailing for the nonlinear optical determinant of these nanowires is the nonlinear scattering [38].

In 2012, M. Eslamifar and N. Mansour studied the enrichment of optical limiting properties with gold nanoparticles (Au NPs) suspended in deionized water. The particle size of Au NPs was about (7) nm and the surface plasmon absorption (SPA) peak was (520-530) nm. Using a laser source (CW) with a wavelength of (532) nm, the nonlinear optical properties were studied. The results of the nonlinear properties showed that there is not nonlinear absorption of the suspension and that the nonlinear refractive index n_2 is negative and its value is (-1.58×10^{-8} cm^2/W). The mechanism responsible for the nonlinear properties is thermal lens formation and self-defocusing. The properties of the optical limiter can be achieved with experimental geometry. Because the results showed that the limitation threshold increased linearly with the increase in the diameter of the circular aperture and decreased linearly with the increase in the distance between the sample and the circular aperture [39].

In the same year, HODA ALEALI *et. al.* studied the tunable of threshold limiter of gold nanoparticles in CASTOR OIL. The particle size of Au nanoparticles is about (25) nm. The nonlinear optical properties of suspension of Au nanoparticles was studied in water and castor oil. By using CW laser source with (532) nm and Z-scan technique, large nonlinear refractive indices were obtained to the suspension in the

water and castor oil in range in oil ((1.61-7.76)× 10^{-7} cm^2/W)) and in water ((0.3-2.5)× 10^{-8} cm^2/W)) as results of concentrations with minus sign. The results was shown that the values of nonlinear refractive induces in castor oil is better than in water because of the difference in thermal conductivity between them. Thermal induced effect is the dominate mechanism of the nonlinear refraction process. The optical limiter results showed that the threshold can be changed by adjusting the set-up and concentration of the suspended Au nanoparticles. The results of the optical limit are attributed to the diffraction of the laser beam when passing through the sample [40].

In 2013, Olivier Muller *et. al.* studied the effect of shape and size on the nonlinear optical behavior of Ag nanoparticles suspended in ethyl alcohol and on the optical limiting in comparison with the suspended carbon black. Using a nanosecond pulsed laser with (532 and 1064) nm wavelengths and Z-Scan technnic. The shapes of the studied particles were Nano plates, spherical, multiplaned, and Nano flowers, with average size ranging from (60 to 70) nm. The results showed that the optical limiting is highly dependent on the size of nanoparticles and that its performance improves with small particles. At the wavelength of (532) nm, the best non-linear attenuation was for spherical nanoparticles, while for other shapes it was twice less and the same behavior for the wavelength of 1064 nm. In addition, the results showed that surface plasmon resonance is not the main influence responsible for the nonlinear processes. They concluded that the optical limiter is highly dependent on the size of the nanoparticles, and its best performance is for small particles, and that the shape does not have a large effect [41].

In 2014, Morvarid Rashidian and Davoud Dorranian Present an exploratory study on the optical determinant of metallic nanoparticles. Where gold and silver

nanoparticles were studied in several concentrations as suspensions in water, with a CW laser wavelength of (532) nm, and they presented the following conclusions: The mechanism of nonlinear refraction is the dominant mechanism for the response of the optical limiting. The efficiency of the optical limiting increases with the decreasing size of the nanoparticles. The threshold power of the optical limiter decreases with increasing concentration of nanoparticles in the suspension. The threshold limit can be improved by changing the geometric design in terms of the dimensions of the set-up and changing the concentrations of the samples. Self-defocusing is predominant by the thermal effect and is largely related to the absorbent properties of the medium. Thermal self-diffraction can be observed if the sample is placed behind the focus [42].

In 2015, Y. C. Gao and C. Y. He, studied the effect of the solvent (host) on the response of the optical limiter to platinum nanoparticles protected by C60. Three different solvents were used (chloroform, ethanol, and dimethylformamide (MDF)). Using a nanosecond laser pulse with a wavelength of (532) nm. The results showed that the optical limiter depends on the thermodynamic properties of the solvents such as thermal conductivity, heat capacity and boiling point. These properties are responsible for causing a rapid local temperature rise in the solvent surrounding the nanoparticles suspended in it or the heat transfer from the nanoparticle to the solvent, which greatly affects the optical limiter [43].

In 2016, Y.S.Tamgadge *et. al.* studied the optical limiting of the nanostructure films of Cu nanoparticles doped with ZnO nanoparticles in PVA with different thicknesses, which were in the range of (120-193) nm. The size of the nanoparticles was about (20) nm. The values of the absorption and excitation peaks were at (343 and 360) nm. A CW laser with a wavelength of (632.8) nm was used to study the

nonlinear optical properties. The values of the nonlinear refractive indices were negative and in the range of (2.8×10^{-4} - 6.5×10^{-4}) cm^2/w, and the values of the negative nonlinear absorption coefficients were in the range of (2.3×10^{-4} – 7×10^{-4}) cm/W and the values of the nonlinear third-order susceptibility are in the order of (2.8×10^{-4} - 6.5×10^{-4}) esu. The results showed that the enrichment of the nonlinear properties is attributed to the effect of self-defocusing, the reverse saturable absorption and the thermal effect. The results showed that the properties of the optical limiter are good and increase with increasing Cu concentration, and the best value for the limiting power was (20) mW and the threshold power was (16) mW [44].

In 2017, Meng Bi *et. al.,* studied the optical limiting properties of liquid crystal elastomer doped with Ag nanoparticles. The size of Ag nanoparticles was about (20) nm. A nanosecond pulsed laser with a wavelength of 532 nm was used to study the properties of nonlinear absorption and optical limiter properties. The results showed that the nonlinear absorption changed from saturable absorption to reverse saturable absorption with increasing incident intensity. The optical limiting properties are good and the limiting threshold value is (3.7) J/cm^2, which is very close to the benchmark of C60 value [45].

In 2018, Dehghanipoor Masoud *et. al.* studied the nonlinear absorption enrichment and optical limiter properties of graphene oxide (GO) mixed with iron oxide nanoparticles (Fe_2O_3), where the mixing ratio was 10:1 volume. The mixing process was done using sonication. A CW laser with a wavelength of (532) nm was used to study the properties of nonlinear absorption and optical limiter properties. The nonlinear absorption properties of the mixture were studied, and the results showed that the nonlinear absorption increased with increasing concentration of iron oxide

nanoparticles. The properties of the optical limiter were studied, and the results showed that the limiting power increases with increasing sample length [46].

In 2019, J. John, R.M. Mathew, I. Rejeena, *et. al.* studied the nonlinear optical limiting of a liquid (not authorized by the researchers) containing green Cu nanoparticles. The size of Cu nanoparticles was (3-6) nm. The nonlinear optical properties were measured using the Z-Scan technique using a nanosecond pulsed laser with a wavelength of (532) nm. The results showed that the value of the nonlinear absorption coefficient of this solution is (7.33) cm/GW and the value of the imaginary third-order susceptibility is (1.24×10^{-10}) esu. The copper nanoparticles showed inverse saturated absorption caused by the two-photon absorption mechanism. The results of the optical limiting showed that it is very effective for high energies, where the limit value was (237) MW/cm^2 and this efficiency is due to the nonlinear absorption of copper nanoparticles [47].

In 2020, Hongyan Zhang *et. al.* studied the preparation of silver nanoparticles of different sizes and optical limiting properties in their acidic solution. The shapes of the nanoparticles were spherical and with sizes of (40, 45 and 78) nm. The results of the nonlinear optical properties and optical limiting properties showed that the nonlinear absorption mechanism resulted from saturated absorption and inverse saturated absorption, and that the limiting efficiency decreased with the increase of the incident intensity of the large nanoparticles, and the efficiency increased with the decrease in the size of the particles. The reason for this is that the high energy absorbed by the large particles leads to its deformation and then its melting and evaporation. Thus, small silver nanoparticles are more suitable for use in high-energy optical parameters [48].

In 2021, Peiran Tian study the ZnO films, ZnO films doped with Ag nanoparticles and ZnO films doped with Cu nanoparticles deposited on quartz substrates. Using the Z-Scan technique with two pulsed lasers, the first in nanoseconds and the second in femtoseconds, with a wavelength of (532) nm, the nonlinear optical absorption properties and optical limiter properties of the films were studied. The results of the non-linear absorption and optical limiter showed that the doping process led to a significant improvement in the non-linear absorption values of the films compared to the non-doped film. The mechanism contributing to this increase in absorption is the two-photon absorption and the inverse saturated absorption. The doping process also led to an improvement in the properties of the optical limiter, as the doped films showed high efficiency to work with the femtosecond and nanosecond pulsed lasers [49].

1.4 Dissertation Structure Overview

A comprehensive overview of the contents of this dissertation will be provided by reviewing what each chapter dealt with and what was highlighted, as follows:

Chapter One included an introduction that reviewed the history of scientists' sensing of nonlinear optical properties, leading to the discovering of the LASER and the invention of its devices, which enhanced this part of physical optics, to the need that led to the protection of optical devices, tools and the eyes of their users through optical limiting. Where these limiters allow the light intensity, transmit to a certain extent commensurate with the system or device to provide protection for it from the occurrence of optical damage. Then, samples of researchers' work for the past twenty years were reviewed. By selecting articles that used materials similars the materials used in this dissertation, as well as the areas of the limiters working with CW lasers

and pulsed lasers. Not to mention the mixing of materials of interest with other materials and its impact on developing the work of optical limiting. Then it included paragraphs to clarify the contents and aim of the dissertation. **Introduction** titled this chapter.

Chapter Two titled the **Theoretical Part**. As each field of science is based on theoretical rules and mathematical equations, by which the results analyzed and the studied parameters were calculated. This chapter included a review of the scientific rules on which explicate of nonlinear optical phenomena. The mechanism that leads to their occurrence, the mathematical equations that describe these mechanisms was described, as well as the mathematical equations that were used to calculate the parameters that were studied for the nonlinear optical properties and the basis for the work of optical limiters and their principle of operation.

Chapter Three included a brief review, with a flowchart, of the overall work carried out in this dissertation. This was followed by a full detail of each step taken, starting with the preparation of the material, Samples preparation, the tests carried out on them, and the results obtained. In addition to a schematic description of the settings used in the study and the brands of devices that provided us with the data. Experimental Part titled this chapter.

Chapter Four is the last chapter of this dissertation. This chapter is titled with **Results, Discussion and Conclusion**. The results of scanning electron microscopy examinations that show the morphological properties of all samples were reviewed. A computer program analyzed all the images for all the samples. This analyzing provide description to the shapes and sizes for the all particles of materials. Then the results of the linear optical tests were reviewed for all samples of the materials used

and for all their concentrations that were represented by graphs showing the linear optical absorption of these samples. Then a description, analysis and conclusion of these diagrams, and an account and measurement of some linear optical parameters followed it. After that, the nonlinear behavior diagrams for all samples were reviewed and the parameters were calculated based on the recorded data from the Z-scan system, was calculated and followed by a description and analysis of its behavior and a calculation of the important parameters to show the results and a conclusion for that behavior and results. Finally, the schematics that describe the behavior of the optical limiting for each sample, which represents the main objective of this dissertation, were reviewed. The required parameters were measured and the behavior of each material was explained based on the concentration, wavelength used, and the laser intensity incidents on it.

1.5 Aim of the Work

The main objective of this dissertation is to study the properties of the optical limiting at the visible spectrum region of the electromagnetic spectrum for a group of metallic nanomaterials (except for one of them was metal oxide).

Shows the effect of the morphology, concentrations, size and type of the nanomaterial on the properties of optical limiter.

Make a mixtures of some of these nanomaterials with two materials for each mixture by using two mixing methods to improve the extent of the optical limiter and studying the effect of these two methods.

Studying the morphological properties, linear optical and nonlinear optical properties of these mixtures and their effects on OL.

Chapter 2

Theoretical Part

CHAPTER 2 Theoretical Part

2.1 Introduction

To find out the theoretical basis on which the studied properties of linear optical properties, third-order nonlinear optical properties and properties of the optical limiting are based, which is the final goal of this thesis. In this chapter, we will review the theoretical and mathematical basis for these properties, and we will discuss the properties of the optical limiting, its general definition, the ideal optical limiting, and its work mechanism, with a mention of the materials used in it and the important requirements of the optical determinant.

2.2 Linear Optical Properties

The interaction between the nature and distribution of the internal charge of the material and the electromagnetic radiation incident on it leads to the emergence of linear optical properties of the material [50]. When the electromagnetic rays incident on the material and interact with it, then many processes will occur. As part of these rays will be reflected from the surface of the material and it is called the (reflected part) and part will pass through it and it is called the (transmitted part) and there is a part that is absorbed by the material and it is called the (absorbed part) [51].

2.2.1 Absorption

Optical absorption is defined as the process by which radiation incident on a material transfers some or all of its energy to it. In other words, it is the process of decreasing the intensity of certain frequencies (certain wavelengths) of electromagnetic radiation. This process leads to the rise of electrons from one level to another level of higher energy. This rising is a product of the process of interaction between the electric dipole moment of the electrons and the electric compound of the electromagnetic ray photons. The absorption potential is proportional to the density of the substance. In the case of solutions or suspensions, the probability of absorbing photons incident on a solution or suspension is directly proportional to the concentration of particles in that sample (the number of particles in the medium). The relationship between the concentration in a sample and its thickness through which the incident ray passes (the length of the optical path) is expressed idiomatically with absorbance or optical density and mathematically by the following equation [52]:

$$A = log_{10}\left(\frac{I_o}{I}\right) = \varepsilon lC \ldots\ldots\ldots\ldots (2.1)$$

The equation (2.1) is known as the Beer-Lambert Law of liquids [53]. Where A: Absorbance C: Concentration, l: The length of the optical path that the ray travels through the material, ε: Molar extinction coefficient (cm^{-1} M^{-1}), I_o: Intensity of incident ray before entrance and I: Transmitted intensity at a specific wavelength.

2.2.2 Linear Absorption Coefficient

The linear absorption coefficient (α_o) or the attenuation of the intensity of light that passes through a material, which is a factor that expresses a portion of the absorbed beam for a unit thickness of the material [54]. According to the "Beer-Lambert law", the absorption coefficient can be found through the following relationship [55]:

$$\alpha_0(cm^{-1}) = 2.303\ \frac{A}{l} \ldots\ldots\ldots\ldots (2.2)$$

$$\alpha_0 = \frac{1}{l} ln\left(\frac{1}{T}\right) \ldots\ldots\ldots\ldots (2.3)$$

Where T: Transmittance of medium, which is the ratio of the penetrating intensity (I) to the incident intensity (I_o) after the medium absorbs part of the incident ray and l: Thickness of medium [56].

$$T = \frac{I}{I_0} \ldots\ldots\ldots\ldots (2.4)$$

$$T = 10^{-A} \ldots\ldots\ldots\ldots (2.5)$$

2.2.3 Linear Refractive Index (n)

An essential parameter of any optical material is the refractive index. Usually, the Maxwell wave equation is the main source for deriving important optical properties, definitions, formulas and basic concepts of materials. The refractive

Index (n) of a transparent optical material is defined as the ratio of the speed of light or electromagnetic wave (C) in a vacuum to the phase velocity (v) of the same wave in the material [57].

$$n = \frac{c}{v} \dots\dots\dots\dots (2.6)$$

The (n) is inversely proportional to the wavelength of the incident wave on the material. With the exception of some materials, the refractive index also changes according to the direction of the electromagnetic waves in the material and these materials are used to change the polarization direction of these waves [58], so the complex refractive index can be given by:

$$\bar{n} = n + ik \dots\dots (2.7)$$

Where k: extinction coefficient or the absorption index (or the imaginary part of the complex refractive index). Both of (k and n) depend on wavelength. When the electromagnetic radiation falls on the material, it works to move the charge in the material, resulting in a dipole. If (υ) is the frequency of the alternating electric field of the incident electromagnetic wave, and therefore the electrical polarization of the particle will fluctuate at the same frequency (υ). So part of the energy of the incident wave will be converted to the vibration energy of the generated electrode dipole and thus reduce the amplitude of the incident wave [59]. The greater the polarization, the greater the effect of the delay, and the higher the refractive index, the lower the speed of light in the material. The material that does not have polarization does not have any delay in returning the light, and therefore its refractive index is (n = 1) [60].

2.3 Nonlinear Optics

When one or more high-intensity electromagnetic waves propagate in a medium, the atoms of the molecules of that medium will vibrate not only at the frequency of the electric field of the electromagnetic wave that is applied to it, but with a different combination of frequencies as a result of the nonlinear response of the medium.

The charged particles of the medium will be displaced from their original equilibrium positions, and then the positive charges will move towards the electric field of the applied electromagnetic wave and the negative charges against it. An electric dipole moment will arise due to the displacement between the positive and negative charges and the dipole moment will induce a polarization in the medium.

From the foregoing, nonlinear optics is a physical phenomenon in which high intensity light such as a laser or a high intensity electromagnetic wave is stimulated in response to a nonlinearity in the medium. In contrast, the medium will adjust the optical fields in a nonlinear manner. In fact, all media are nonlinear mediums of a certain degree of intensity [61 & 62].

When the medium is exposed to an electromagnetic wave of not high intensity, it causes the atoms (charges) of the medium to vibrate. This vibration of the charges is consistent with the frequency of the incident ray, that is, it has the same frequency where the displacement of the charges is proportional to the value of the electric field of the incident ray. Because of that, a ray of the same frequency of the incident ray may be emitted or non-radiative processes like heat in the material or any other energy transformation processes may transform the energy absorbed by

The material. Therefore, the linear induced polarization given by the following equation [63]:

$$\vec{P}_L = \varepsilon_0 \chi^{(1)} \vec{E} \ldots\ldots\ldots (2.8)$$

Whereε_0: Permittivity in vacuum (dielectric constant),$\chi^{(1)}$: The first order linear optical susceptibility which responsible for linear absorption and linear refraction and$\vec{E}$: Applied electric field.

When applying high enough electric fields, then it will induce a non-linear polarization that depends on these fields, and it can be expressed by:

$$\vec{P} = \varepsilon_0 \chi^{(1)} \vec{E} + \varepsilon_0 \chi^{(2)} \vec{E}^2 + \varepsilon_0 \chi^{(3)} \vec{E}^3 + \cdots = \vec{P}^{(1)} + \vec{P}^{(2)} + \vec{P}^{(3)} + \cdots (2.9)$$

Where$\chi^{(2)}$: The second order nonlinear susceptibility which responsible for sum and difference frequency mixing, optical rectification and electro-optic effect and $\chi^{(3)}$: The third order nonlinear susceptibility which responsible for nonlinear refraction indices, implicitly to the optical limiting phenomenon [64].

The solution of Maxwell's equations (2.10 and 2.11) is necessary to describe the nonlinear light interaction with matter [65].

$$\nabla \times H = \frac{\partial D}{\partial t} \ldots\ldots\ldots\ldots (2.10)$$

$$\nabla \times H = 0 \ldots\ldots (2.11)$$

Where *D*: Displacement related through $D\ (E) = \varepsilon_0 E + P\ (E)$ where the electric polarization *P (E)* is the dipole per unit volume, H: related through $B=\mu_o H$ (B: magnetic field

and μ_o Permittivity of free space). By separating the linear part from nonlinear part in equation (2.9), then the equation become [65]:

$$\vec{P}\,(E) = \varepsilon_0\,(\varepsilon_1 - 1)\vec{E} + \vec{P}_{NL} \dots\dots\dots\dots (2.12)$$

Where ε_1: Linear dielectric constant.

$$(\varepsilon_1 - 1) = \chi^{(1)}$$

$$\varepsilon_1 = \chi^{(1)} + 1 \dots\dots\dots (2.13)$$

In this form the electric displacement becomes:

$$D\,(E) = \varepsilon_0\varepsilon_1\vec{E} + \vec{P}_{NL} \dots\dots\dots (2.14)$$

Maxwell's equations can be written as:

$$\nabla \times H = \frac{\partial}{\partial t}\left(\varepsilon_0\varepsilon_1\vec{E} + \vec{P}_{NL}\right) = \varepsilon_0\varepsilon_1\frac{\partial\vec{E}}{\partial t} + \frac{\partial\vec{P}_{NL}}{\partial t} \dots\dots (2.15)$$

$$\nabla \times \vec{E} = \frac{\partial}{\partial t}\,(\mu_o\,H) = -\mu_o\frac{\partial H}{\partial t} \dots\dots (2.16)$$

To extract the nonlinear wave equation need to solve equations (2.15 and 2.16). The rotation of equation (2.16) is:

$$\nabla \times \nabla \times \vec{E} = \nabla \times \left(-\mu_o\frac{\partial H}{\partial t}\right) = = -\mu_o\frac{\partial}{\partial t}\,(\nabla \times H) \dots\dots (2.17)$$

By substituting equation (2.15) in the equation (2.17) get:

$$\nabla \times \nabla \times \vec{E} = -\mu_o\frac{\partial}{\partial t}\,(\varepsilon_0\varepsilon_1\frac{\partial\vec{E}}{\partial t} + \frac{\partial\vec{P}_{NL}}{\partial t}) \dots\dots (2.18)$$

By using general identity, $\nabla \times \left(\nabla \times \vec{E}\right) = \nabla\left(\nabla . \vec{E}\right) - \nabla^2 \vec{E}$ the equation (2.18) becomes:

$$\nabla\left(\nabla . \vec{E}\right) - \nabla^2 \vec{E} = -\mu_o \frac{\partial}{\partial t}\left(\varepsilon_0 \varepsilon_1 \frac{\partial \vec{E}}{\partial t} + \frac{\partial \vec{P}_{NL}}{\partial t}\right) \ldots\ldots\ldots (2.19)$$

In general $\nabla . \vec{E} = 0$ this simplifies equation (2.19) as:

$$\nabla^2 \vec{E} - \frac{\varepsilon_1}{c^2} \frac{\partial^2 \vec{E}}{\partial t^2} = \frac{1}{c^2 \varepsilon_0} \frac{\partial^2 \vec{P}_{NL}}{\partial t^2}, \qquad \ldots\ldots\ldots (2.20)$$

Where $\mu_o \, \varepsilon_0 = c^{-2}$ (c: Speed of light in vacuum. The equation (2.20) is known the nonlinear inhomogeneous equation [66]. According to the solution to obtained nonlinear wave equation by [67]. And by using the assumption which is known "slowly varying envelope approximation (SVEA)" through neglecting the first and the second order temporal derivatives of nonlinear polarization and the order spatial and temporal derivatives of the amplitude of the electric field of electromagnetic wave by [68] the nonlinear wave equation be [65]:

$$\frac{\partial \vec{E}_j}{\partial z} + \frac{n_j}{c} \frac{\partial \vec{E}_j}{\partial t} = i \frac{\omega_j}{c \, n_j} \frac{1}{2\varepsilon_0} \vec{P}_{NL_j} e^{ik_j z} \quad \ldots\ldots\ldots (2.21)$$

Where, $k_j = \frac{n_j \omega_j}{c}$, ω_j: The frequencies of plane waves, n_j: refractive index of plane waves $n_j = \sqrt{\varepsilon_j}$

2.3.1 Processes of Optical Third-order Nonlinear

According the equation (2.9) which refers to inducing a non-linear polarization that depends on electric fields and by considering the sinusoidal field equation, which is, clearly describes of optical behavior as follow:

$$E(z,t) = E_o \cos(\omega t - kz) \dots\dots\dots (2.22)$$

With $k^2 = \varepsilon\omega^2/c^2$, where, E_o: The amplitude of the field, k: The propagation vector, characterizing the phase of the optical wave with respect to a reference point, *kz* describes the relative phase of the wave . By substituting equation (2.22) in to equation (2.9) get:

$$P = \chi^{(1)}E_o \cos(\omega t - kz) + \chi^{(2)}E_o^2 \cos^2(\omega t - kz) + \chi^{(3)}E_o^3 \cos^3(\omega t - kz) \dots\dots\dots\dots\dots\dots\dots\dots (2.23)$$

Equation (2.23) shows, a du to nonlinear polarization, a new frequency components presence [69].

The third-order nonlinear susceptibility ($\chi^{(3)}$) is the subject of the study which leads to nonlinear refractive index (n_2) and nonlinear absorption coefficient (β). The ($\chi^{(3)}$) equation consist of two parts (really and imaginary). In general, the ($\chi^{(3)}$) can expressed in the following form [63, 70]:

$$\chi^{(3)} = Re\left(\chi^{(3)}\right) + Im\left(\chi^{(3)}\right) \dots\dots\dots (2.24)$$

Where $Re\left(\chi^{(3)}\right)$: The real part of the third-order nonlinear susceptibility, $Im\left(\chi^{(3)}\right)$: The imaginary part of the third-order nonlinear susceptibility [70].

$$Re\left(\chi^{(3)}\right)(e.s.u) = 10^{-4}\frac{\varepsilon_o\, n_o^2 c^2}{\pi} n_2 \ldots\ldots\ldots (2.25)$$

$$n_2 = \frac{\pi}{10^{-4}\,\varepsilon_0\, n_0^2\, c^2}\,\chi^{(3)} \ldots\ldots\ldots\ldots (2.26)$$

n_2, in unit ($\frac{cm^2}{W}$): Nonlinear refractive index of material, *c*: velocity of light in space, n_o: Linear refractive index of material. The $Im\left(\chi^{(3)}\right)$, can be expressed in terms of the nonlinear absorption coefficient (β) [70]:

$$Im\left(\chi^{(3)}\right)(e.s.u) = 10^{-2}\,\frac{\varepsilon_0\, n_0^2\, c^2\, \lambda}{4\,\pi^2}\,\beta \ldots\ldots\ldots (2.27)$$

$$\beta = 10^{-2}\,\frac{4\,\pi^2}{\varepsilon_0\, n_0^2\, c^2\, \lambda}\,\chi^{(3)} \ldots\ldots\ldots\ldots (2.28)$$

β, In unit ($\frac{cm}{W}$), λ: Wavelength for incident ray.

2.3.1.1 Nonlinear Refraction

One of the major and important nonlinear optical effect is nonlinear refraction. It plays a large and influential role in many optical and electro-optical applications. The nonlinear refractive index (n_2) is defined as the change in the refractive index of the material under the influence of the high intensity of the electromagnetic wave incident to the material, such as the laser beam. It can be described in the following relationship [71]:

$$n(I) = n_0 \pm n_2\, I \ldots\ldots\ldots (2.29)$$

CHAPTER 2 Theoretical Part

The change in the refractive index of the material under the influence of the high intensity of the laser beam can result in many effects. One of the most important effects is self-focusing and self-defocusing [72]. These effects are of great importance in optical limiter and optical switch applications. Self-focusing is one of the nonlinear processes that can occur due to the dependence of the refractive index on the intensity. This process causes spatial variation in the laser beam, where a beam of high intensity changes the optical properties of the medium in such a way that the beam is focused inside the material so that the material acts as a positive lens (convex lens, n2 > 0 is positive). This focus of the laser beam will induce a difference in the refractive index inside the material where the refractive index will be greater in the center of the beam than in its periphery. This process is of great practical importance because the intensity at the self-focusing spot is large enough to cause optical damage to the material [73 & 74]. As for the self-defocusing, it increases the spacing of the laser beam, which leads to the widening of the beam and thus leads to a decrease in transmittance and the material acts as a negative lens (concave lens, n2 < 0 negative) [75 & 76]. For more explanation, the following must be clarified:

Permeability and permittivity ($\mu \; and \; \varepsilon$) are a parameters every substance possesses them. These parameters determine the interactive method between light and material. The real refractive index must be possessed by the material transmitting electromagnetic rays and the $\mu \; and \; \varepsilon$ must have the same sine [77]. Which material have both negative sign of ($\mu \; and \; \varepsilon$) termed as left-hand material because the electric and magnetic fields form a left set of vectors with the wave vector [78 & 79]. Also called negative-refractive index material (NRM) and as

is demonstrated both theoretically and experimentally by [80], lenses and optics made from (NRMs) will produce unusual optics. From the equation of the dielectric permittivity of propagation of Transverse electric polarized (TE- polarized) in nonlinear Kerr-type (NRM) below:

$$\varepsilon = \varepsilon_1 + \varepsilon_2 |E|^2 \text{.....(2.30)}$$

On the right-hand side of above equation (2.30), the first and second terms characterize the linear property and the Keer-type nonlinearity , respectively. For a normal medium, ($\varepsilon_2 > 0 \; and \; \varepsilon_2 < 0$) correspond to "self-focusing" and "self-defocusing" medium, respectively. There are necessary conditions for a light beam "self-focusing" and "self-defocusing". An optical beam scattered in a nonlinear medium subjected to "self-focusing or defocusing" depends on the additional phase shift caused by the nonlinear refractive index [81 & 82]. Therefore, it is useful to discuss the effect on a beam of nonlinear effect alone. From the growth equation for the electric field envelop A:

$$2ik\frac{\partial A}{\partial z^2} + \nabla_\perp^2 A + k^2 \frac{\varepsilon_2}{\varepsilon_1}|A|^2 A = 0 \text{ ... ... (2.31)}$$

Where $k = \sqrt{\varepsilon_1 \mu \omega}/c$. If we neglect the deviation in the equation (2.31), we have the following solution [83]:

$$A(r_\perp, z) = A(r_\perp, 0)\exp[i\phi_{NL}(r_\perp, z)] \text{ ... . (2.32)}$$

Where $r_\perp$: Coordinate vector, ϕ_{NL}: Nonlinear phase.

$$\phi_{NL}(r_\perp, z) = k\frac{\varepsilon_2}{2\varepsilon_1}|A(r_\perp, 0)|^2 z \text{ ... ... (2.33)}$$

Equation (2.33) indicates that the transverse distribution of the nonlinear phase is similar to that of input beam . The transverse component of the wave vector at a transverse point r⊥ in a beam is [83] :

$$\boldsymbol{K}_{\perp}(r_{\perp},z)=\nabla_{\perp}\phi_{NL}(r_{\perp},z)=k\frac{\varepsilon_2}{2\varepsilon_1}\nabla_{\perp}|A(r_{\perp},0)|^2 z\ldots\ldots \text{ (2.34)}$$

This result is independent of the beam profile. This variation can be viewed as a spatial chirp. From the equation (2.34) get a conditions for self-focusing and self-defocusing of an optical beam in (NRM). From the foregoing, it is clear that the light propagates in the opposite direction to the flow of energy in the material (NRM). Meaning that the direction of the wave vector K is opposite to the propagation direction of z, and therefore the $k<0$ in addition, as a symmetric Gaussian wave with circular symmetry and more intense in the center, then $\varepsilon_1<0$ and $\nabla_{\perp}|A(r_{\perp},0)|^2<0$. From the foregoing, the following conclusions will be drawn:

- For $\varepsilon_2<0$, an optical beam will probably self-focuses. This is because of that $\boldsymbol{K}_{\perp}>0$, i.e. the direction of transverse wave vector is the same as that of transverse coordinate vector r⊥ in this case. When a Gaussian beam with an initially uniform wave front propagating in such a medium, its uniform wave front will evolve to a converging spherical wave front, as Fig. (2.1 a) shows [83].
- For $\varepsilon_2>0$, an optical beam will probably "self-defocuses". This is because of that $\boldsymbol{K}_{\perp}<0$, i.e. the direction of transverse wave vector is opposite to that of transverse coordinate vector r⊥ in this case. When a Gaussian beam with an initially uniform wave front propagating in such a medium, its uniform wave front will evolve to a divergent spherical wave front, as Fig. (2.1 b) shows [83].

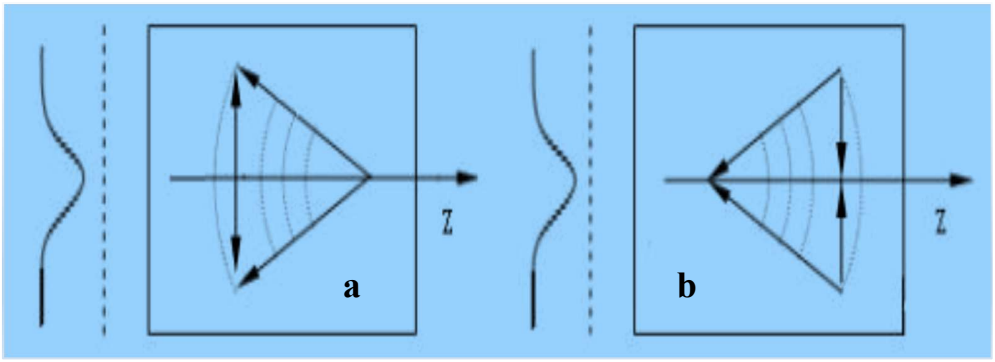

Fig. (2.1): a: Self-focusing $\varepsilon_2 < 0$ for Gaussian beam propagate in (NRM), b: Self-defocusing $\varepsilon_2 > 0$ for Gaussian beam propagate in (NRM) [83].

2.3.1.2 Nonlinear Absorption

Nonlinear absorption means, the change of permeability of a material as a function of density or fluence. Electromagnetic waves of high intensity such as lasers can cause profound changes in the optical properties of a material resulting in a nonlinear response of the real and imaginary parts of polarization [84]. The imaginary part is related to the nonlinear polarization. The nonlinear absorption is proportional to the intensity square or proportional to the intensity of the higher orders as it refers to the change in the permeability of the material as a function of the intensity falling on it [85] as there are different effects that can be produced by nonlinear absorption, including:

2.3.1.2.1 Two Photon & Multi Photon Absorption

A transition from ground state (1) of a material to a higher-lying state (2) by the simultaneous absorption of two photons via an intermediate virtual state known as Two photon Absorption (TPA) , as it shown in Fig. (2.2).

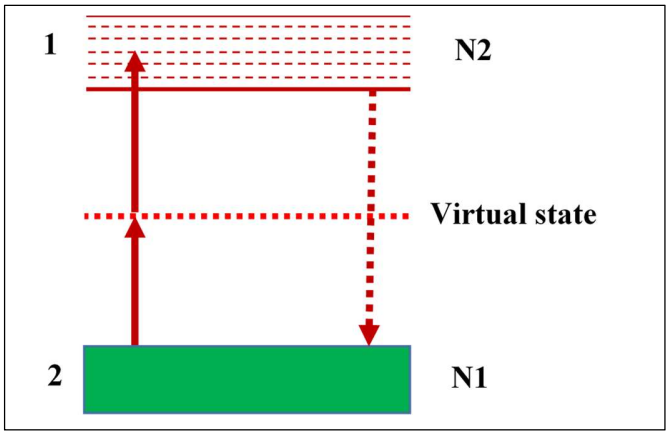

Fig. (2.2): Two-photon absorption (TPA) Schematic diagram [86]

The probability of a substance absorbing more than one photon before it relaxes to the ground state can be greatly improved at sufficiently high intensities. In 1931, Göppert-Mayer derived using the theory of second-order quantum perturbation, the probability of the transmission of two photons in a system [86].

Multiple photon absorptions (MPA) are very promising for frontier optical [87], 3D microfabrication [88], optical data storage [89] and biomedical applications [90]. The process of absorption of more than two photons is a process of higher orders, in which three or more photons are absorbed. It refers to the absorption of (n) photons from a single beam or more than one beam, as shown in Fig. (2.3).

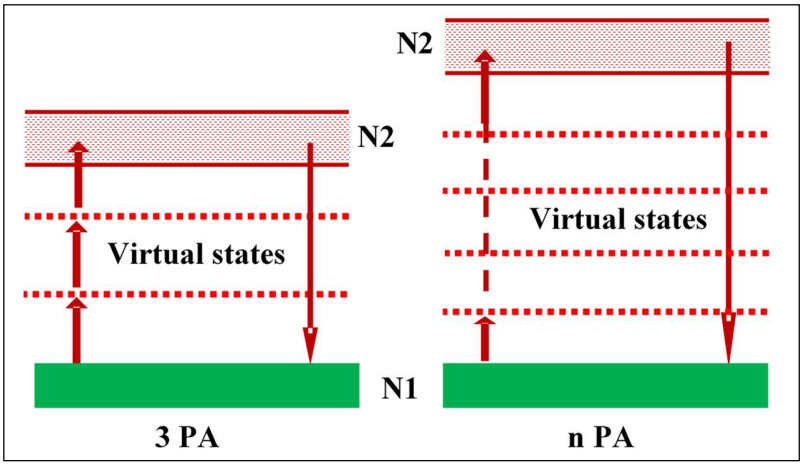

Fig. (2.3): Three and multi photon absorption (MPA) Schematic diagram [85]

where the absorption of photons with Rank (n + 1) can be given by the following equation [85]:

$$\frac{dI}{dz} = -(\alpha_0 + \gamma^{(n+1)} I^n) I \dots\dots\dots (2.35)$$

Where I: The intensity of the transmitted light, $\gamma^{(n+1)}$: The absorption coefficient of an ordered photon (n + 1), $\frac{dI}{dz}$: Decreases intensity of light with the depth of propagation in the medium. Since the nonlinear absorption of two photons is one of the forms of multi-photon absorption, then the nonlinear absorption of two photons will be proportional to the square of the intensity as in the following equation [85]:

$$\frac{dI}{dz} = -\alpha_0 I - \beta I^2 \dots\dots\dots (2.36)$$

Where, α_0: Linear absorption coefficient and β: Nonlinear absorption coefficient for two photons. When the intensity is not sufficient to show the nonlinear properties,

in this case the absorption is negligible and neglected. Thus, the equation (2.36) is in the following form:

$$\frac{dI}{dz} = -\alpha_0 I \dots\dots\dots (2.37)$$

2.3.1.2.2 Excited state absorption (ESA)

When high-intensity light falls on the material, the excited state absorption (ESA) can become significant due to the large number of excited sites. The excited electrons will rapidly move to the higher excited states before decaying back to the ground state. The possibility of a number of higher states that can be associated with these intermediate states is also included in which the energy differences are in a state of quasi-resonance with the energy of the incident photon. In such a case, before the electron is completely relaxed to the ground state, it may undergo an absorption that raises it to another higher state. The ESA mechanism of nonlinear absorption understood by a five-level model. That indicates five featured electronic states [69, 85] is shown in Fig. (4).

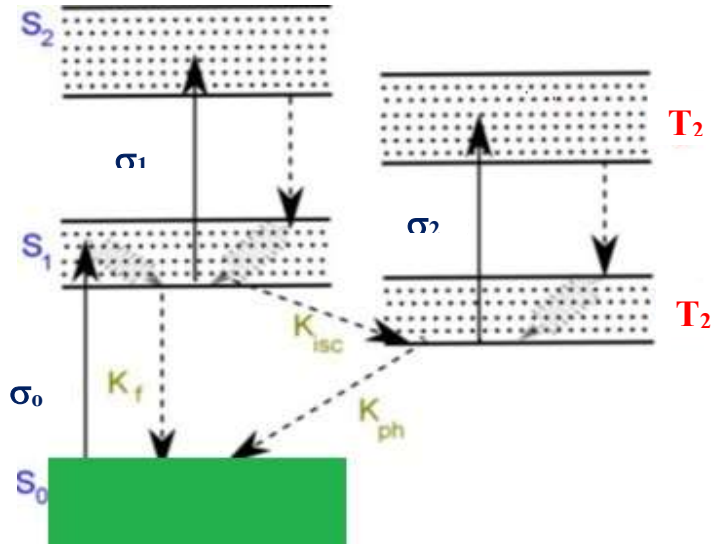

Fig. (2.4) Five energy levels for the excited state absorption (ESA) schematic diagram [85]

From the Fig. (2.4), the absorption of the incident photon leads to an increase in the number of electrons in the first excited single state (S1), where the electrons will move from the ground state (So) to the excited state (S1). Then the following possibilities can be (1) The electron can relax back to the ground state by radiant or non-radiative transition with a rate constant (k_f). (2) Can undergo a spin transition to a triplet state (T1) (a transit in the system between two different levels of multiplicity) with a rate constant (kisc). (3) The material can absorb another photon sufficient to enhance the number of electrons in the higher level (S2), from which it can relax back to the first excited single state (S1). Accordingly, the electrons in the aforementioned three possibilities have two options: (a) They can relax back to the ground state by another spin-reversal transition and this leads to the

phosphorescence process (b) The material can absorb another photon boosting the electrons into a state Triple above (T2) after which it can relax back to the (T1) state.

The main difference between (TPA) and (ESA) is that the first includes very short-lived intermediate virtual states, while in the second they are intermediate real states where the chronological age is not determined by (Heisenberg's imprecision) relations, but their lifetimes are determined by the electronic structure of the molecules in the materials. The (TPA) depend on the intensity (energy per unit time per unit area) of the incident light while (ESA) processes depend on the fluence (energy per unit area) of the incident light. The (TPA) depends on the intensity of the incident light while (ESA) depends on the fluorescence (energy per unit area) of the incident light [91].

2.3.1.2.3 Saturable Absorption (SA)

Saturated absorption is the process in which the absorption cross-sectional area of the excited state (2σ) is less than the cross-sectional area of ground-state absorption (1σ). The transmittance of the material will increase with the increase in the intensity of the laser beam, so the material will absorb light and then become more transparent so that it reaches the state of saturation (Bleaching). Is not to mention that it is a third-order nonlinear optical process [85 & 92]. Saturated absorption is of great importance due to its use in many applications, including those of the Passive Q-Switching Laser [85 & 93]. In general, when a laser beam passes through a saturated absorbent medium, the nonlinear absorption of the system can be expressed by the following relationship [92].

$$\alpha(I) = \frac{\alpha_0}{1 + \left(\frac{I}{I_s}\right)} \dots\dots\dots (2.38)$$

Where I_s: Saturation Intensity.

2.3.1.2.4 Reverse Saturable Absorption (RSA)

Reverse Saturable Absorption (RSA) can be experiential in a method that absorbs additional in the excited state than in the ground state. If the cross section for the absorption from the ground and the excited states are in that order ($\sigma_{1)}$ and (σ_2), the material develops more transparent when ($\sigma_2 > \sigma_1$) . This is because the population change between the ground and the excited states reductions when the system absorbs light, the total absorption rises [94]. These materials are known as Reverse Saturable Absorbers (RSA) as shown in Fig. (2.5). The simplest electronic system possessing (RSA) has three vibronecally broadened electronic energy levels. In contrast to (TPA and RSA) cannot cause an ideal optical limiting (OL), i.e. zero transmittance at high intensities. The minimum transmittance that can be attained by RSA mechanism is $T_{RSA} = (T_0)^{\sigma 2/\sigma 1}$ which revealed by [95] where T_0: is the linear transmittance.

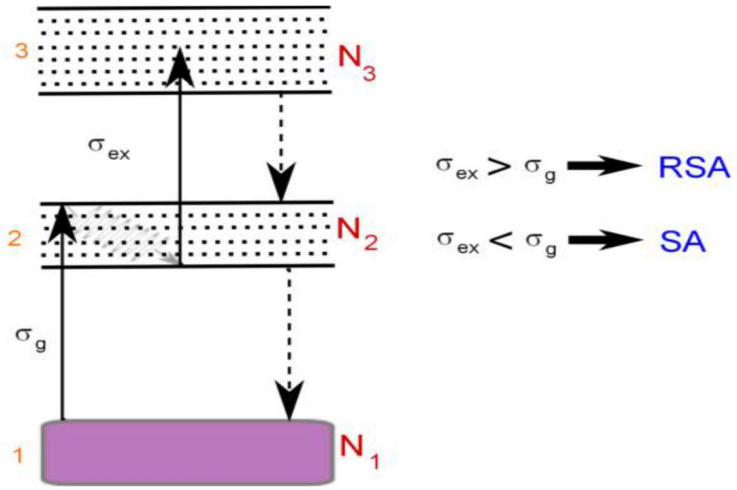

Fig. (2.5): Reverse Saturable Absorption (RSA) schematic energy level diagram [85].

2.3.1.2.5 Free-carrier Absorption (FCA)

One-photon or two-photon exciting in semiconductors can generate carriers. By absorbing additional photons, the electron/hole pairs can be excited to states higher/lower in the conduction/valence band. 'Free-carrier Absorption' the process named, and it is similar to ESA in molecular system [96]. There are four possible processes in a free carrier absorption (FCA) medium, linear absorption (LA), Two-photon Absorption (TPA), One-photon induced free carrier absorption (FCA) and Two-photon induced free carriers absorption (FCA). For the simplest case, the linearly excited One-photon induced free carrier absorption (FCA) in Fig. (2.6) can be described by the propagation equation in the following form [97]:

$$dI/dz = -(\alpha + \sigma_{FCA}N)I \quad \ldots\ldots\ldots (2.39)$$

Where α: is linear absorption coefficient, σ_{FCA}: The total (electron-hole) cross section, N: The number of (electron-hole) pairs which is given by:

$$dN/dt = \frac{\alpha I}{h\nu} \text{ ..... (2.40)}$$

By the approximation solution for propagation equation, get [95]:

$$T = T_0 / [1 + (1 - T_0)(F_0 \sigma_{FCA} / 4h\nu)] \text{ ..... (2.41)}$$

Where T_0 : Linear transmission. When the fluence of the peak incident increase, the total transmission (T) decrease resulting an optical limiting effect (OL) [98].

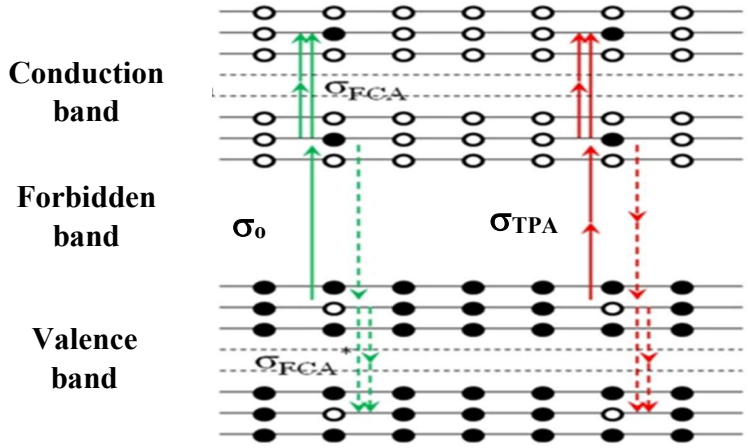

Fig. (2.6): Free-carrier absorption in semiconductor [97]

2.3.1.2.6 Light Scattering

The processes of light scattering of the important processes in the field of photonics. They are of three forms, namely Rayleigh, Raman, and Brillion Scattering, as shown in Fig. (2.7). Rayleigh scattering is the process by which a material changes the direction of an incident photon. It includes an elastic interaction (energy conservation), such that the scattered photon has the same energy as the incident photon, as shown in Fig. (2.7 a). Rayleigh scattering occurs in gases, liquids, and solids. It was generated by changing in the medium such as inhomogeneous random refractive index in the glass causing an attenuation of the intensity of the light transmitted through it [99]. As for Raman scattering, it is carried out by a photon of energy hν_1, after interaction with matter, it appears either at a lower energy ($h\nu_s = h\nu_1 - h\nu_R$) (Stokes-Scattering), or at a higher energy ($h\nu_A = h\nu_1 + h\nu_R$) (Anti-Stokes Scattering), as shown in Figure (2.7 b and c) [100]. Raman scattering occurs in gases, liquids, and solids. Unlike Rayleigh scattering, Raman scattering is inelastic in that a change in the photon's frequency is induced by an energy exchange ($h\nu_R$) with the rotational and/or vibrational position of the molecule. In Stokes-Scattering, the photon gives energy to the material system while the opposite occurs in Anti-Stokes Scattering. Thus, the spectrum of light scattered from the material generally contains a Rayleigh scattering component [101]. As for “Brillouin-Scattering”, it is similar to Raman scattering, but the vibrations are acoustic instead of molecular vibrations as shown in Figure (2.7 d) [102].

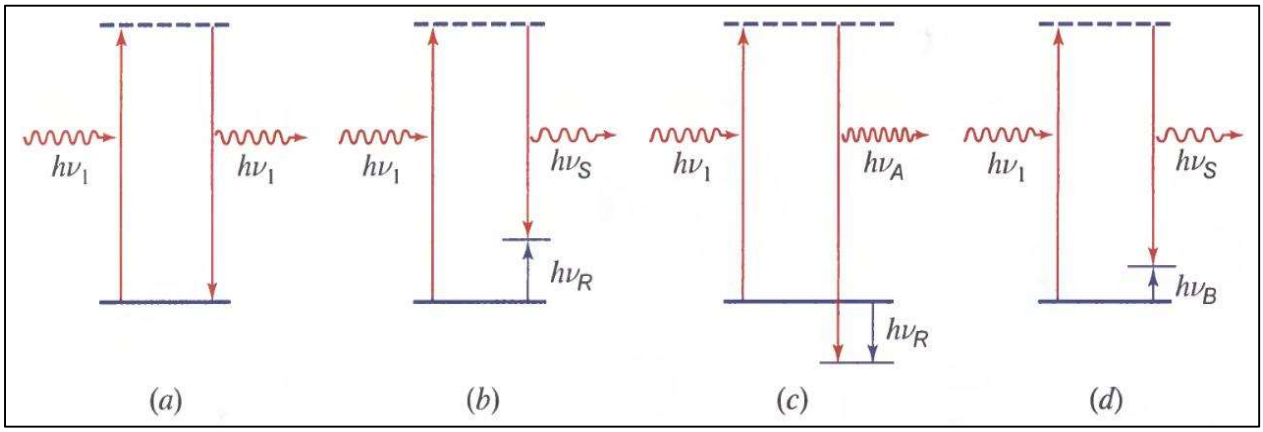

Fig. (2.7): Light scattering, a: Rayleigh-Scattering, b: Raman Stokes-Scattering, c: Raman Anti-Stokes Scattering, d: Brillouin-Scattering [100]

2.3.2 Measuring Techniques for $\chi^{(3)}$ Nonlinearity

For characterizing and determining the applicability of any material as a nonlinear optical device, the magnitude and response of third-order nonlinear susceptibility are important parameters. The techniques for measuring these parameters include [103-106]:

- Z-scan (For measuring of sign and magnitude of third-order nonlinearity).
- Degenerate Four Wave Mixing DFWM (for measuring of both magnitude and response time of the third-order nonlinearity).
- Third Harmonic Generation (THG) (for measurement of magnitude of third-order nonlinearity only).

- Time-resolved Optical Kerr Effect and Transient Absorption Techniques (for the study of photon-physical processes determining the nonlinearity).
- Time Correlated Single Photon Counting (TCSPS) (to measure the radiative lifetimes) [107].

In this study, the Z-Scan technique used, and we will discuss in details.

2.3.2.1 The Z-Scan technique

The Z-scan technology is certainly a popular and reliable method for characterizing third- and high-order nonlinear processes. Mansour Sheikh Baha et al. [70 & 108] described the basic Z-Scan technology in 1989 when the FWM (Four Wave Mixing) technology was replaced by. It was the main technique used to describe third-order processes in optical materials. Several updates and improvements to the original technology have been implemented since 1990 taking into account the geometric and optical parameters such as the shape of the laser beam [109].

Using Z-Scan technology to measure and characterize nonlinear optical materials due to its accuracy and simplicity. This method has become widely used to study the optical properties of non-linear refractive and non-linear absorption [109 & 110]. Its working principle is that the model is scanned longitudinally through the focal region of a focused Gaussian beam (TEM_{00}) [111] where the passage of the laser beam through a nonlinear medium will change its intensity as the model moves along the (Z) axis. This is because the model experiences different laser intensities that depend on the position (Z) relative to the focus (z = 0). The method

is done by calculating the transmittance through the model as a function of the position (z) of the model. There are two systems of optical scanning methods, the first is a closed-aperture system for detecting nonlinear refraction (n_2) and an open-aperture system for detecting nonlinear absorption (β) [110, 112]. Fig. (2.8) shows a schematic diagram of the Z-scan setup.

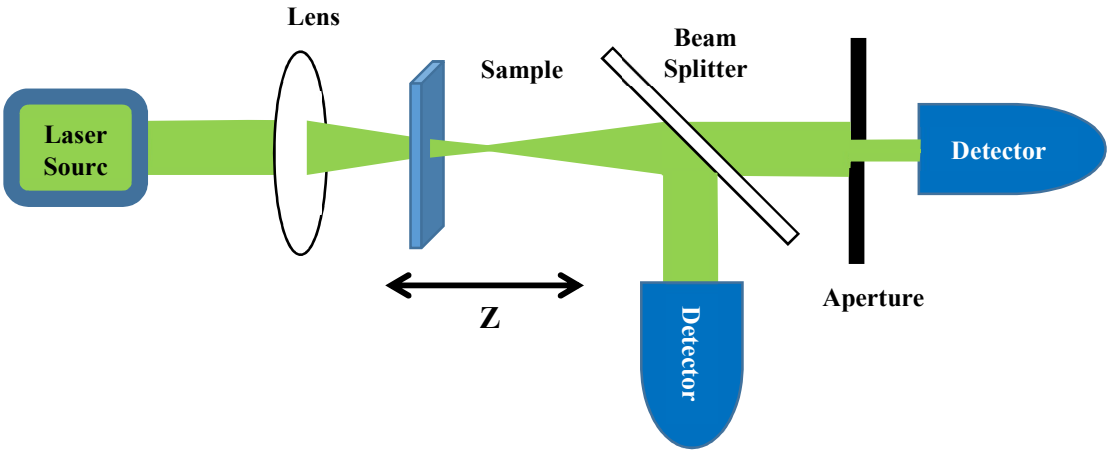

Fig. (2.8): Diagram of Z-scan setup

Z-Scan Closed Aperture System

When the sample is placed across the focal area of the beam and an aperture is placed in front of the detector as shown in Fig. (2.8), the detector measures the intensity that passes through the aperture that is transmitted through the sample. The intensity of the laser beam falling on the detector will vary due to the Kerr-lens generated in the material by the intensity of the laser beam [113]. To show how the transmittance of the Z-Scan as a function of (Z) is related to the nonlinear refraction of the sample if there is a medium with a negative nonlinear refractive index and a

thickness smaller than the diffraction length of the focused beam it can be considered as a thin lens with variable focal length.

At the far field (Z<<0) the beam strength is low and the nonlinear refraction is negligible. In this case the measured transmittance remains constant (i.e. independent of Z). As the sample approaches the focus, the intensity of the laser beam increases, resulting in the formation of self-lens in the sample. A negative subjective lens before the focus of the beam tends to collect the beam on the aperture in the far field increasing the transmittance measured after the focus. Out of focus (Z > 0) again the refraction is slightly nonlinear resulting in transmittance independent of Z. The maximum transmittance (peak) followed by the minimum transmittance (bottom) is evidence of a negative value of nonlinear transmittance (negative refractive index). Whereas the Z-scanning curve (i.e. bottom followed by a top) characterizes the nonlinear transmittance, (the material has a positive nonlinear refractive index). Fig. (2.9), shows the nonlinear transmittance represented by the positive and negative nonlinear refractive index [114].

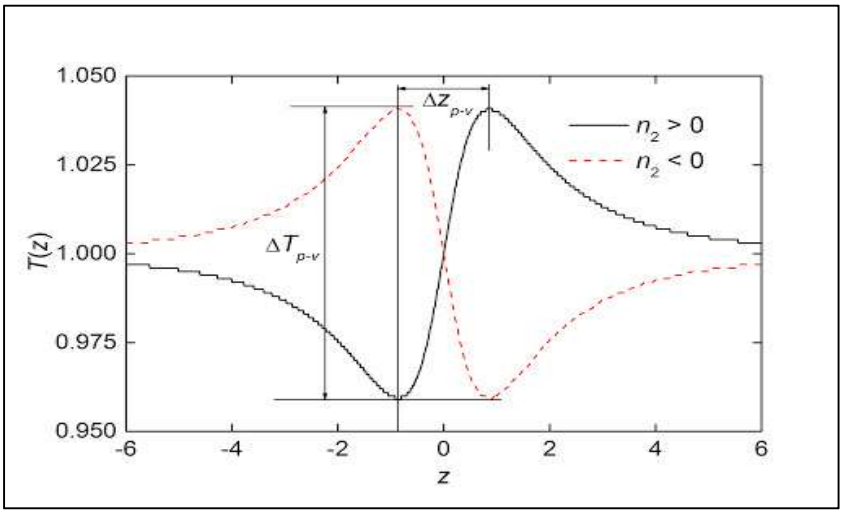

Fig. (2.9): Z-scanning technique for positive nonlinear refraction (black line) and the negative (red line) [115]

The nonlinear refractive index (n_2) of the top-to-bottom difference for normal transmittance is calculated (experimentally) with the following formula [116 & 117]:

$$n_2 = \frac{\Delta\emptyset_0}{(I_0\, L_{eff} K)} \text{ ..... (2.42)}$$

Where, I_0: Incident light intensity, $K = 2\pi/\lambda$ (K: Wave number and λ: Wave length of the beam), $\Delta\emptyset_0$: Nonlinear phase shift of the top on the axis at focus when:

$$\Delta T_{p-v} = 0.406\ (1 - S)^{0.25}\ |\Delta\Phi_o| \text{ ... ... (2.43)}$$

Where, ΔT_{p-v}: The change in the normal transmittance between the top and the bottom is equal to: $|T_p - T_v|$ [116 &118].

$$S = 1 - exp\left(\frac{-2\,r_a^2}{w_a^2}\right) \ldots\ldots\ldots (2.44)$$

Where, S: Linear transmittance of the aperture, r_a^2 : Square of aperture radius and w_a^2: Square of laser beam radius at the aperture [119]. The effective length of the sample can be determined by the following relationship [110]:

$$L_{eff} = \frac{(1 - e^{-\alpha_0 L})}{\alpha_0} \ldots\ldots\ldots (2.45)$$

Where, L: Length of sample. To calculate the intensity at the focus point, it can used the formula [116]:

$$I_0 = \frac{2\,P_{peak}}{\pi\,\omega_0^2} \ldots\ldots\ldots (2.46)$$

Where, P: Power of laser beam, ω_0^2: Square of laser beam radius at the focus point.

Z-Scan Open Aperture System

When the sample is placed across the focus area of the beam. The detector calculates the total window intensity as shown in Fig. (2.8). In this case excluding the aperture. The optical scan insensitive to nonlinear refraction so by the transmittance graph against the sample position for such a Z-scan. For the open-aperture it must be symmetrical about the focus because the distribution of the Gaussian beam density is symmetrical around the focus. When the nonlinear absorption is very small it can be neglected due to the low excitation power. So as in equation (2.37) and (2.38) will be re-examined when the excitation power is sufficient. To show the nonlinear properties, replace the following:

$$\alpha\,(I) = \alpha + \beta I \ldots\ldots\ldots (2.47)$$

$$\frac{d\Delta\phi(r,t,z,L)}{dz} = \Delta n(I)k \ldots\ldots\ldots (2.48)$$

Where Δn: Change in refractive index. Solutions of these differential equations produce the intensity and phase shift distribution of the laser beam at the sample output as follows [120]:

$$I_e\,(z,r,t) = \frac{I\,(z,r,t)\,e^{-\alpha L}}{1+q\,(z,r,t)} \ldots\ldots\ldots (2.49)$$

$$\Delta\phi\,(z,r,t) = \frac{k\gamma}{\beta} ln[1+q\,(z,r,t)] \ldots\ldots\ldots (2.50)$$

Where, $q\,(z,r,t) = L_{eff}/(1+\frac{z^2}{z_o^2})$. By using these equations (2.49) and (2.50), the complex electric field at the output of the sample is as follows:

$$E_e = E(z,r,t)e^{-\alpha L/2}\,(1+q)^{(\frac{ik\gamma}{\beta}-\frac{1}{2})} \ldots\ldots\ldots (2.51)$$

When no linear absorption (TPA) occurs, the equation is as follows [121]:

$$E_e = E(z,r,t)e^{-\alpha L/2}\,e^{i\Delta\phi\,(r,z,t)} \ldots\ldots\ldots (2.52)$$

The normal optical transmittance (T(z)) can be calculated from [121]:

$$T_{(z)} = \frac{\int_{-\infty}^{\infty} P_T\big(\Delta\phi_0(t)\big)dt}{S\int_{-\infty}^{\infty} P_i(t)dt} \ldots\ldots\ldots (2.53)$$

Where P_T: Power transmittance through the aperture. With the aperture removed, the Z-Scan transmittance becomes insensitive to nonlinear refraction and therefore

is just a function of nonlinear absorption. Thus, equation (2.49) can be integrated in the absence of the aperture (S=1) without the need to include the free space scattering process at (z) with respect to (r), we get the average transmittance of the power:

$$P(z,t) = P_i(t)\, e^{-\alpha L}\, \frac{ln[1 + q_0(z,t)]}{q_0(z,t)} \dots\dots\dots (2.54)$$

$$q_0(z) = \frac{\beta I_0 L_{eff}}{1 + \frac{z^2}{z_0^2}} \dots\dots\dots (2.55)$$

Where, $P_i(t)$: Instantaneous input power (inside the sample). From the definition of ($P_i(t)$) as in equation (2.53), assuming the presence of a Gaussian pulse, equation (2.54) can be combined with time to give us the natural energy permeability [121]:

$$T(z) = \frac{1}{\sqrt{\pi} q_0(z)} \int_{-\infty}^{\infty} ln\left[1 + q_0(z) e^{-r^2}\right] dT \dots\dots\dots (2.56)$$

When ($|q_0| < 1$) the transmittance function can be rewritten more appropriately for numerical analysis i.e.:

$$T(z) = \sum_{m=0}^{\infty} \frac{[-q_0(z)]^m}{(m+1)^{3/2}} \dots\dots\dots (2.57)$$

Thus once the optical scanning with an open aperture (S = 1) is performed, the nonlinear absorption coefficient can be deduced unambiguously and with the knowledge of (β) the Z scanning with the aperture in place (S < 1) can be used to extract the remaining unknown, i.e. the modulus (γ).

When moving the sample from the region in which the intensity is low (-Z) from the near field to the other end the far field (+Z) through the focus of the beam (Z = 0). The intensity of the laser beam is high and sufficient to show nonlinear properties and as a result of changing the intensity can be one of the two effects is either saturated absorption (SA) or reverse saturable absorption (RSA). We notice from Figure (2.10) that when the absorption curve is as high as possible at the position (Z = 0), the material has a saturated absorption (SA) as shown in Figure (2.10 a), but when the absorption is minimal in the (Z = 0) region. (Z = 0) The material has saturated reverse absorption (RSA) as shown in Figure (2.10 b) [70]. The nonlinear absorption coefficients can be easily calculated from the transmittance curves [113]:

$$\beta \left(\frac{cm}{W}\right) = \frac{2\sqrt{2}}{I_0 L_{eff}} \Delta T \ldots\ldots\ldots (2.58)$$

Where, (ΔT) is the single peak or bottom of the open-scan Z-scan curve.

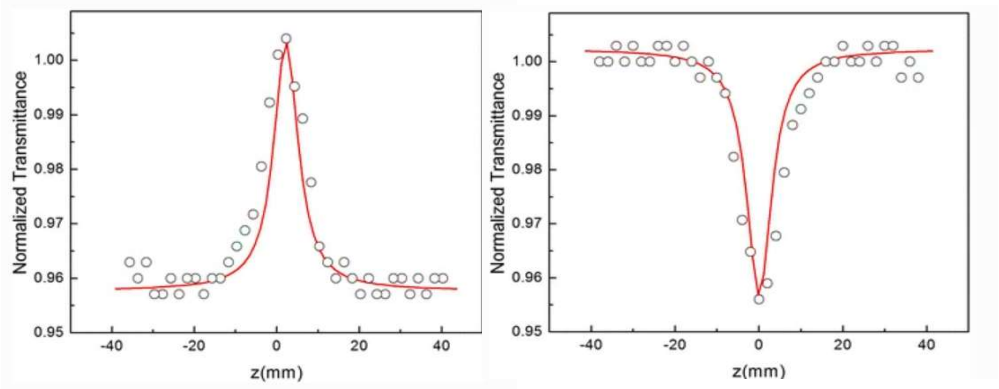

Fig. (2.10): The scanning technique on the open aperture Z-Scan, a: saturated absorption (SA) and b: reverse saturable absorption (RSA) [119]

2.4 Optical Limiting (OL) Concepts

The ideal optical limiter (OL), the transmittance begins to change in a linear with the transmitted power through it. Then the transmittance changes suddenly at an intensity of a certain value known as the critical intensity or the threshold limit, as the optical limiter shows at those critical areas or the threshold its independence on the intensity and fixed the transmittance intensity for a limit and definite amount despite the increased intensity. Fig. (2.11) Illustrates this.

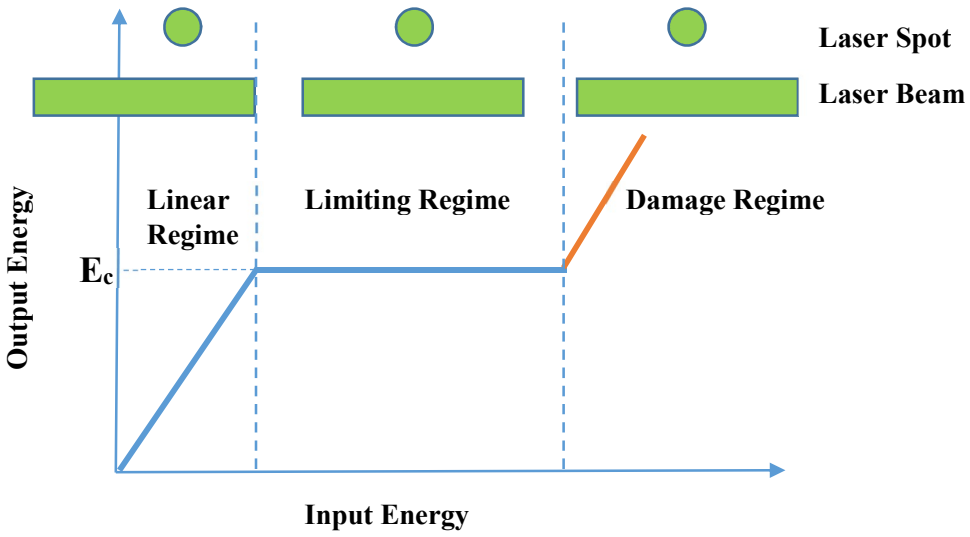

Fig. (2.11): The behavior of an ideal optical limiter schematic [12]

If the severity of the limiter fixed at a certain amount is less than the intensity causing its damage, then the limiter is an important protective device. The limiting threshold of the material is defined as the input intensity/fluence passing through the material, which leads to reduce the transmittance through the material to 50% of

its linear transmittance [12]. "Clamping threshold" of the material is defined, as the point at which the transmittance begins to remain constant to the input intensity/fluence passing through the optical limiter. The optical limiter can work for a certain range, which may be wide for the input intensity/energy values passing through it, but for a certain limit the limiter may collapse. Therefore, a suitable optical limiter need to be selected for the intensity to be limited. The value of the input intensity/energy that causes damage is known, the damage threshold. The ratio between the damage threshold and the limiting threshold of the optical limiter is called its dynamic range [12]. A good optical limiter has the following characteristics [123]:

1- Large dynamic range and low limiting threshold.

2- Sensitive response to broadband.

3- Fast response time.

4- High linear transmittance, ease of carrying, resistance to breakage, and resistance to atmospheric influences.

The processes that lead to optical limiting are:

1- Nonlinear refraction effecting (self- focusing, self-defocusing, induced aberration, induced scattering, induced refraction, etc.) [123].
2- Nonlinear absorption {(ESA), (RSA), (FCA), (TPA) and (MPA)}. The mechanism, which leads to optical limiting, classified in to two mechanisms. First is energy spreading, second, is energy absorption [123]. The block diagram in Fig. (2.12) illustrates this mechanism.

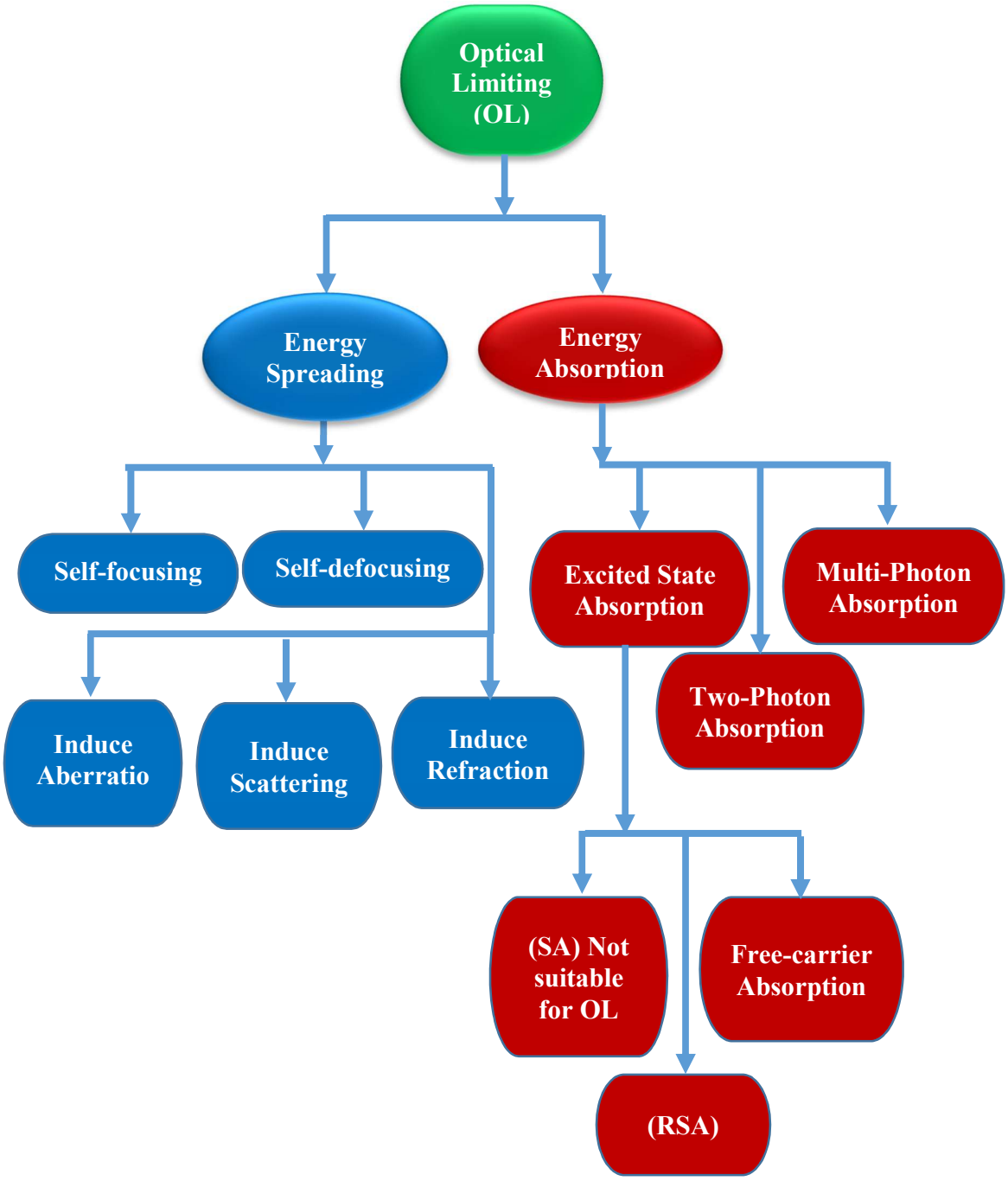

Fig. (2.12): The mechanisms responsible for optical limiting (OL) [123]

2.4.1 Energy Absorption Type of Optical Limiter

Nonlinear absorption is one of the mechanisms that plays an important role in optical limiting. The optical limiting is based on the fact that the transmittance of the nonlinear medium decreases with the increase in the intensity of the laser entering the medium. At high intensities to cause nonlinear changes, the probability of the substance being absorbed by one of the nonlinear absorption methods mentioned in paragraph (**2.3.1.2**) will increase. An optical limiting device that works by a mechanism based on nonlinear absorption is called an energy-absorption type.

2.4.2 Energy Spreading Type of Optical Limiter

The process of placing a hole or aperture in front of the detector directed towards the laser is considered the key to the process of energy spreading. The process of limiting the exposed laser beam is based on the change in the spatial distribution of the energy of the transmitted beam. The large refraction of the incident laser beam will propagate in a solid angle range when the intensity/fluence of the entering laser increases due to passing through the hole or aperture. The diameter of the hole or aperture has a significant impact on this process. It can be said that the optical limiter here will not depend on the intensity of the incident laser rays only, but on the diameter of the hole or aperture and on the geometrical configuration of the system. For most materials that work with the principle of energy spreading, the principle of heat inducing a change in the refractive index is the main actor. Fig. (2.13) shows the effects that work in materials that work on the principle of energy spreading.

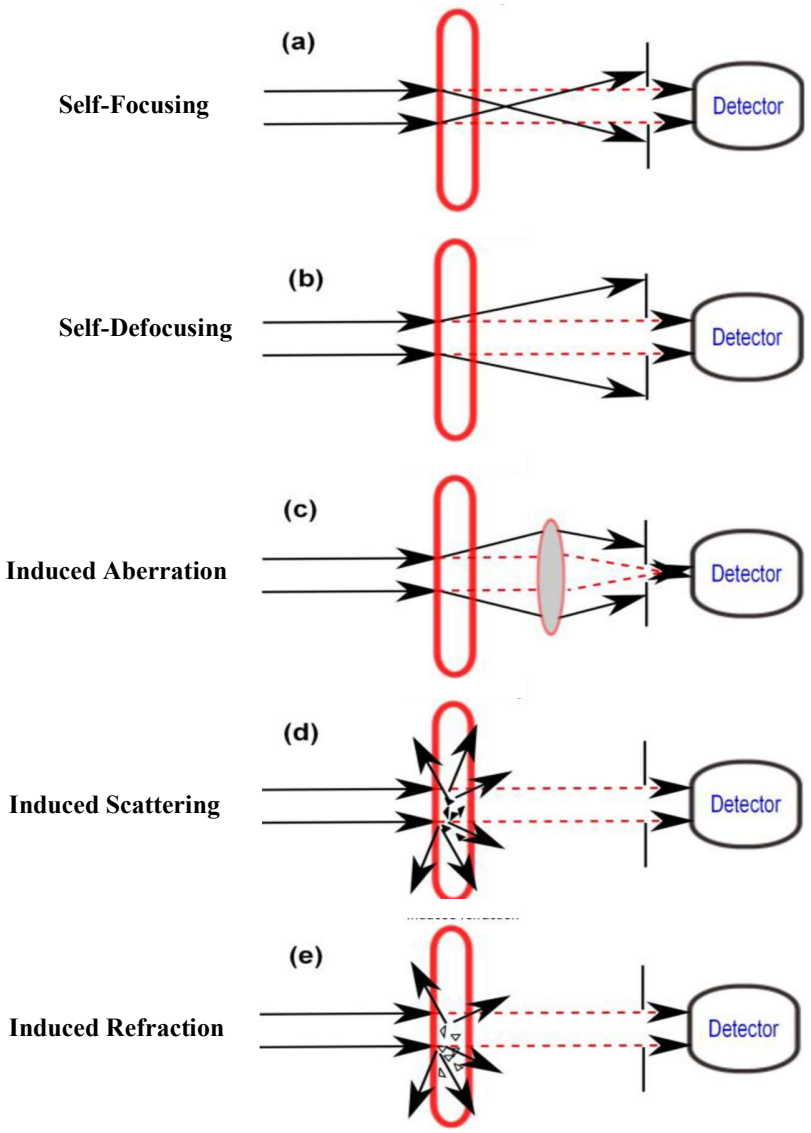

Fig. (2.13): Optical limiter of energy spreading type [85]

In Fig. (2.13 a and b), the detected energy will be greatly reduced due to its diffusion through the hole. Fig. (2.13 c) indicates the diffraction of the light where the induction of a variable refractive index occurs as a function of the local distri-

bution of the intensity of the laser beam within the nonlinear medium passing through it. Because of the non-uniform local change, random refractive indexes will be produced at high intensity sites that lead to aberration [85 & 95]. Fig. (2.13 d and e) shows, an optical limiting based on the fact that, high laser intensity induces scattering and refraction. In the case of inducing scattering, the limiting medium is a random distribution system of linear absorption particles in a transparent host that changes by a principle arising from negligible light absorption. Therefore, at high intensity, the absorption induces heat of the center and the medium becomes very heterogeneous, leading to the small part of the energy passing through the hole and the spreading of the greater part of it to a wider spatial scale [124].

In the case of refraction induction, the medium is composed of two microscopic components with the same refractive index static but different in phase (a mixture of liquid and solid). If one of these components is transparent and the other absorbs the incident laser beam, the selective heating is able to make the system heterogeneous at the boundaries between the two components [107].

All these mechanisms lead to a slow temporal response, but the change of refractive index caused by the thermal optical effect is important for the optical limit. The impurities or particles in this case, even if they cause only a small linear absorption and a non-resonant absorption, but this small absorption is sufficient to cause thermal changes that induce a refractive index at the high intensity of the input laser. Even at not high intensities of the input laser, the inductance of a variable refractive index is important for a medium with linear and resonant absorption.

Chapter 3

Experimental Part

CHAPTER 3 Experimental Part

3.1 Introduction

In this chapter, provide a complete description of the sample preparation process and the steps for measuring linear, morphological and nonlinear optical properties of them. Review the devices used in the examination. A description of the setup of the experiments that were used in the preparation or that were used to examine the nonlinear properties of the oil-scan system.

3.2 Outline of the Experimental Part

The block diagram in Fig. (3.1) illustrates the steps that will be emphasized in our experimental work to produce optical determinants. It includes the process of obtaining the nanomaterials that were used in this work and then the process of preparing samples for the Nano suspensions, then the linear optical properties, morphological and the nonlinear optical properties of these suspensions are measured and examined. Where this diagram will help to understand the work steps that were followed in this thesis, starting from preparing the materials to the last examination of the samples to obtain the results by tracing its steps.

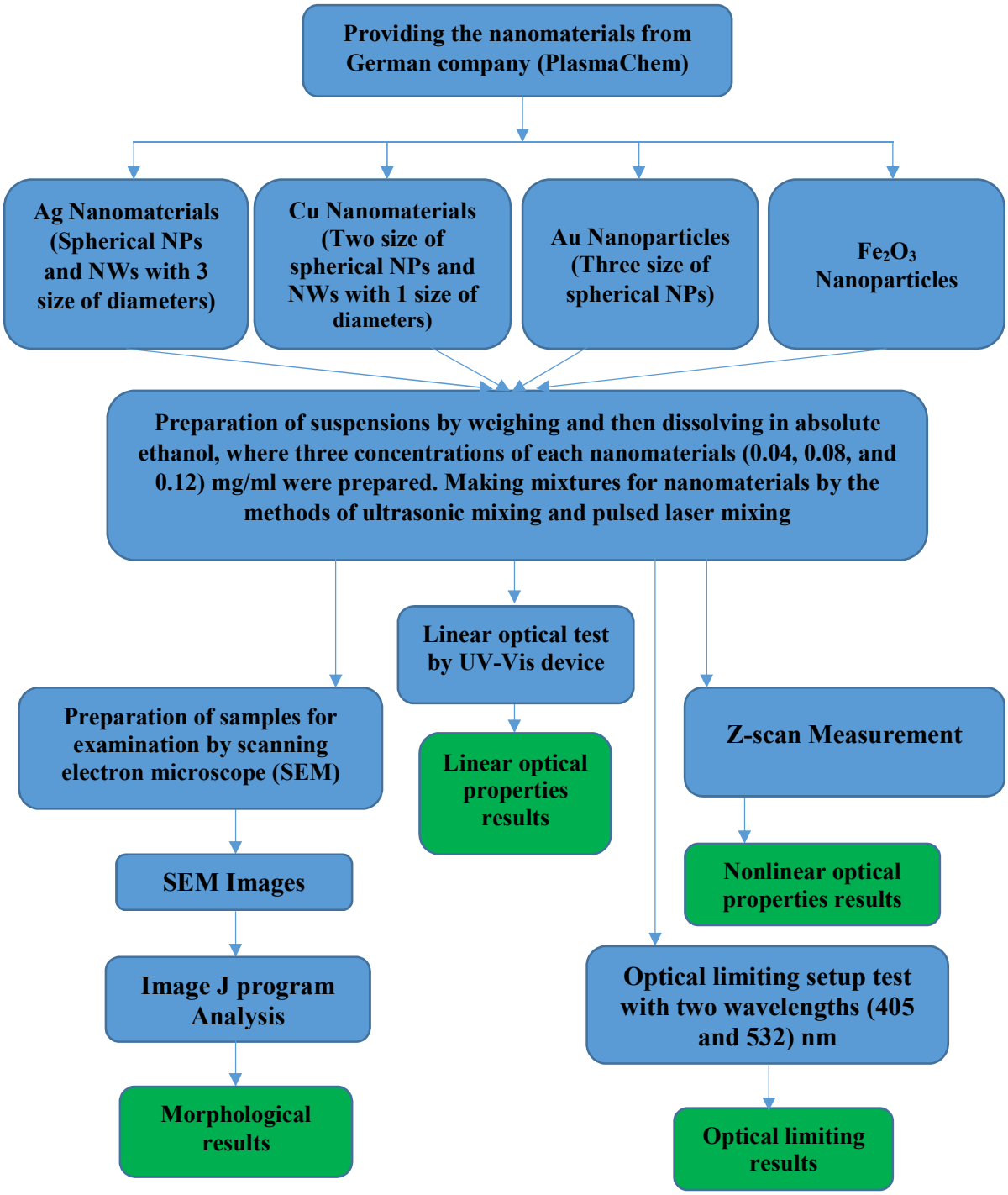

Fig. (3.1) Flow chart of the experimental part in this project

3.3 Providing nanomaterials

The nanomaterials used in this project were purchased from the German company (PlasmaChem) in the form of glass containers for the materials. The materials were in the form of powders, except for iron oxide (Fe_2O_3), which was prepared in the form of an aqueous suspension, and all of these materials were hydrophilic except for gold, which was hydrophobic. The materials are:

1- Spherical gold nanoparticles (Au NPs) of three sizes (2, 4 and 6) nm then became (4, 6 and 8) nm. They were named as (Au1, Au2 and Au3) respectively.

2- Spherical silver nanoparticles (Ag NPs) with a size of (6-7) nm, then became (70) nm.

3- Silver nanowires (Ag NWs) of three different diameters (50, 100 and 200) nm and have the same length, ($5 < length < 50$) microns. They were named as (Ag NWs D50, Ag NWs D100 and Ag NWs D200) respectively, where latter (D) refers to diameter.

4- Spherical copper nanoparticles (Cu NPs). It was supplied in two sizes, the first (20) nm then became (50) nm and the second (less than 100) nm. They were named as (Cu1 and Cu2) respectively.

5- Copper nanowires (Cu NWs) with a diameter of (50) nanometers and a length greater than 5 microns and less than 50 microns. It was named as (Cu NWs D50).

6- Iron oxide spherical nanoparticles (Fe_2O_3), a 5% aqueous suspension, with a size of (8) nm, then became (65) nm with Nano fragments shape. It was named as (Fe_2O_3 Nano fragments).

3.4 Host Liquid (Absolute Ethanol)

It is also called ethyl alcohol, an organic chemical compound with the chemical formula (C_2H_6O), a volatile, flammable, colorless liquid with a slight characteristic odor. Ethanol is naturally produced by fermenting sugars by yeasts or by petrochemical processes such as hydration of ethylene. It has medicinal applications as a disinfectant and disinfectant. It is used as a polar chemical solvent and as used in the synthesis of organic compounds. Ethanol is a versatile solvent, miscible with water and with many organic solvents [125], the physical properties of ethanol mainly stem from the presence of its hydroxyl group and the shortness of its carbon chain. The hydroxyl group in ethanol can participate in hydrogen bonds, making it more viscous and less volatile than less polar organic compounds of similar molecular weight, such as propane. Since ethanol also has a low boiling point, it is easy to remove from the solution that was used to dissolve other compounds [126], it can also participate in hydrogen bonds because it has O-H bonds, as in Table (3.1).

Table (3.1): Specification and molecular structure of ethanol [126]

Molecular structure of ethanol	Bipolar Moment	Polarity (Dielectric Constant)	Boiling Degree C^0	Molecular Density gm/cm^3	Molecular Weight gm/mol
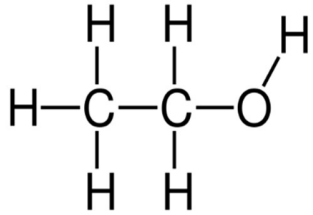	1.65	25	80	0.78945	46.07

3.5 Preparation of Samples

The first step: From each material and for each size according to the materials and their sizes mentioned in paragraph (3.4), the following weights (0.4, 0.8 and 1.2) mg were weighed by a sensitive electronic scale with four digits after the comma. Each of these weights was placed in a glass bottle marked with its name and weight.

Second step: (10) ml of absolute ethanol was added to each glass bottle. Thus, the concentration of the packages according to the weights becomes (0.04, 0.08 and 0.12) mg/ml.

The third step: A (125 W) sonication probe device (UP-VCX130PB) mixed the contents of each package.

Thus, we have (33) samples, each size of samples have three concentrations, distributed as follows:

1- (Au NPs) **Nine** samples. three concentrations for each size (Au1, Au2 and Au3).

2- (Ag NPs) **Three** samples.

3- (Ag NWs) **Nine** samples. Three concentrations for each size (Ag NWs D50, Ag NWs D100 and Ag NWs D200).

4- (Cu NPs) **Six** samples. Three concentrations for each size (Cu1 and Cu2).

5- (Cu NWs D50) **Three** samples.

6- (Fe_2O_3 Nano fragments) **Three** samples. A procedure preceded the process of preparing iron oxide samples in the aforementioned method, where this material was received in the form of an aqueous suspension. To get rid of the water, a sample of this aqueous suspension was taken and dried at room temperature. The drying

resulted in a chips of iron oxide. The required weight was taken from this chips and placed in absolute ethanol and using the ultrasonic probe to prepared the three weight ratios of samples. Fig. (3.2) illustrate the steps of preparation of samples.

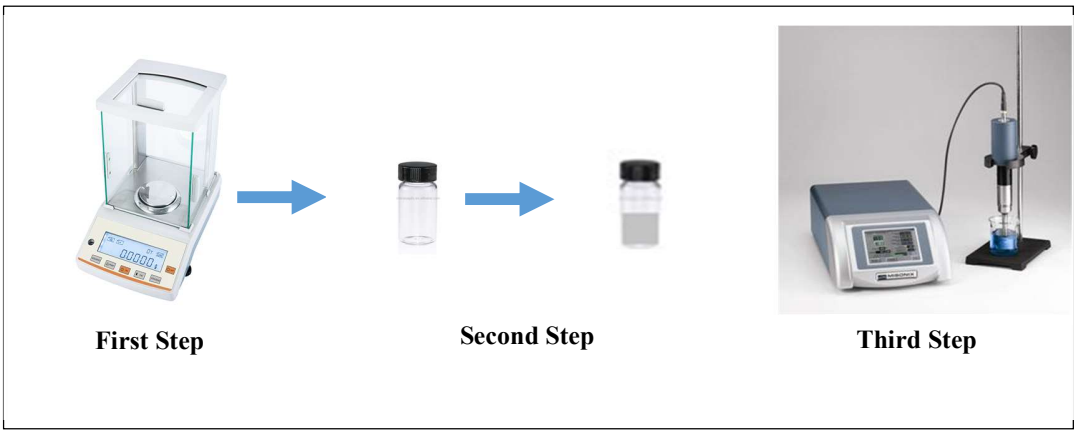

Fig. (3.2): Illustration the steps of preparation of samples

3.6 Preparation of Mixtures Samples

Through the scientific literature on the topic of nanomaterials, the follower of them finds that the methods followed for the synthesis of two nanomaterials are mostly chemical or using the pulsed laser ablation method to form core-shell structures [127]. Since the composite of a nanomaterial with another or decorating and coating a nanomaterial with another produces a composition that differs in its physical and optical properties from the original nanomaterials [128]. In order to obtain structures that improve the performance of the optical-limiting compared to a single material and the synthesis of its different working mechanisms, led us to think about making mixtures of some the materials we prepared. The mixing process was done by two simple physical methods showed important results that may lead to a new line in the matter of superimposing or decorating nanomaterials.

3.6.1 Preparation of (Cu2+Ag NWs D200) and (Ag NPs + Cu NWs D50)

In this mixture, one volume of concentration (0.12) mg/ml of (**Cu2**) was taken and added to one volume (1:1) at the same concentration of (**Ag NWs D200**) and mixed using an ultrasound probe with a power of (15) watts for a period of twenty minutes with placing the mixing vial in a beaker of groats. ice for cooling. The same method was followed with the second mixture, for the same volumes and concentrations

3.6.2 Preparation of (Ag NPs + Fe_2O_3 Nano fragments) and (Cu1+Fe_2O_3 Nano fragments)

In this mixture, one volume of concentration (0.12) mg/ml of (**Ag NPs**) was taken and added to three volume (1:3) at the same concentration of (**Fe_2O_3 Nano fragments**). The mixing process was carried out using two methods. First one by using an ultrasound probe with a power of (15) watts for a period of thirty minutes with placing the mixing vial in a beaker of groats ice for cooling. The second method is by using pulse laser (Nd:YAG Pulses Laser (SHG) (532) nm with (100) pulses, (300) mJ). The laser beams were shed laterally on the vial of the mixture with a convex lens (focal length=10) cm to focus the laser beams so that the focus is in the center of the mixture. A magnet was placed inside it for the purpose of continuous movement when exposed to laser pulses. The same methods were followed with the fourth mixture, for the same volumes and concentrations. Fig. (3.3) shows the setup of the devices for the second method. We summarize the above in the process of preparing mixtures in Table (3.2).

Table (3.2): Preparations of mixtures samples

Materials of Mixtures	Ratios of volumes mixing	Concentration of each materials (mg/ml)	Mixing methods
Cu2+Ag NWs D200	1:1	0.12 & 0.12	Sonication Probe
Ag NPs + Cu NWs D50	1:1	0.12 & 0.12	Sonication Probe
Ag NPs + Fe2O3 Nano fragments	1:3	0.12 & 0.12	Sonication Probe & Pulse laser
Cu1 + Fe2O3 Nano fragments	1:3	0.12 & 0.12	Sonication Probe & Pulse laser

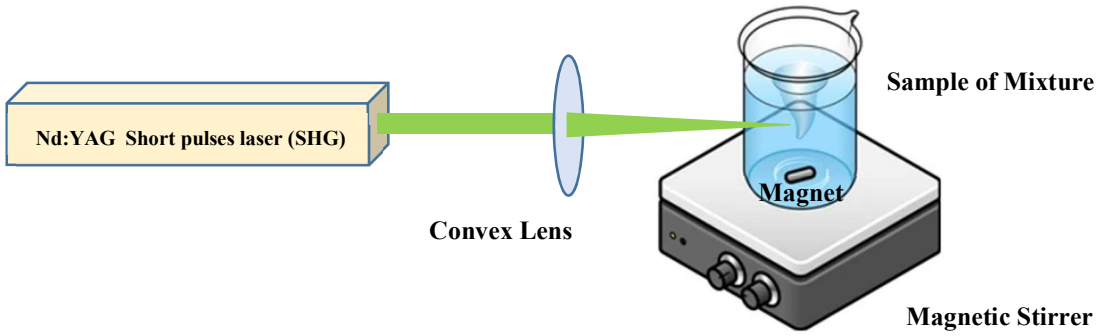

Fig. (3.3): The setup of the devices for the pulsed laser method of preparation of mixtures

3.7 Linear optical properties Measurements and preparations Samples for SEM

By using a UV-Vis spectrophotometer device (CECIL 7200 AQUARIUS) as in Fig (3.4), linear absorbance were measured for all prepared samples and for all concentrations within the spectral range (190-900) nm in the advance laboratory in college of science for women in University of Babylon . Each sample loaded with (1) cm thick quartiz cuvette. The linear absorption coefficient was calculated from the linear absorbance of each material and at the four wavelengths that were used to study the nonlinear optical properties of materials, and its values will be included in the subsequent Tables with the nonlinear refractive index values of the materials.

Fig. (3.4): The UV-Vis spectrophotometer device (CECIL 7200 AQUARIUS)

The linear refractive index of the suspensions of all materials was measured by using an Abbe-Model (RMT) type refractometer as in the Fig (3.5), and its value ranged between (1.357) and (1.359) for all samples. The variance in the values of the linear refractive index of the prepared samples was in the fourth place after the sorter for the value of the refractive index. This discrepancy was neglected because it did not affect the accounts, and only three ranks were adopted after the sorter.

Fig. (3.5): The Abbe-Model (RMT) type refractometer

For examination by scanning electron microscope SEM (FEI Nova NanoSEM 450) as in the Fig (3.6),

Fig. (3.6): The scanning electron microscope SEM (FEI Nova NanoSEM 450)

samples were prepared in the department of physics of college of sciences in University of Basrah. By placing droplets from each sample on a (1) cm^2 highly conductive silicon substrate and sending them all for examination to determine the

morphological properties of the samples and mixtures. SEM images were analyzed with a computer program version (Image J) (1.8.0).

3.8 Z-scan Measurements

To detect the nonlinear optical transmittance, a Z-Scan system was used, the parts of which are shown in Fig. (3.7).

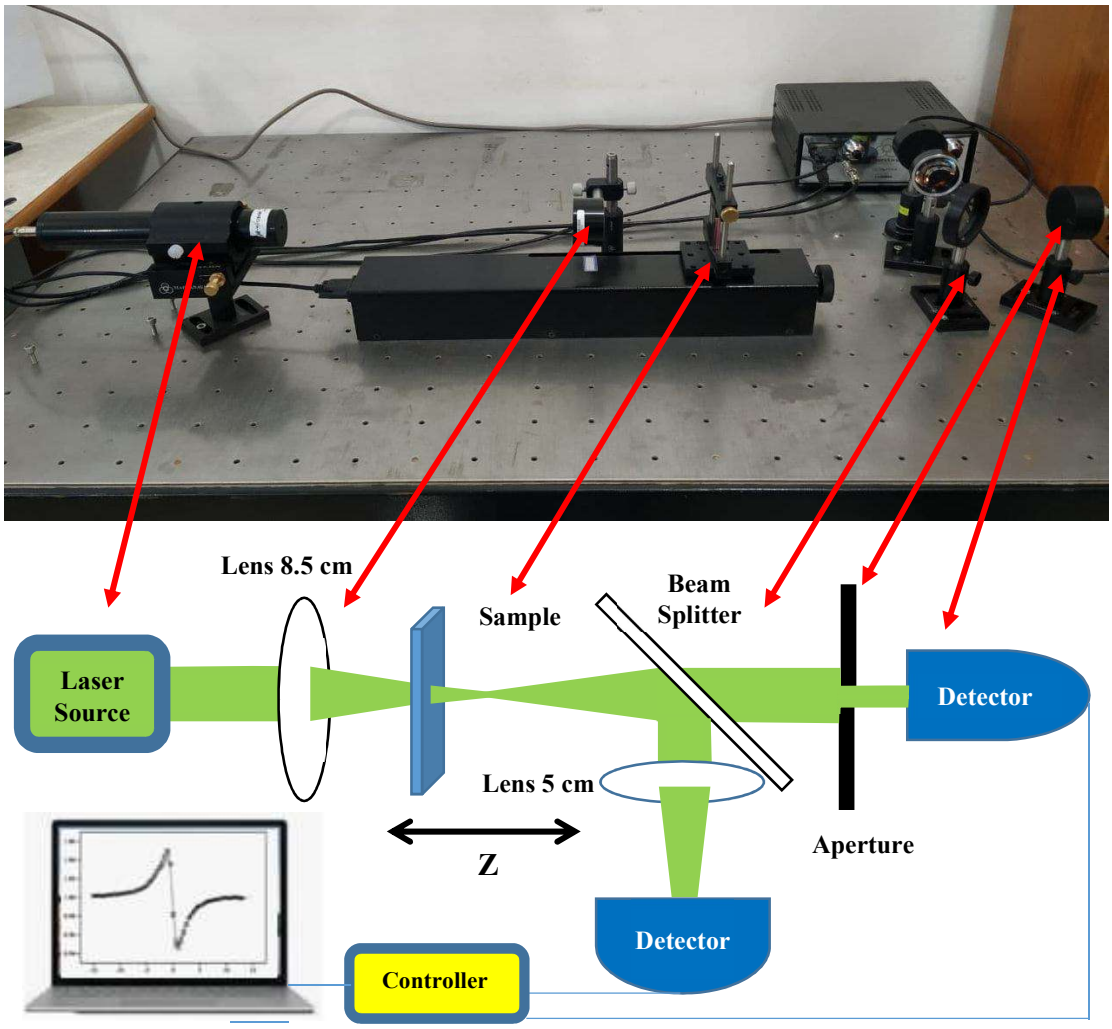

Fig. (3.7) The setup of the Z-scan system

This setup (Z-SCAN-VER-8) is equipped from (MAHFANAVAR) and consists of:

1 - (CW) Lasers with different wavelengths.

2 - Different optical attenuators to control the intensity of the laser beam falling on the sample.

3 - Optical lenses with different focal lengths (5, 8.5 cm). A convex lens with a focal length of (8.5) cm was used.

4 - Laser beam splitter (50:50) to split the beam between the detectors.

5- Motorized sample holder. The movement of the holder controlled it by controller and the step between each reader is (0.15) micron. Each sample loaded with (1) mm thick quartz cuvette.

6 - The first detector is directly beyond the beam bisector and its aperture diameter is (1) mm to detect nonlinear refraction, and a post-mid beam detector is to detect nonlinear absorption.

7 - A lens before the nonlinear absorption detector to collect the equilibrated laser beam on it. A convex lens with a focal length of (5) cm was used.

8 - Connecting wires to transmit signals from the detectors to a (Controller) device, and then connected to a (USB) wire to a computer.

9 - The controller device contains two ports to connect to the detectors and a regulator through which we can control increasing or decreasing the sensitivity and gain of the detectors according to the permeability of the sample.

Before starting work, the sample is placed and dragged before and after the focus and through it in order to know the amount of beam amplitude due to the non-linearity of the sample and also to control the increase or decrease of the gain of the laser so that we can obtain the correct nonlinear transmittance. Each model was

calibrated with the power of the laser placed on it, so that the lowest power at which the nonlinear change would occur regularly was chosen.

10- The measurement process was carried out using four semiconductor lasers of different wavelengths (405, 473, 532 and 650) nm. The lasers used are characterized by efficiency and high stability. In general, the shape of the laser beam for these lasers is almost Gaussien.

11- The laser beam diameter for each laser was measured using the beam scanning method and was determined at the level($\frac{1}{e^2}$).

12- The laser power meter used shown in Fig. (3.8) was used to measure the optical power of the laser beam passing through the sample with a range (0-40) mW. From Japanese company (Sanwa) model (mobiken LP1); the power meter device was supplied. This device works within a wide spectral range (400-110) nm with a sensitivity that depends on the wavelength.

Fig. (3.8): The power meter device

3.9 Optical Limiting measurements

Fig. (3.9) shows the setup of the optical limiter system. The laser device, lens, sample, and power meter are aligned with the sample. A power meter for laser beam is placed between the lens and the sample and is movable to measure the power of the laser beam each time it is changed. Two sources of (CW) semiconductor lasers were used. The first wavelength (405) nm and the second wavelength (532) nm. Optical-limiting measurement was carried out for all samples at the two indicated wavelengths. Each time the sample is placed very close to the focus and not completely in focus, in order to avoid focusing the high intensity on the sample, which in turn leads to the collapse of the laser beam. Before starting the measurement with each sample, the position of the power meter is adjusted after the sample to ensure that the laser beam does not depart from its surroundings. Using attenuators of different value, they are placed in front of the laser source sequentially. With the setting of each attenuator, the power entering the sample is measured by a mobile power meter, and then it is removed to measure the power leaving it. Thus, we have obtained values for the incoming and outgoing powers of the sample. By sequencing the steps, we obtain values for the two input and output powers to be represented graphically to show the behavior of the optical-limiter for each sample.

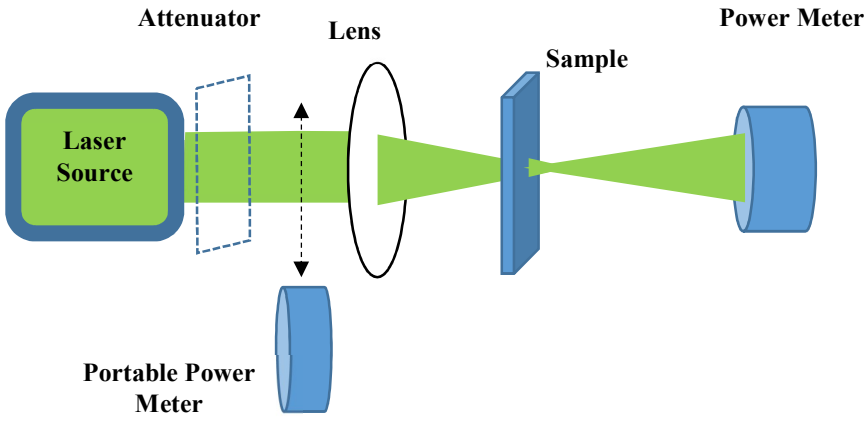

Fig. (3.9): The optical-limiting setup

Chapter 4

Results, Discussion

and conclusion

4.1 Introduction

This chapter presents all the experimental results for the prepared samples of the studied materials. The morphology of the samples, the sizes, shapes and the decoration shapes for mixtures are presented in details. In addition, the results of the linear optical properties, linear absorption spectrum, and linear absorption coefficient. Furthermore, this chapter includes a comprehensive discussion about the third order nonlinear optical properties; include the nonlinear refractive index and third-order susceptibility and then optical limiter properties.

4.2 Morphological Properties

4.2.1 (Ag) Nanoparticles group

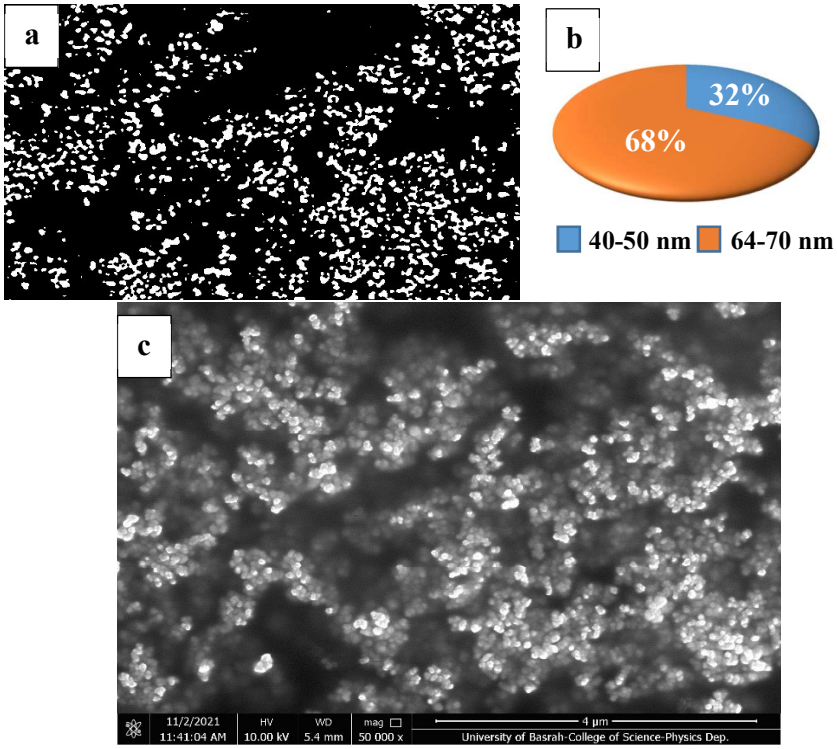

Fig. (4.1): (a) Image of (Image J) program of Ag nanoparticles, (b) size distribution by (Image J) program and (c) original SEM image.

The results of scanning electron microscope (SEM) measurements are presented in Fig. (4.1) and (4.2). The Ag nanoparticles group consist of two shapes. First, is spherical shape as shown in Fig. (4.1) with size distribution (40-70) nm. It can be observed that the dominated particles size is about (70) nm. They will be denoted as Ag NPs. The second shape is set of three nanowires with the same lengths but different in diameters (Diameters= 50, 100 and 200) nm and the length is about (5-50) μm as shown in Fig. (4.2), they will be denoted by the symbols Ag NWs D50, Ag NWs D100 and Ag NWs D200 according the diameter respectively.

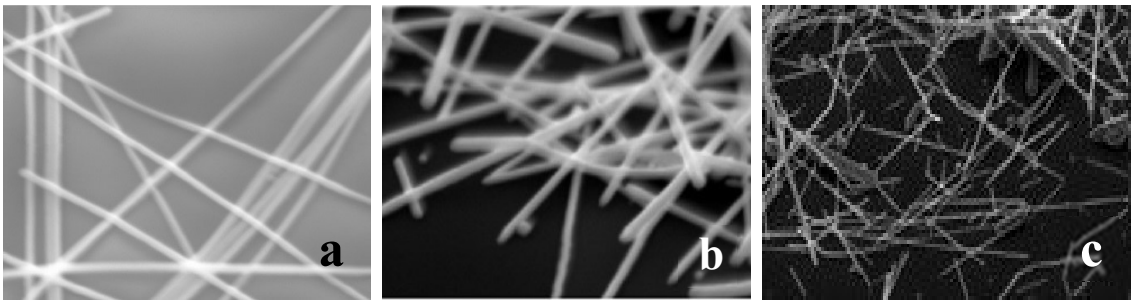

Fig. (4.2): SEM images of Ag nanowires, a: Ag nanowire with diameter 50 nm and length (5-50) μm, b: Ag nanowire with diameter 100 nm and length (5-50) μm and c: Ag nanowire with diameter 200 nm and length (5-50) μm.

4.2.2 (Cu) Nanoparticles group

The results of (SEM) images in Figs. (4.3, 4.4 and 4.5) show that the Cu group consist of two shapes, first one presented in Figs. (4.3 and 4.4) are spherical with two ranges of size distribution Cu1 and Cu2. The range size distribution of Cu1 is from (40-50) nm with predominate size of (50) nm. The range size distribution of Cu2 is (65-99) nm and it is clear that predominate size is (90-99) nm. The Second is Cu nanowire with diameter about (40-50) nm and length of (50) μm. They will be denoted as Cu NWs D50.

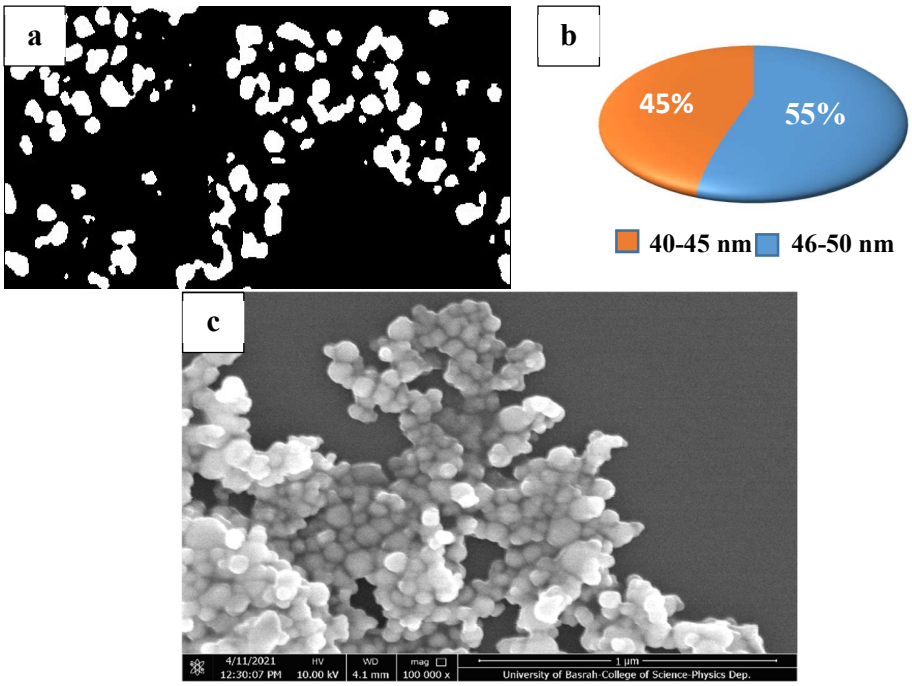

Fig. (4.3): (a) Image of (Image J) program of Cu1 nanoparticles, (b) size distribution by (Image J) program and (c) original image of SEM.

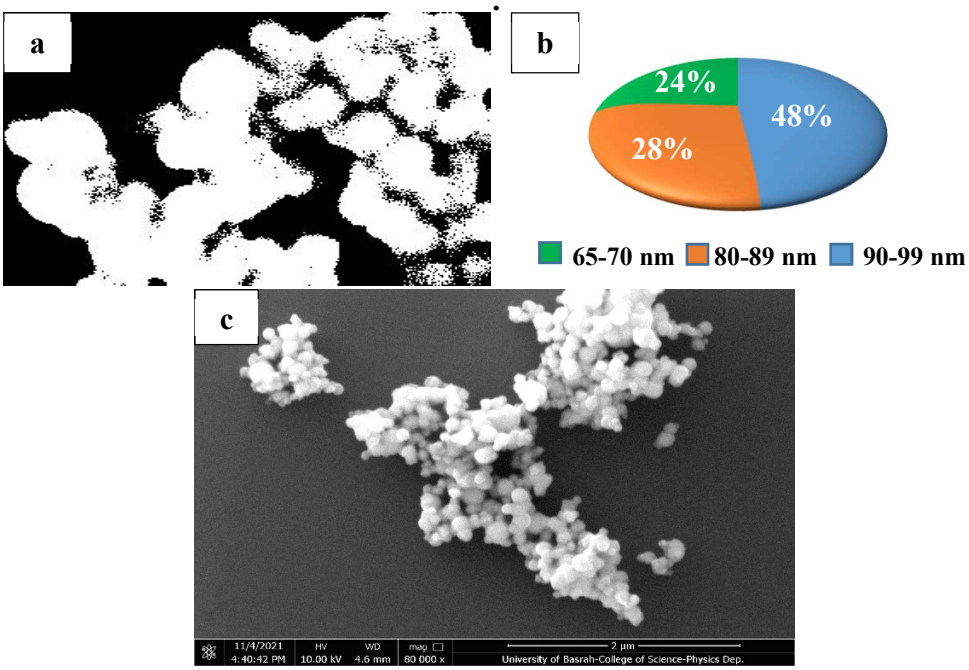

Fig. (4.4): (a) Image of (Image J) program of Cu2 nanoparticles, (b) size distribution by (Image J) program and (c) original image of SEM.

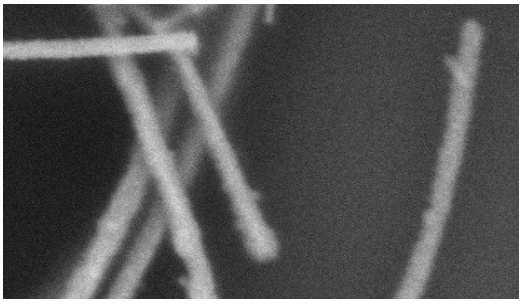

Fig. (4.5): SEM image of Cu nanowires shape with diameter (40-50) nm and length (50) μm.

4.2.3 Au Nanoparticles group

This group was brought as Au nanoparticles of spherical shape with three sizes (2, 4 and 6) nm, which will be referred to as (Au1, Au2 and Au3) respectively. These three sizes were suspended in absolute Ethanol as was illustrated in chapter (3). The images of SEM as in Fig. (4.6) showed that these particles have been agglomerated and coalesced and become out of Nano scale.

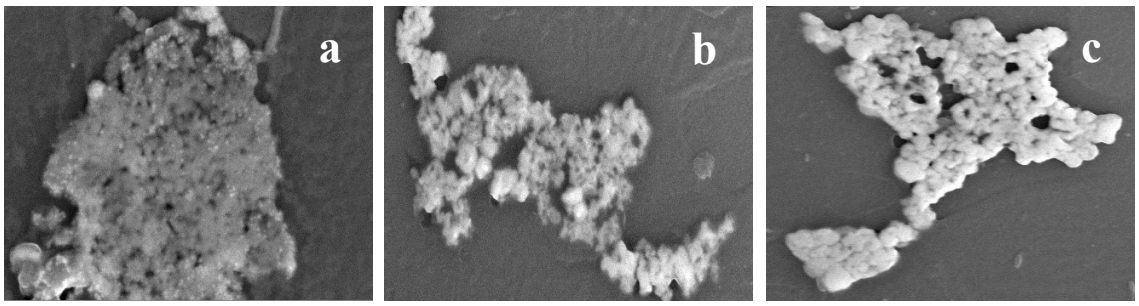

Fig. (4.6): SEM images of Au nanoparticles, a: Au1 nanoparticles, b: Au2 nanoparticles and c: A3 nanoparticles. As primary suspension samples

In order to overcome this situation, the samples prepared in the form of suspensions each was exposed to hundred laser pulses at (532 nm) with (300 mJ) per

pulse, as explained previously in Chapter (3). This results, in reversing the agglomeration action and separates the particles, as shown in Fig. (4.7).

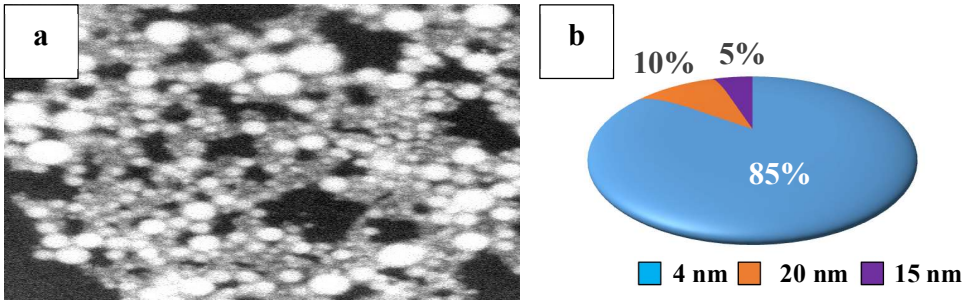

Fig. (4.7): (a) SEM image of Au1 spherical nanoparticles after pulse laser treatment, (b) sizes distribution of nanoparticles by (Image J) program.

The SEM image in Figure (4.7) shows that the laser treatment process has returned the particles to a size very close to the size with which they were prepared. The size distribution became (85%) of Au1 nanoparticles with size (4 nm), (10%) in size (20 nm) and (5%) with size (15 nm) all of spherical shapes. The dominate size was (4 nm).

Applying the same methodology to the Au2 and Au3 in the Figs. (4.8 And 4.9). In the Fig. (4.8), the SEM image and its statistical distribution shows that the spherical nanoparticles size distribution was (90%) with size (6 nm), (5%) at about (36 nm) and (5%) in scale larger than (50 nm). The dominate nanoparticles size of the Au2 samples was (6 nm). From Fig. (4.9), the statistical distribution of the spherical nanoparticles was (88%) with size (8 nm), (6%) with size (11 nm), (3%) with size (18 nm) and (1%) with sizes (13, 15 and 25) nm. The dominate nanoparticles size of the Au3 sample is (8 nm).

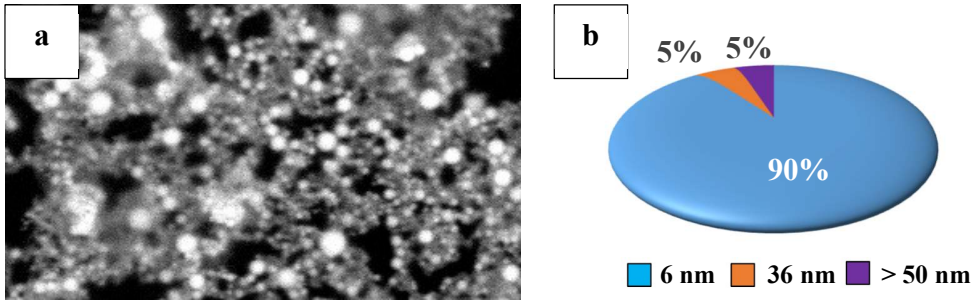

Fig. (4.8): (a) SEM image of Au2 spherical nanoparticles after pulse laser treatment, (b) sizes distribution of nanoparticles by (Image J) program.

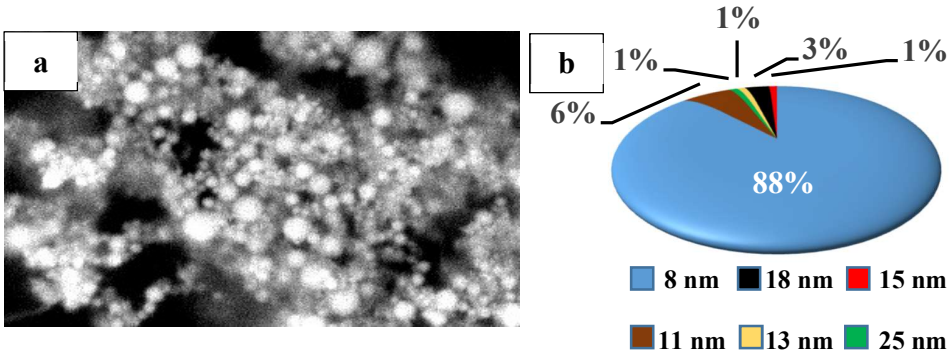

Fig. (4.9): (a) SEM images of Au3 spherical nanoparticles after pulse laser treatment, (b) sizes distribution of nanoparticles by (Image J) program.

This indicates that dispersing the Au nanoparticles in Ethanol can be achieved by applying high power ultrasonic waves. This can be performed either by using direct high power ultrasonic waves or by applying high-energy short laser pulses.

It is worth mentioning that the use of ultrasonic probe with high energies or exposing to laser pulses is not suitable for nanoparticles of tubular or wire shapes because it leads to the destruction of their shapes and sizes. Instead, a low power ultrasonic probe (15 W), is suitable for nanotube and nanowire structures.

4.2.4 Fe_2O_3 Nano fragments

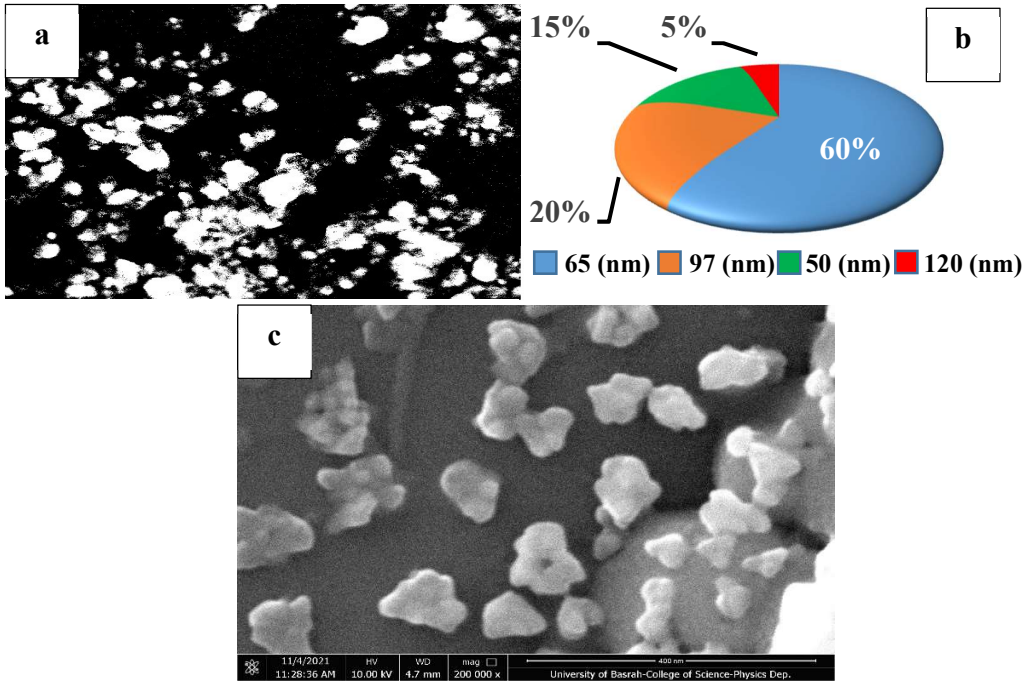

Fig. (4.10): (a) Image of (Image J) program of of Fe_2O_3 Nano fragments, (b) sizes distribution of Nano fragments by (Image J) program and (c) original image of SEM.

The drying process of the aqueous suspension of spherical iron oxide nanoparticles was explained in chapter (3), led to the deformation of the shapes of the spherical nanoparticles and forming as fragments with nanoscale as in the image of SEM in Fig. (4.10). The Nano fragments size distribution became (60%) with size (65 nm), (20%) with size (97 nm), (15%) with size (50 nm) and (5%) with size (120 nm) with randomly shaped fragments. The predominate fragments size was (65 nm).

4.2.5 Mixtures group

This section include the morphological results of a number of mixtures of different nanomaterials.

4.2.5.1 Mixture of (Cu2+Ag NW D200) (1:1)

In this sample, two equal volumes (1:1) of Cu2 and Ag NWs D200 suspension were mixed (each of them with (0.12 mg/ml) concentration) by using ultrasonic probe with power (15 W). The images of SEM in Fig. (4.11) show the adhesion of Cu2 nanoparticles (90-99) nm on the Ag NWs D200. The images in Fig. (4.11) show clear adhesions between Cu2 and Ag NWs D200. The percentage of the number of Cu2 in the suspension is much more than the percentage of the number of Ag NWs D200 in it, because of the different sizes and their equal concentration. This issue enhances the bounding condition not to mention the adhesion of the copper nanoparticles with the silver nanowires. The adhesion between them is due to the presence of unsaturated dangling bonds [129].

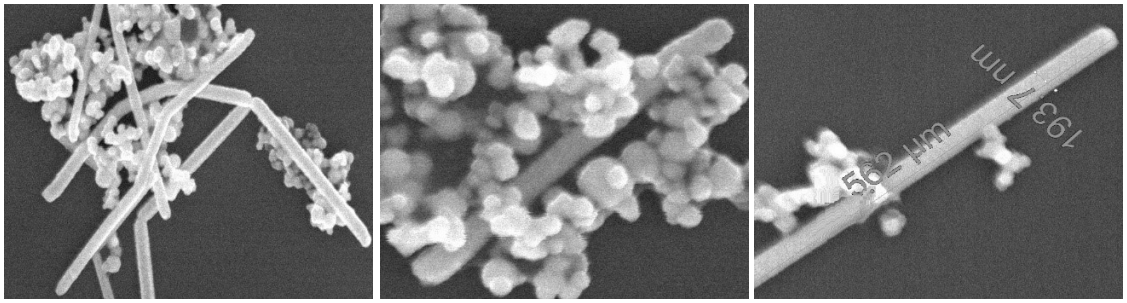

Fig. (4.11): SEM image of Cu2+Ag NW shows the adhesion between Cu2 spherical nanoparticles and Ag NWs D200

4.2.5.2 Mixture of (Ag NPs + Cu NWs D50) (1:1)

In this sample, spherical Ag NPs were mixed with Cu NWs D50. The images of SEM in Fig. (4.12) show the adhesions between these two types of nanoparticles. It appears that the adhesion of spherical Ag NPs to the Cu NWs is more homogeneous than that of the spherical Cu2 to the Ag NWs D200 when compared with the Fig. (4.11). This homogeneity is attributed to the surface energy of the

nanoparticle, where the smaller the particles, the higher the surface energy for them. In addition to their crystal growth orientation, affects the dangling bonds. In this case, the particle size of Ag NPs is smaller than Cu2 therefore the surface energy is greater.

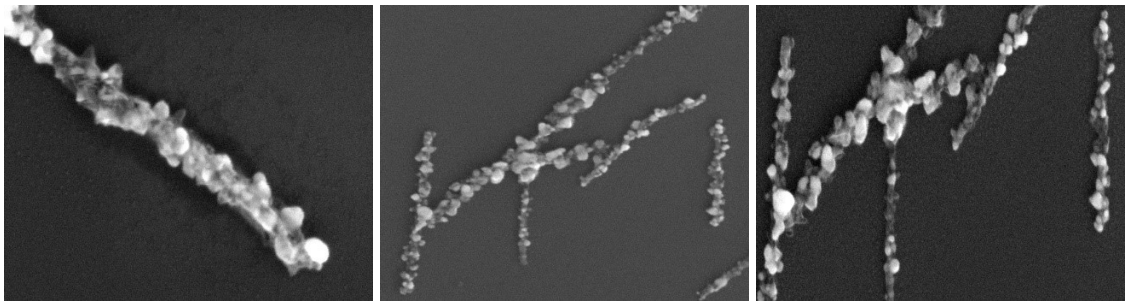

Fig. (4.12): SEM image of Ag NPs + Cu NWs D50 shows the adhesion between spherical Ag NPs and Cu NWs D50

4.2.5.3 Mixture of spherical (Ag NPs + Fe_2O_3 Nano fragments) (1:3)

In this mixture, two mixing methods were used. In the first, one volume of (0.12 mg/ml) concentration of spherical Ag NPs was mixed with three volumes of concentration (0.12 mg/ml) too of Fe_2O_3 Nano fragments using an ultrasound probe with a power of 15W. As for the second method of mixing with the same quantities, it was using a pulsed laser with a wavelength of (532 nm) with a pulse energy of (300 mJ) and a number of 100 pulses, as detailed in Chapter (3).

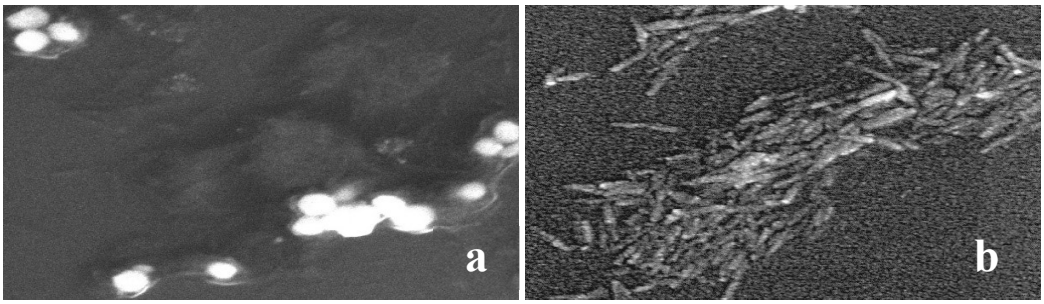

Fig. (4.13): SEM image of spherical Ag NPs + Fe_2O_3 Nano fragments, (a): mixing by ultrasonic probe, (b): mixing by pulse laser

In the Fig. (4.13), the SEM of (a) image indicates the adhesion of spherical Ag NPs to the Fe2O3 Nano fragments by the mixing effect with the ultrasonic probe. In (b), the laser effect appears clear by changing the shape of the iron oxide fragments to be in a granular or needle-shaped form and the adhesion is clearly too. Not to mention the change in the color of the suspension as it appeared in Chapter (3).

4.2.5.4 Mixture of spherical (Cu1 + Fe_2O_3 Nano fragments) (1:3)

The Cu1 and the Fe2O3 Nano fragments of (0.12) mg/ml were mixed by the following the same methods followed in section (4.2.5.3).

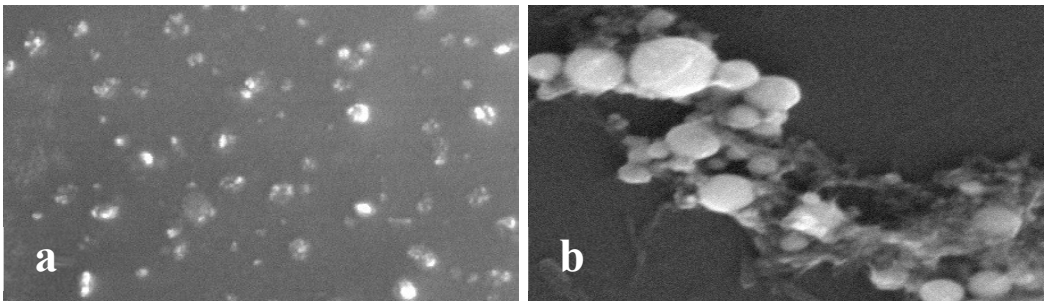

Fig. (4.14): SEM image of spherical Cu1 + Fe_2O_3 Nano fragments, (a): mixing by ultrasonic probe, (b): mixing by pulse laser

In Fig. (4.14), the SEM of (a) image shows the adhesion of spherical Cu1 to the Fe2O3 Nano fragments when mixed with the ultrasonic probe. In frame (b), the adhesion is clearly too and the laser effect appears clear by changing the shape of the iron oxide fragments to be in a granular or needle-shaped form, not to mention the change in the color of the suspension as it appeared in Chapter (3).

4.3 Linear Optical Properties

The absorption spectrum depends on the shape, size, concentrations and number of nanoparticles per volume. The linear absorption spectrum of each of the studied groups will be viewed according to the concentrations that have been prepared. All graphs and the effect of concentration and shape change on linear absorbance will be discussed.

4.3.1 Linear optical properties for (Ag) nanoparticles group

Based on what was referred to in paragraph (4.2.1), this group consists of two shapes; first, one is spherical Ag NPs and second is Ag NWs. Fig. (4.15) shows three broad linear absorption spectra of three concentrations of Ag NPs (0.04, 0.08 and 0.12) mg/ml. It can be said that it almost covers the entire visible region of the spectrum.

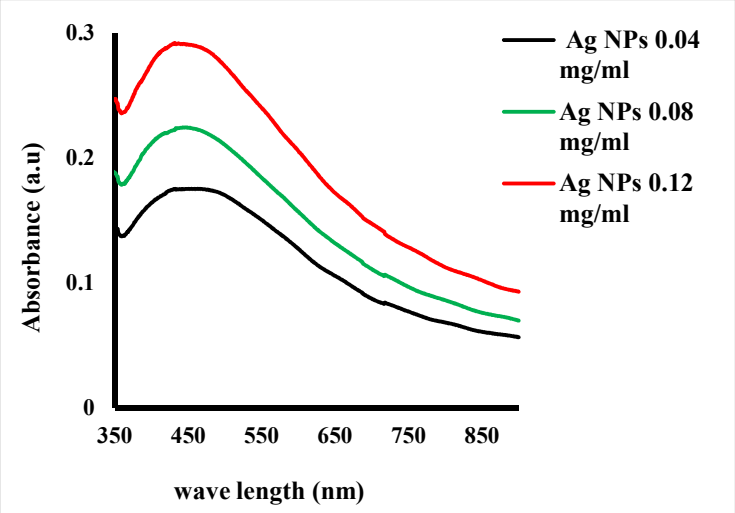

Fig. (4.15): UV- visible absorption spectra of spherical Ag NPs of three different concentrations

It was found that the peak absorption of surface plasmon resonance (SPR) of Ag NPs spanning the large part of visible region. The average value of $\Delta\lambda$ was about (238) nm. It is clearly that the absorbance increases with the increase of concentrations. The increase of concentration means, the number of particles per unit volume was increased, therefore the absorption has been increased. The λ_{max} (the position of the peak of curve) is slightly shifted towards the blue region with the increasing of concentrations. λ_{max} values are (448, 443 and 432) nm respectively. It is known that λ_{max} increases with decreasing nanoparticle size. In our case, we consider the size of the nanoparticles to be constant even if the concentrations change, but the probability of the presence of small nanoparticles in the larger concentration is more than in the lower concentrations, which may cause this shift of the blue region and this is consistent with the results in [130].

Fig. (4.16 a, b and c) Show the absorption spectra of three sizes of Ag NWs with three concentrations of each size (0.04, 0.08 and 0.12) mg/ml. Each spectrum exhibits two peaks. These two peaks correspond to the transvers and longitudinal plasmon bands. The transvers plasmon band is caused by diameter of Ag NWs, while the longitudinal is attributed to the absorption over the lengths of Ag NWs. Fig. (4.16 a) shows that the λ_{max} of each concentration is approximately at (400) nm and average $\Delta\lambda$ is about (324) nm. Fig. (4.16 b) also shows that the λ_{max} for each concentrations is at (380) nm and $\Delta\lambda$ is about (137) nm, while in Fig. (4.16 c) the λ_{max} at (420) nm and $\Delta\lambda$ is about (329) nm. From observing the three graphs in Fig. (4.16), we find that the absorbance decreases with the increase in the diameter of the Ag NWs, and [131 & 132] confirmed this.

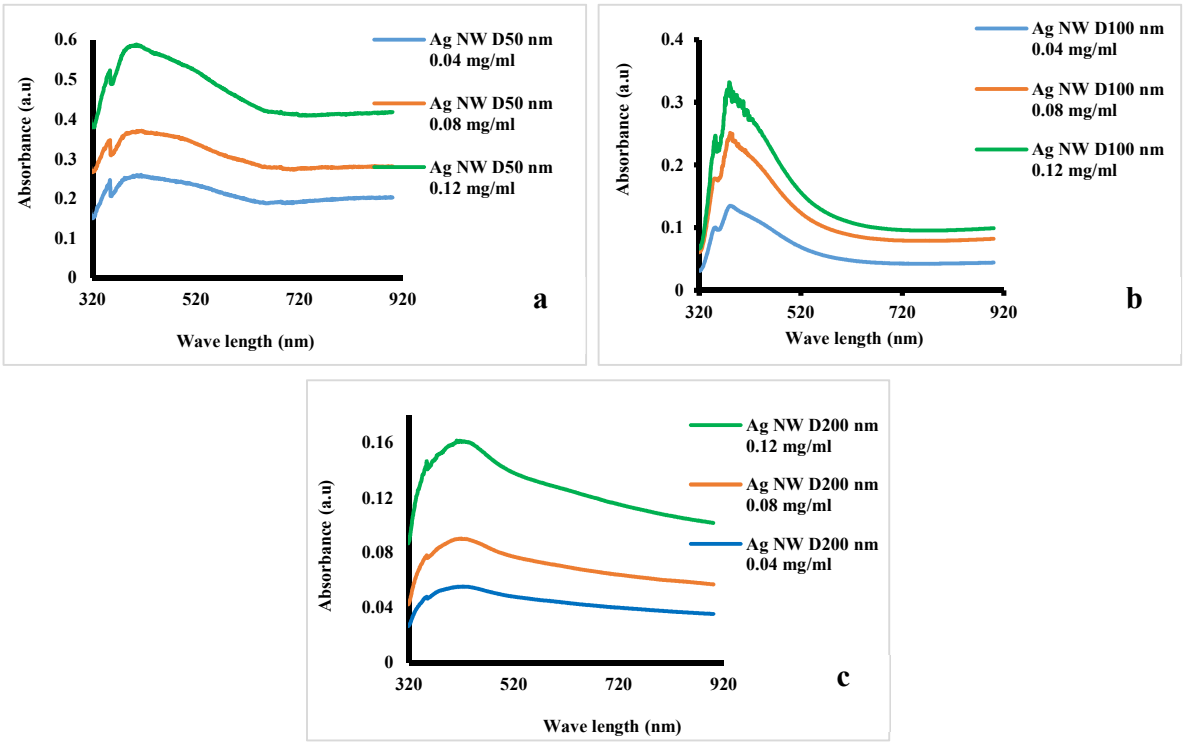

Fig (4.16): UV- visible absorption spectra of Ag NWs with three concentrations, (a): Ag NW D50, (b): Ag NW D100, (c): Ag NW D200

4.3.2 Linear optical properties of (Cu) nanoparticles group

As indicated in the paragraph (4.2.2), this group includes two shapes of (Cu) nanoscales, the first one is spherical Cu NPs (Cu1 and Cu2) with two sizes, and the second is Cu NWs with one size (Cu NWs D50). The results of the linear optical absorption measurement of the three concentrations are presented in Fig. (4.17) below.

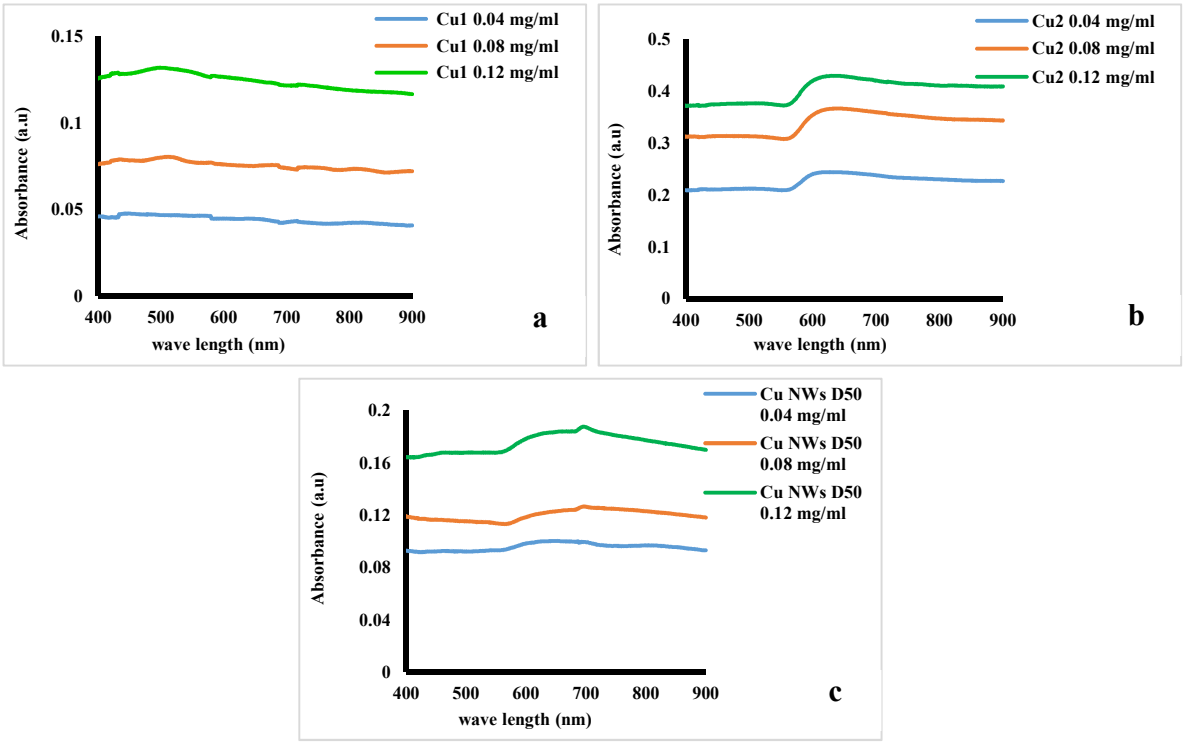

Fig (4.17): UV- visible absorption spectra of Cu nanoparticles group with three concentrations, (a): Cu1, (b): Cu2 and (c) Cu NWs D50

Fig. (4.17 a) shows three curves of the linear absorption spectrum of three concentrations of Cu1 suspension in absolute Ethanol. It is clear that the shape of the absorption spectrum appears flat over the whole visible region of the spectrum. With increasing concentration, the absorbance increases with the possibility of the appearance of an absorption peak at the wavelength of (510) nm. Fig. (4.17 b) also shows three linear absorption spectrum curves for Cu2 at the same three concentrations. It is very clear that the amount of linear absorbance increases with increasing concentration. The absorption spectra in this figure appear differently as compared to the spectra shown in the previous figure (4.17a), although the difference between them is only in the particle size. It can be seen that at the wavelength of

about (570) nm, which is very close to the SPR peak [133], the linear absorbance values start to increase. The absorption peak can be recorded at the wavelength (630) nm. It is clear that the absorption curve of Cu1 and Cu2 is broad due to the scale of size distribution [134].

Fig. (4.17 c) shows three curves of absorption spectrum for Cu NWs suspended in absolute ethanol of three concentrations. The absorbance increases with increasing the concentration and the absorption curves appear broad. From observing the absorption spectrum curves of Cu NWs we find, that it is possible to identify two regions for increasing absorption. The first absorption region at a wavelength of about (570) nm, where the absorption begins to increase to be its highest value at a wavelength of about (660) nm, then the absorption peak of the second region appears at the wavelength of about (700) nm. The appearance of these two absorption regions is attributed to the effect of the length and diameter of the nanowire. The second region influence by length and the first region by diameter and this supported by [135]. The absorption spectrum of copper nanowires shows a broad region, which is attributed to excitation of surface plasmon resonance (SPR) or interband transitions and this also supported by [136].

4.3.3 Linear optical properties for (Au) nanoparticles group

Fig. (4.18) shows surface plasmon absorption of three schematics of the linear absorption spectrum curves of three sizes of spherical Au nanoparticles and each of three concentrations. It is clear that the absorbance increases with increasing concentration.

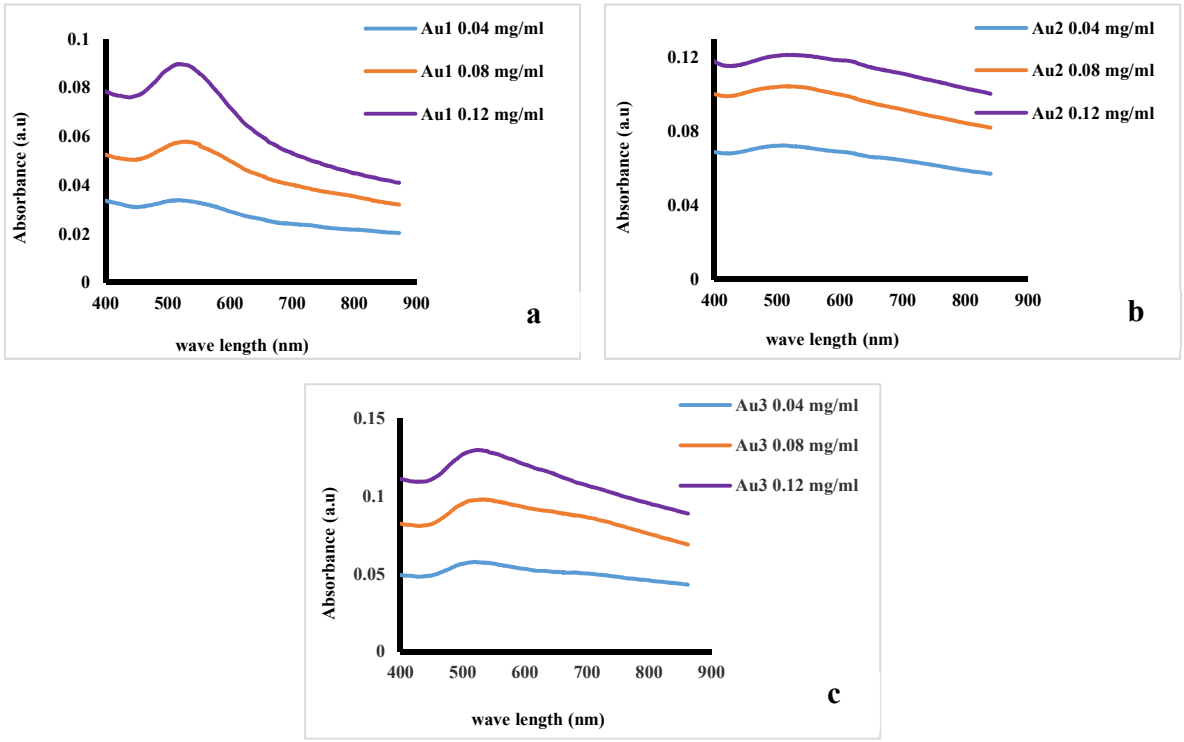

Fig (4.18): UV- visible absorption spectra of Au nanoparticles group with three concentrations, (a): Au1, (b): Au2 and (c): Au3

Fig. (4.18 a) shows the absorbance of spherical Au1 Nanoparticles, in which the predominant size was (4 nm). For the three concentrations (0.04, 0.08 and 0.12) mg/ml, the absorption peaks λ_{max} were (517, 520 and 522) nm and the $\Delta\lambda$ was (50) nm. Fig. (4.18 b) shows the absorption spectra of three concentrations of spherical Au2 nanoparticles in which the predominant size was (6 nm). The values of the absorption peaks λ_{max} were (520, 523 and 525) nm and the $\Delta\lambda$ was (35) nm. As for Fig. (4.18 c), it shows the absorption spectrum of three concentrations of spherical Au3 nanoparticles, in which the predominant size was (8 nm). The values of the absorption peaks λ_{max} were (525, 528 and 530) nm and the $\Delta\lambda$ was range (55) nm.

The Fig. (4.19) depicts the variation of the peaks absorption λ_{max} with the variation of particle sizes at the same concentration. It appears that as the particle size decreases, the spectrum shifts towards the blue region. The absorption peaks values for Au1, Au2 and Au3 were (522, 525 and 530) nm respectively.

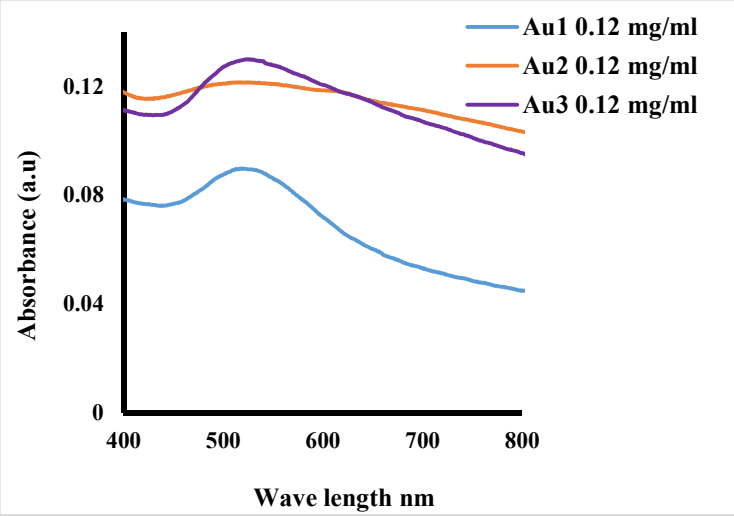

Fig (4.19): UV- visible absorption spectra and peaks blue shift of Au1, Au2 and Au3 spherical nanoparticles at the same concentration with different sizes

4.3.4 Linear optical properties for (Fe_2O_3) Nano fragments

Fig. (4.20) shows three linear absorption curves of Fe_2O_3 Nano fragments, and it is clear that the absorption increases with increasing concentration. From observing the curves, we find that the absorption spectrum of this material decreases with increasing wavelength. It appears that the absorption region starts from the wavelength (280) nm, i.e. from the ultraviolet region, and decreases in the visible region of the visible spectrum to be at its lowest at the wavelength (550) nm, meaning that the absorption is weak in the visible region.

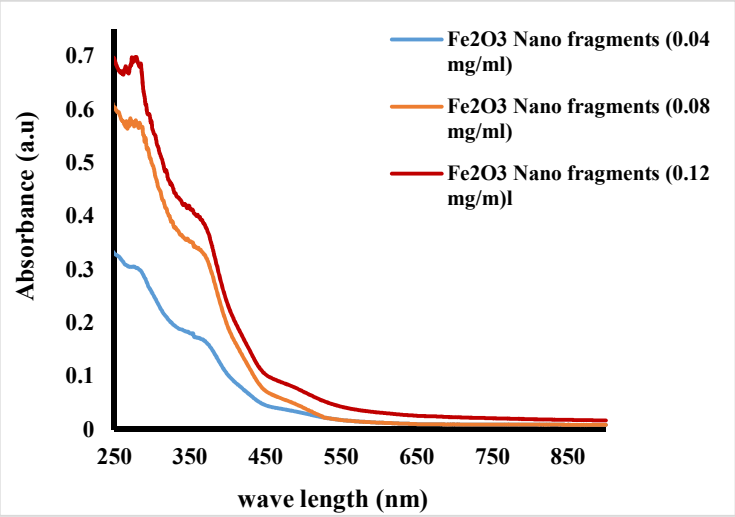

Fig (4.20): UV- visible absorption spectra of Fe_2O_3 Nano fragments with three concentrations

4.3.5 Linear optical properties for Mixtures groups

This section will include a presentation of the linear optical properties results of a number of mixtures of different nanomaterials that have been prepared.

4.3.5.1 Linear optical properties for mixture of (Cu2+Ag NW D200)

Fig. (4.21) shows the linear absorption of the three samples suspended in absolute ethanol, Cu2 (0.12 mg/ml), Ag NWs D200 (0.12 mg/ml), and their mixture with ratio (1:1). The Curve shapes for silver nanowires and copper nanoparticles are described in the paragraphs (4.3.1) and (4.3.1) respectively. As for the mixture, the absorption curve appears as lowest state under the curves of the Ag NWs D200 and Cu2. This reduction is due to the dilution of the concentrations of the two components in the mixture. The appearance of the spectrum of the mixture in this way without a distinct new peak indicates that there are no bonds or interference

levels of energy between the silver nanowires and the copper nanoparticles. The absorption of the suspension is mainly due to the excitation of (SPR), which is a specific property of the metallic nature of the particles.

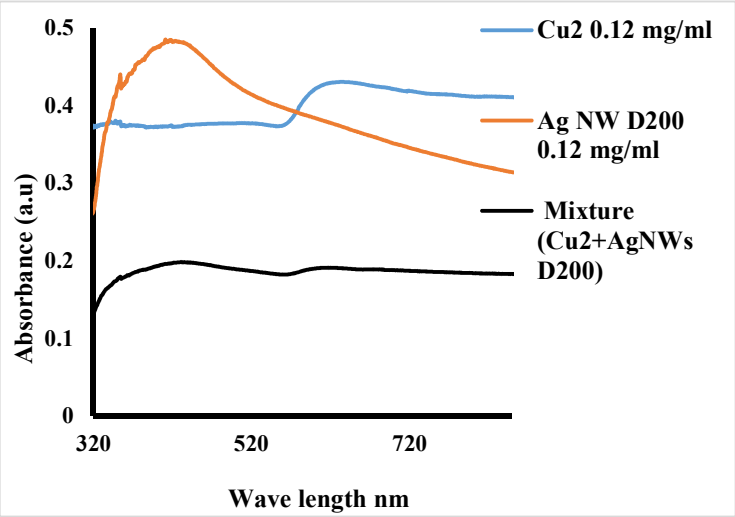

Fig. (4.21): UV- visible absorption spectra of (0.12 mg/ml) Cu2 (0.12 mg/ml), Ag NWD200 and mixture (Cu2 and Ag NW D200) with volume mixing ratio (1:1) for each component

4.3.5.2 Linear optical properties for mixture of (Ag NPs + Cu NWs D50)

Fig. (4.22) shows the linear absorption of the three samples of suspensions in absolute ethanol, spherical Ag NPs (0.12 mg/ml), Cu NWs D50 (0.12 mg/ml), and the mixture at (1:1) mixing ratio. The Curve shapes for silver nanoparticles and copper nanowires are described in the paragraphs (4.3.1) and (4.3.1) respectively. As for the mixture, the absorption curve appears as lowest state under the curves of the Ag NPs and Cu NWs D50. This reduction is due to the dilution of the concentrations of the two components in the mixture. The linear absorption of this mixture appears as a union between the two absorption spectra of the two mixed

materials before mixing. It is a clear that the absorption peak λ_{max} due to Ag NPs with an absorption peak at (422 nm), then it goes flat to the region of the near IR Spectrum to appear as the absorption spectrum of Cu NWs D50, with a slight shift towards the blue region. These shifts in the spectrum, which were clear in its first part, about (26 nm) towards the blue region, may be due to the adhesions between Ag NPs and Cu NWs D50, which in turn changed the surface area of the particles. The absorption of the suspension is mainly due to the excitation of Surface Plasmon Resonance (SPR).

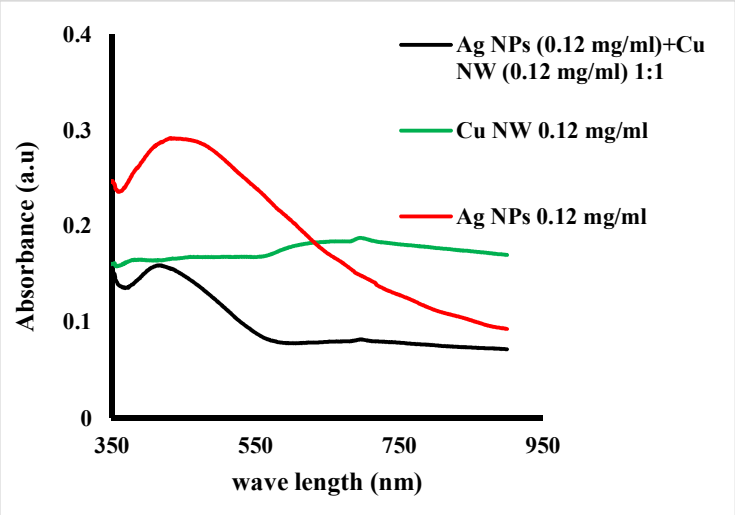

Fig (4.22): UV- visible absorption spectra of the mixture Ag NPs (0.12 mg/ml) + Cu NW D50 (0.12 mg/ml) (1:1) and both before mixing

4.3.5.3 Linear optical properties mixture of spherical (Ag NPs + Fe_2O_3 Nano fragments) (1:3)

Fig. (4.23) shows four curves of the linear absorption spectra, two curves for Ag NPs and Fe_2O_3 Nano fragments with two mixing methods and two curves for the individual components. The curve in green color represents the linear absorption spectrum of Fe_2O_3 Nano fragments suspended in absolute ethanol at concentration

(0.12 mg/ml), which shows that its absorbance is limited at Δλ about (125 nm) with a steep slope. The curve in purple represents the linear absorption spectrum of spherical Ag NPS, which has its λ_{max} at wavelength (448 nm). The curve in blue shows the linear Absorbance of the mixture consisting of one volume of spherical Ag NPs (0.12 mg/ml) with three volumes of Fe_2O_3 Nano fragments at (0.12 mg/ml). The mixing process was carried out by using a pulse laser as explained in Chapter (3). The curve in orange color represents the linear absorption spectrum of the same mixture above, but the mixing process was carried out by using an ultrasonic probe.

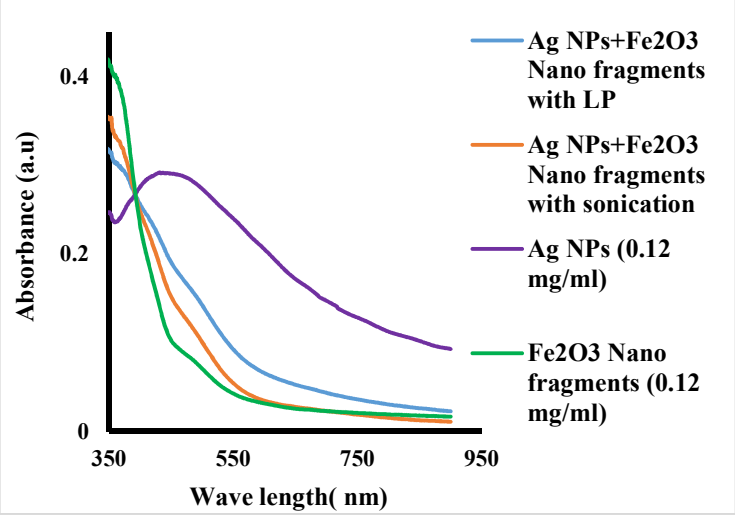

Fig (4.23): UV- visible absorption spectra of the mixture Ag NPs (0.12 mg/ml) + Fe_2O_3 Nano fragments (0.12 mg/ml) (1:3) and both before mixing

The two curves of the two mixtures show a new shape of the absorption spectrum which may idicate the formation of the core-shell. This result is consistent with the result obtained in the reference [137], which indicates the formation of the core-shell structure using the sol-gel method. The formation of the core-shell structure may be more pronounced in the curve of the mixture that has been treated

with laser, which can be attributed to the high energy of the laser. The two curves show the disappearance of the absorption spectrum of spherical Ag NPs and the appearance of convexity in the region between wavelength (396 nm) and wavelength (443 nm). When compared with the Fe_2O_3 Nano fragments curve alone. In addition to the increase in exposing the absorption area to be at a rate of $\Delta\lambda$ (200 nm). This indicates that the iron oxide absorption area is exposed due to mixing and the formation of a new structure.

4.3.5.4 Linear optical properties mixture of spherical (Cu1 + Fe_2O_3 Nano fragments) (1:3)

Fig. (4.24) shows four curves of the linear absorption spectrum, marked with different colors.

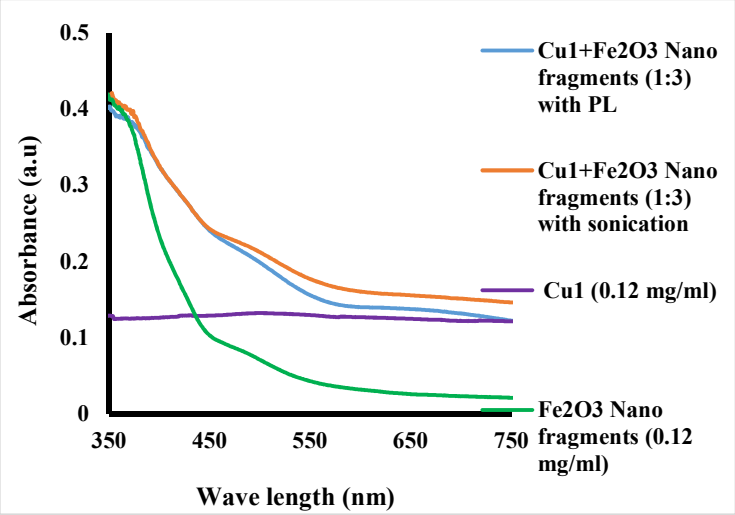

Fig (4.24): UV- visible absorption spectra of the mixture Cu1 (0.12 mg/ml) + Fe_2O_3 Nano fragments (0.12 mg/ml) (1:3) and both before mixing

The curve in green color represents the linear absorption spectrum of Fe_2O_3 Nano fragments suspended in absolute ethanol at concentration of (0.12 mg/ml). Which

shows that its absorbance is limited at Δλ about (125 nm) with a steep slope. The flat curve in purple represents the linear absorption spectrum of spherical Cu1. The curve in orange represents the linear absorption spectrum of the mixture consisting of one volume of spherical Cu1 (0.12 mg/ml) with three volumes of Fe_2O_3 Nano fragments (0.12 mg/ml). The mixing process of this sample was carried out by using an ultrasonic probe. The curve in blue shows the linear absorbance of the same mixture above, but the mixing process was carried out by using a pulse laser as explained in Chapter (3).

The linear absorption spectra of the two mixtures in Fig. (4.24) show different shapes than the linear absorption curves of the materials that make up them. This may be due to the adhesions between the particles of the two materials that is caused by the ultrasound and laser energy. This may have formed a core-shell structure. As in the silver nanoparticles in the previous mixture, especially that the amount of Fe_2O_3 Nano fragments is three times greater than the amount of spherical Cu1 nanoparticles because the mixing ratio was (1:3). The curves of the two mixtures shows an exposure to the absorption region for Fe_2O_3 Nano fragments absorption, where Δλ became about (250 nm) tow times greater than Δλ for Fe_2O_3 Nano fragments. This indicate that the mixing Cu with Fe_2O_3 can lead to raise the overall absorbance of the sample in comparison with that of the Fe_2O_3 fragments alone.

4.4 Nonlinear Optical Properties

This section determined and discussed the empirical results for the nonlinear optical properties of all the preparation samples. These results include nonlinear refractive index and nonlinear third order susceptibility at four wave lengths (405, 473, 532 and 650) nm and three concentrations for each sample by Z-scan technology.

The appropriate value of the power has been determined depending on the nonlinear response of the suspension at the specific wavelength. In other words, low power has been used when the nonlinear response is relatively high and vice versa. This insures that no ultrahigh intensity effects happen rather than the third order effects e.g. beam collapse, beam filamentation, and some other phenomena that happen in nonlocal nonlinear material. The open aperture nonlinear characterization indicates not nonlinear absorption for all the materials suspensions included in this study at all the wavelengths used within the conditions of the present study. The closed aperture nonlinear characterization indicates that all suspensions for all materials have a negative refractive index at all the wavelengths used. The results showed that the nonlinear refractive index of these materials is of thermal origin. The nonlinear investigation has shown that all suspensions have a defocusing nonlinear refraction in absolute ethanol over the visible region. The real part of the third-order nonlinear optical susceptibility ($Re\chi^{(3)}$) was calculated and the imaginary part was not calculated because there is no nonlinear absorption coefficient.

4.4.1 Nonlinear optical properties for (Ag) nanoparticles group

We mentioned above that this group consists of two shapes, the first one is spherical silver nanoparticles and the second is silver nanowires with three different diameters.

4.4.1.1 Nonlinear optical properties for spherical Ag NPs

Fig. (4.25) shows the normalized transmittance of Z-scan measurements as a function of distance from the focus of Gaussian beam. A close-aperture curves for spherical Ag NPs at three concentrations with four wavelengths. Form the Fig (4.25 a, b, c and d), it is evident that all the samples have negative refractive indices at all the wavelengths. The asymmetry at the ends of the nonlinear refractive index curves in the above figure May be due to nonlinear scattering [138].

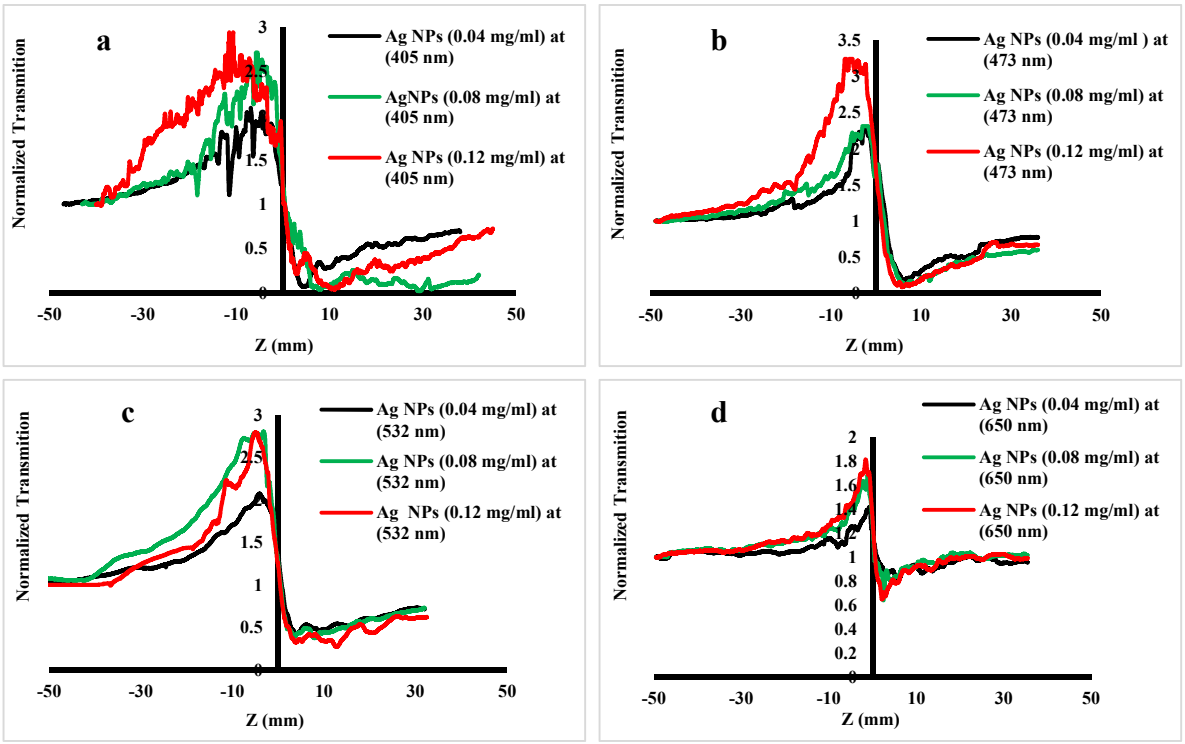

Fig (4.25): Z-scan closed aperture curves for spherical Ag NPs suspension in three concentrations ((0.04, 0.08 and 0.12) mg/ml). with excitation wavelength (a) 405 nm, (b) 473 nm, (c) 532 nm and (d) 650 nm and powers of (2, 4.8, 11 and 13.8) respectively

CHAPTER 4 Results, Discussion and Conclusion

The numerical values of the refractive indices (n_2) and the real part of the third-order nonlinear optical susceptibility ($Re\chi^{(3)}$) are listed in Table (4.1). The values of n_2 have been calculated by using equations (2.42). ($Re\chi^{(3)}$) values have been calculated by using equation (2.25).

Table (4.1): The values of n_2 and $Re\chi^{(3)}$ at the different concentrations and wavelength for spherical Ag NPs

Ag NPs Wavelength (405 nm), power (2 mW) and intensity (13.49 MW/m^2)				
Concentration (mg/ml)	**Linear absorption coefficient α (m^{-1})**	**Linear refractive index n_o**	**Nonlinear Refractive index -n_2 (m^2/W)**	**Susceptibility $Re\chi^{(3)}$(esu)**
0.04	38.37112743	1.357	2.47681× 0^{-11}	1.1563×10^{-5}
0.08	49.40364893	1.357	3.31870× 0^{-11}	1.5494×10^{-5}
0.12	64.4653457	1.357	4.31252× 0^{-11}	2.0134×10^{-5}
Ag NPs Wavelength (473 nm), power (4.8 mW) and intensity (4.98 MW/m^2)				
Concentration (mg/ml)	**Linear absorption coefficient α (m^{-1})**	**Linear refractive index n_o**	**Nonlinear Refractive index -n_2 (m^2/W)**	**Susceptibility $Re\chi^{(3)}$(esu)**
0.04	40.23356353	1.357	8.2361×10^{-11}	3.8452×10^{-5}
0.08	50.7224235	1.357	8.5735×10^{-11}	4.0027×10^{-5}
0.12	65.97580663	1.357	1.2371×10^{-10}	5.7757×10^{-5}
Ag NPs Wavelength (532 nm), power (11 mW) and intensity (5.79 MW/m^2)				
Concentration (mg/ml)	**Linear absorption coefficient α (m^{-1})**	**Linear refractive index n_o**	**Nonlinear Refractive index -n_2 (m^2/W)**	**Susceptibility $Re\chi^{(3)}$(esu)**
0.04	36.2777772	1.357	6.19672×10^{-11}	2.89×10^{-5}
0.08	44.67896767	1.357	9.13483×10^{-11}	4.26×10^{-5}
0.12	57.98462693	1.357	9.54751×10^{-11}	4.46×10^{-5}
Ag NPs Wavelength (650 nm), power (13.8 mW) and intensity (13.51 MW/m^2)				
Concentration (mg/ml)	**Linear absorption coefficient α (m^{-1})**	**Linear refractive index n_o**	**Nonlinear Refractive index -n_2 (m^2/W)**	**Susceptibility $Re\chi^{(3)}$(esu)**
0.04	24.29035513	1.357	1.9772×10^{-11}	5.59×10^{-6}
0.08	30.2994195	1.357	2.0099×10^{-11}	9.38×10^{-6}
0.12	39.55786333	1.357	2.25072×10^{-11}	1.05×10^{-5}

From the data in Table (1), it is clear that, at the same wavelength, the linear absorption coefficients (α), nonlinear refractive index (n_2) and third-order nonlinear optical susceptibility ($Re\chi^{(3)}$) increases with increasing the concentration of the sample. The largest absolute value of the nonlinear refractive index and the real part of the third-order nonlinear optical susceptibility ($Re\chi^{(3)}$) are at (473 nm) this is because the (473) nm wavelength is within the peak of the absorption band of Ag NPs. The value of the nonlinear refractive index starts decreasing with the increase of the wavelength due to the decreasing linear absorbance. Due to the (SPR) of Ag NPs suspensions, the energy of light is absorbed efficiently and then transfered to ethanol via non-irradiative relaxation processes. This increases the local temperature in ethanol. The temperature gradient filed results in a change in the local refractive index because the local refractive index decreases with the increase of temperature for most liquids such as ethanol. The large values of the nonlinear refractive index at the short wavelength may be attributed to the higher energy of these photons relative to the other wavelengths. The higher energy photons can excite the samples to higher energy levels. This means more non-radiative relaxation processes, hence higher temperature, which results in a higher associated nonlinearity.

4.4.1.2 Nonlinear optical properties for Ag NWs D50

The Fig. (4.26) shows the Z-scan closed aperture curves of the suspension of Ag NWs D50. Fig. (4.26 a) shows the nonlinear change of three concentrations at the wavelength of (405 nm) with (2.2 mW) power of the laser beam used. It shows the increase of the nonlinear change with the increasing concentrations. The same is true for Fig. (4.26 b, c and d) at wavelengths (473, 532 and 650) nm with powers (8.7, 15.6 and 13.6) mW respectively.

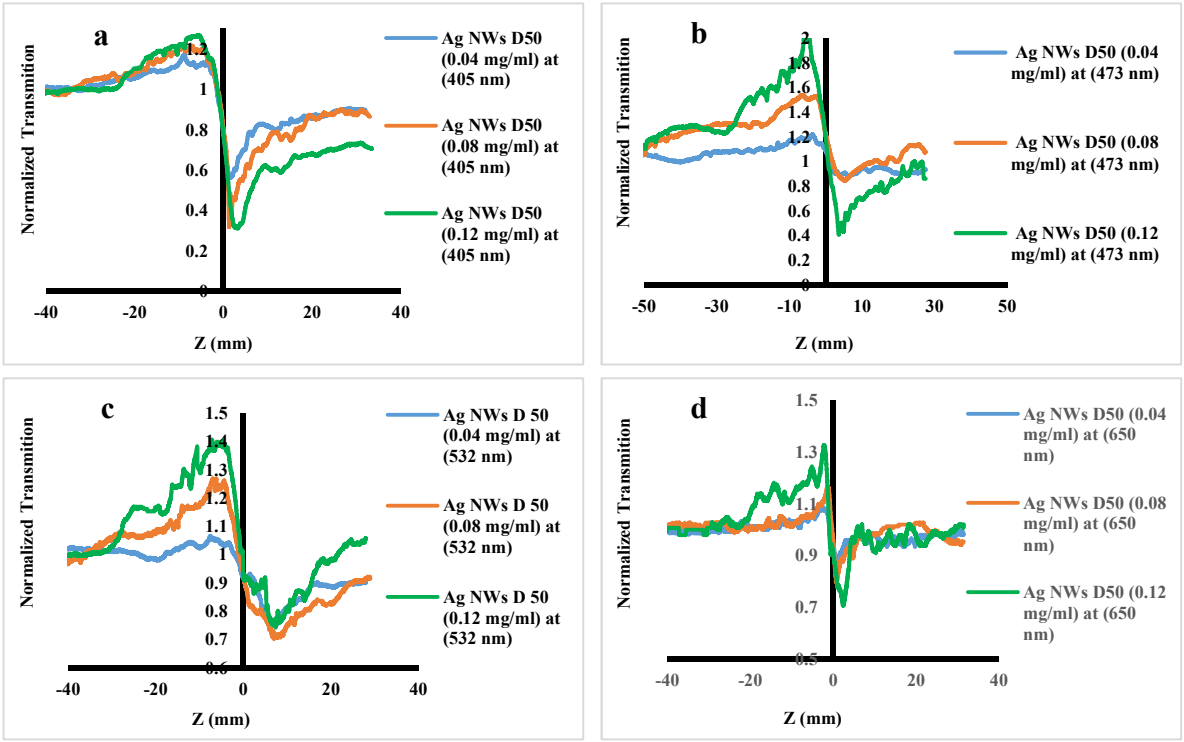

Fig (4.26): Z-scan closed aperture curves for Ag NWs D50 suspension in three concentrations ((0.04, 0.08 and 0.12) mg/ml), with excitation wavelength (a) 405 nm, (b) 473 nm, (c) 532 nm, and (d) 650 nm and powers of (2.2, 8.7, 15.8, and 13.8 mW) respectively.

From the observation of the values listed in Table (4.2), it appears that, the values of the linear absorption coefficient appear to be are close at all the wavelengths used. However, this did not prevent the emergence of a significant variation in the nonlinear changes of the suspension at these wavelengths. The highest value of the nonlinear refractive index and the third-order nonlinear optical Susceptibility were for the concentration (0.12 mg/ml) at the wavelength (473 nm), although this wavelength does not fall within the absorption peak of these nanowires, but within its broad-spectrum region. The lowest values of the nonlinear refractive index and the third-order nonlinear optical susceptibility were shown for the

concentration (0.04 mg/ml) at the wavelength (650 nm). Because this wavelength is located, at the end of the linear absorption region of the nanowires. The energy of the photons does not lead to sufficient or large non-radiative (thermal) decays in the nanowire material.

Table (4.2): The values of n_2 and $Re\chi^{(3)}$ at different concentrations and wavelengths for spherical Ag NWs D50

Ag NWs D50 Wavelength (405 nm), power (2.2 mW) and intensity (14.83 MW/m^2)				
Concentration (mg/ml)	**Linear absorption coefficient α (m^{-1})**	**Linear refractive index n_o**	**Nonlinear Refractive index -n_2 (m^2/W)**	**Susceptibility $Re\chi^{(3)}$(esu)**
0.04	59.38362267	1.357	6.8765×10^{-12}	3.1204×10^{-6}
0.08	84.97686167	1.357	1.0233×10^{-12}	4.7774×10^{-6}
0.12	135.434824	1.357	1.1151×10^{-11}	5.206×10^{-6}
Ag NWs D50 Wavelength (473 nm), power (8.7 mW) and intensity (9.03 MW/m^2)				
Concentration (mg/ml)	**Linear absorption coefficient α (m^{-1})**	**Linear refractive index n_o**	**Nonlinear Refractive index -n_2 (m^2/W)**	**Susceptibility $Re\chi^{(3)}$(esu)**
0.04	56.248472	1.357	7.5121×10^{-12}	3.51×10^{-6}
0.08	82.25318033	1.357	1.5203×10^{-11}	7.10×10^{-6}
0.12	126.515305	1.357	3.7838×10^{-11}	1.77×10^{-5}
Ag NWs D50 Wavelength (532 nm), power (15.6 mW) and intensity (8.21 MW/m^2)				
Concentration (mg/ml)	**Linear absorption coefficient α (m^{-1})**	**Linear refractive index n_o**	**Nonlinear Refractive index -n_2 (m^2/W)**	**Susceptibility $Re\chi^{(3)}$(esu)**
0.04	52.690337	1.357	8.6013×10^{-12}	4.02×10^{-6}
0.08	76.259239	1.357	1.5271×10^{-11}	7.13×10^{-6}
0.12	117.858328	1.357	1.8241×10^{-11}	8.52×10^{-6}
Ag NWs D50 Wavelength (650 nm), power (13.6 mW) and intensity (13.32 MW/m^2)				
Concentration (mg/ml)	**Linear absorption coefficient α (m^{-1})**	**Linear refractive index n_o**	**Nonlinear Refractive index -n_2 (m^2/W)**	**Susceptibility $Re\chi^{(3)}$(esu)**
0.04	43.816878	1.357	4.6769×10^{-12}	2.20×10^{-6}
0.08	64.17386267	1.357	7.4309×10^{-12}	3.49×10^{-6}
0.12	97.135934	1.357	1.2535×10^{-11}	5.8910^{-6}

4.4.1.3 Nonlinear optical properties for Ag NWs D100

Fig. (4.27) shows the nonlinear change of optical transmittance of Ag NWs D100 at three different concentrations. The nonlinear change of these samples was

examined at four wavelengths covering the visible region of the electromagnetic spectrum as mentioned earlier. Nonlinear investigation showed that the suspension of Ag NWs D100 has a defocusing nonlinear refraction in ethanol over the visible region and all the samples have negative refractive indices at all the wavelengths.

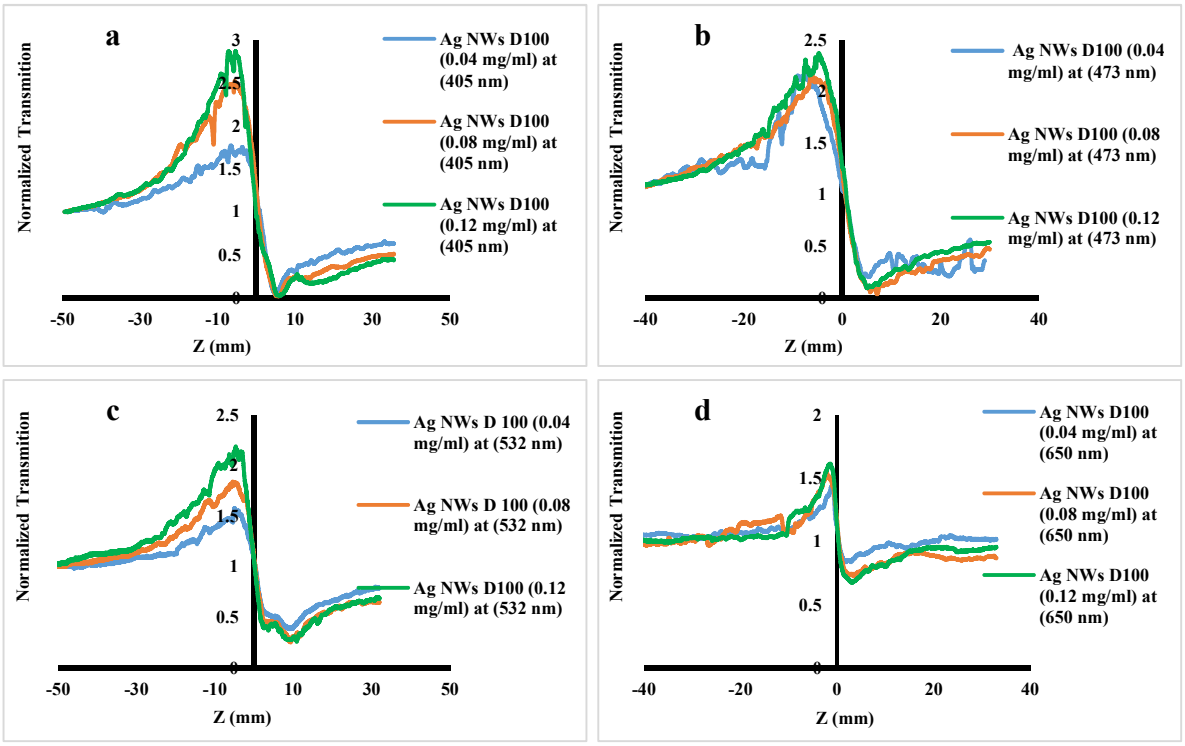

Fig (4.27): Z-scan closed aperture curves for Ag NWs D100 suspension in three concentrations ((0.04, 0.08 and 0.12) mg/ml), with excitation wavelength (a) 405 nm, (b) 473 nm, (c) 532 nm, and (d) 650 nm and powers of (2.2, 8.7, 15.8, and 13.8 mW) respectively.

Figs. (4.27 a, b, c and d) show that the nonlinear change increases with increasing concentrations and depends on the wavelength.

Table (4.3): The values of n_2 and $Re\chi^{(3)}$ at different concentrations and wavelengths for spherical Ag NWs D100

Ag NWs D100 Wavelength (405 nm), power (2.2 mW) and intensity (13.83 MW/m^2)				
Concentration (mg/ml)	Linear absorption coefficient α (m^{-1})	Linear refractive index n_o	Nonlinear Refractive index -n_2 (m^2/W)	Susceptibility $Re\chi^{(3)}$(esu)
0.04	28.4754435	1.357	1.9190×0^{-11}	8.959×10^{-6}
0.08	51.56649859	1.357	2.8097×0^{-11}	1.311×10^{-5}
0.12	67.00857419	1.357	3.2130×0^{-11}	1.500×10^{-5}
Ag NWs D100 Wavelength (473 nm), power (8.7 mW) and intensity (9.03 MW/m^2)				
Concentration (mg/ml)	Linear absorption coefficient α (m^{-1})	Linear refractive index n_o	Nonlinear Refractive index -n_2 (m^2/W)	Susceptibility $Re\chi^{(3)}$(esu)
0.04	21.01136932	1.357	4.1619×0^{-11}	1.94×10^{-5}
0.08	37.69074447	1.357	4.5936×0^{-11}	2.14×10^{-5}
0.12	48.2888434	1.357	4.8943×0^{-11}	2.29×10^{-5}
Ag NWs D100 Wavelength (532 nm), power (15.6 mW) and intensity (8.21 MW/m^2)				
Concentration (mg/ml)	Linear absorption coefficient α (m^{-1})	Linear refractive index n_o	Nonlinear Refractive index -n_2 (m^2/W)	Susceptibility $Re\chi^{(3)}$(esu)
0.04	14.90624427	1.357	3.1235×0^{-11}	1.46×10^{-5}
0.08	26.79069664	1.357	4.1790×0^{-11}	1.95×10^{-5}
0.12	33.72387814	1.357	5.0948×0^{-11}	2.38×10^{-5}
Ag NWs D100 Wavelength (650 nm), power (13.6 mW) and intensity (13.32 MW/m^2)				
Concentration (mg/ml)	Linear absorption coefficient α (m^{-1})	Linear refractive index n_o	Nonlinear Refractive index -n_2 (m^2/W)	Susceptibility $Re\chi^{(3)}$(esu)
0.04	10.39141748	1.357	1.1500×0^{-11}	5.37×10^{-6}
0.08	19.24942079	1.357	1.6099×0^{-11}	7.52×10^{-6}
0.12	23.52227904	1.357	1.8295×0^{-11}	8.54×10^{-6}

From observing the nonlinear refractive index values and the third-order nonlinear optical susceptibility values listed in Table (4.3), we find that the highest values of the linear absorption index were recorded at wavelength (405 nm) and this is expected because this wavelength is located at the top of the linear absorption spectrum of the Ag NWs D100. The highest values of the nonlinear refractive index and the third-order nonlinear optical susceptibility values were recorded at the wavelength (473 nm), and as we mentioned earlier, that this wavelength is located in the region of the broadband linear absorption spectrum of this material, that is,

within the effective region of absorption. The highest value of the nonlinear refractive index and the third-order nonlinear optical susceptibility were recorded at a concentration of (0.12 mg/ml) at (473 nm) and power of (7.8 mW) for the laser beam used. The lowest value for these two factors were recorded for a concentration of (0.04 mg/ml) at (650 nm).

4.4.1.4 Nonlinear optical properties for Ag NWs D200

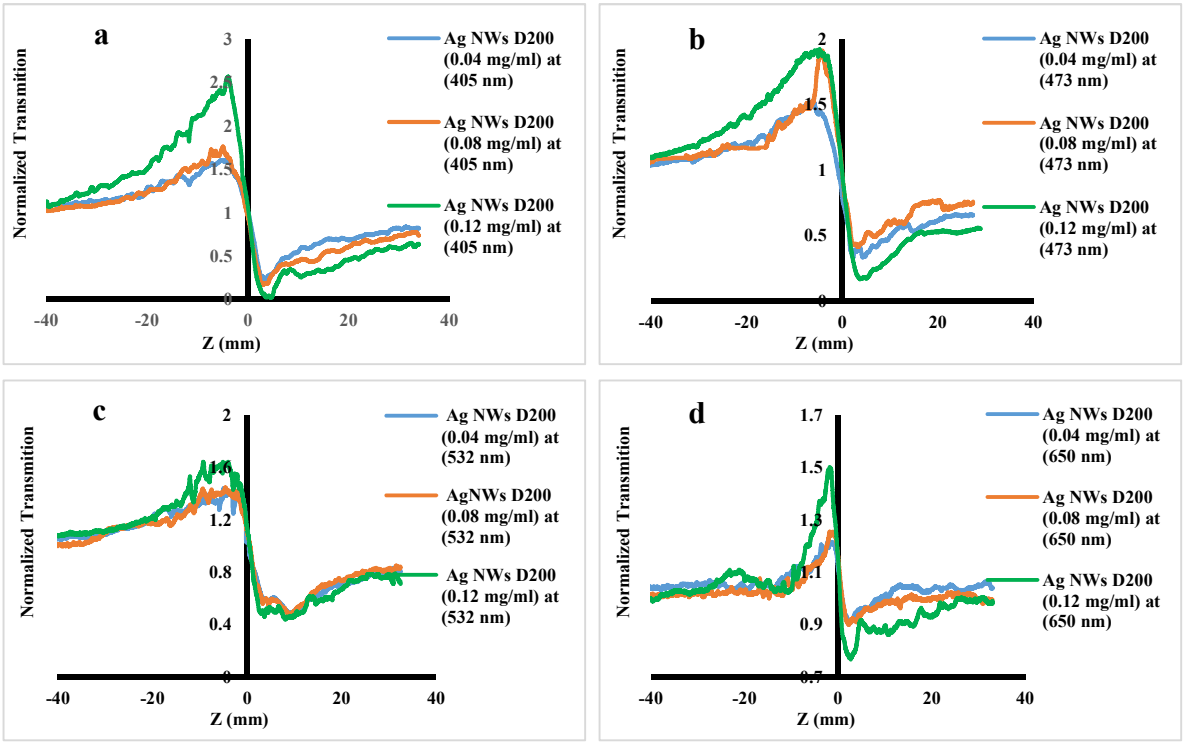

Fig (4.28): Z-scan closed aperture curves for Ag NWs D200 suspension in three concentrations ((0.04, 0.08 and 0.12) mg/ml), with excitation wavelength (a) 405 nm, (b) 473 nm, (c) 532 nm, and (d) 650 nm and powers of (2.2, 8.7, 15.8, and 13.8 mW) respectively.

Fig. (4.28) shows the nonlinear change of optical transmittance of Ag NWs D200 at three different concentrations. The nonlinear change of these samples was examined at four wavelengths covering the visible region of the electromagnetic spectrum as mentioned earlier. Nonlinear investigation showed that the suspension

of Ag NWs D200 has a defocusing nonlinear refraction in ethanol over the visible region. All the samples have negative refractive indices at all the wavelengths. Figs. (4.27 a, b, c and d) show that the nonlinear change increases with increasing concentrations and depends on the amount of wavelength.

Table (4.4): The values of n_2 and $Re\chi^{(3)}$ at different concentrations and wavelengths for spherical Ag NWs D200

Ag NWs D200 Wavelength (405 nm), power (2.2 mW) and intensity (14.84 MW/m^2)				
Concentration (mg/ml)	**Linear absorption coefficient α (m^{-1})**	**Linear refractive index n_o**	**Nonlinear Refractive index -n_2 (m^2/W)**	**Susceptibility $Re\chi^{(3)}$(esu)**
0.04	12.62041441	1.357	1.5354×0^{-11}	7.1684×10^{-6}
0.08	20.57382491	1.357	1.7631×0^{-11}	8.2316×10^{-6}
0.12	36.64751106	1.357	2.8339×0^{-11}	1.3231×10^{-5}
Ag NWs D200 Wavelength (473 nm), power (8.7 mW) and intensity (9.03 MW/m^2)				
Concentration (mg/ml)	**Linear absorption coefficient α (m^{-1})**	**Linear refractive index n_o**	**Nonlinear Refractive index -n_2 (m^2/W)**	**Susceptibility $Re\chi^{(3)}$(esu)**
0.04	11.8680499	1.357	2.5408×0^{-11}	1.19×10^{-5}
0.08	19.18286409	1.357	3.1779×0^{-11}	1.48×10^{-5}
0.12	34.36290947	1.357	3.7441×0^{-11}	1.75×10^{-5}
Ag NWs D200 Wavelength (532 nm), power (15.6 mW) and intensity (8.21 MW/m^2)				
Concentration (mg/ml)	**Linear absorption coefficient α (m^{-1})**	**Linear refractive index n_o**	**Nonlinear Refractive index -n_2 (m^2/W)**	**Susceptibility $Re\chi^{(3)}$(esu)**
0.04	10.89915221	1.357	2.5110×0^{-11}	1.17×10^{-5}
0.08	17.48176593	1.357	2.5522×0^{-11}	1.20×10^{-5}
0.12	31.32960258	1.357	3.1780×0^{-11}	1.49×10^{-5}
Ag NWs D200 Wavelength (650 nm), power (13.6 mW) and intensity (13.32 MW/m^2)				
Concentration (mg/ml)	**Linear absorption coefficient α (m^{-1})**	**Linear refractive index n_o**	**Nonlinear Refractive index -n_2 (m^2/W)**	**Susceptibility $Re\chi^{(3)}$(esu)**
0.04	9.738644922	1.357	5.9483×0^{-12}	2.78×10^{-6}
0.08	15.57964147	1.357	6.8817×0^{-12}	3.21×10^{-6}
0.12	28.17776796	1.357	1.4321×0^{-11}	6.69×10^{-6}

From observing the nonlinear refractive index values and the third-order nonlinear optical susceptibility values listed in Table (4.4), we find that the highest values of the linear absorption index were recorded at wavelength (405 nm) and this

is expected because this wavelength is located at the top of the linear absorption spectrum of Ag NWs D200. The highest values of the nonlinear refractive index and the third-order nonlinear optical susceptibility values were recorded at the wavelength (473 nm), and as we mentioned earlier that this wavelength is located in the region of the broadband of the linear absorption spectrum of this material, that is, within the effective region of absorption. The highest value of the nonlinear refractive index and the third-order nonlinear optical susceptibility were recorded at a concentration of (0.12 mg/ml) at a wavelength of (473 nm) and a power of (7.8 mW) for the laser beam used. The lowest value for these two factors were recorded for a concentration of (0.04 mg/ml) at a wavelength of (650 nm).

By reviewing the results in Tables (2, 3 and 4) for Ag NWs with diameters (50, 100 and 200) nm respectively, we note that the highest values of the two nonlinear optical properties were recorded for Ag NWs D100, which is a diameter that lies between the other two diameters used. According to the results of the researchers in [139]. The thermal conductivity of the silver nanowire increases with decreasing the diameter of the silver nanowire. The non-linear changes in this study depend on the heat resulting from the non-radiative electronic transitions and the transfer of this heat to the host and cause the occurrence of nonlinear optical changes, and based on the above, the highest results are supposed to be recorded for Ag NWs D50. The highest values recorded for Ag NWs are D100. This may be attributed to the fact that the high thermal conductivity of the small diameter silver nanowire leads to rapid heat exchange between the nanowire and the host and the heat drains quickly, resulting in unsustainable thermal change of the host material, which in turn affects the value of the nonlinear properties. For Ag NWs D100, its diameter is twice as large, meaning that its thermal conductivity is lower than that of Ag NWs D50,

but the highest results were recorded for this value of diameters for nanowires. The reason for this is likely to be that there is a state of proportionality between the width of this wire and the amount of heat transmitted from it to the host, so that the thermal conductivity between it and the host provides a longer sustainability to maintain the temperature sufficient to cause a non-linear turbulence in the host material. Thus provide a longer perturbation time and better non-linear results . For Ag NWs D200, the thermal conductivity is lower due to the increase in diameter, so the heat will be dispersed along the nanowire body and thus not a large amount of heat is transmitted to the host and thus obtaining lower values for nonlinear optical changes.

4.4.2 Nonlinear optical properties for (Cu) nanoparticles group

We have mentioned that in this group, we have three samples, two of them are spherical of two different sizes and the other is wire-shaped. The nonlinear properties were measured using four wavelengths covering the visible region of the spectrum like all other samples of materials.

4.4.2.1 Nonlinear optical properties for Cu1

From Fig. (4.29 a, b, c and d), it is clear that all the samples have negative refractive indices at all the wavelengths. Later, we will discuss the effect of changing the concentrations, and the wavelengths of the laser beam used, and the size of this sample and the other sample Cu2 material on the nonlinear optical properties.

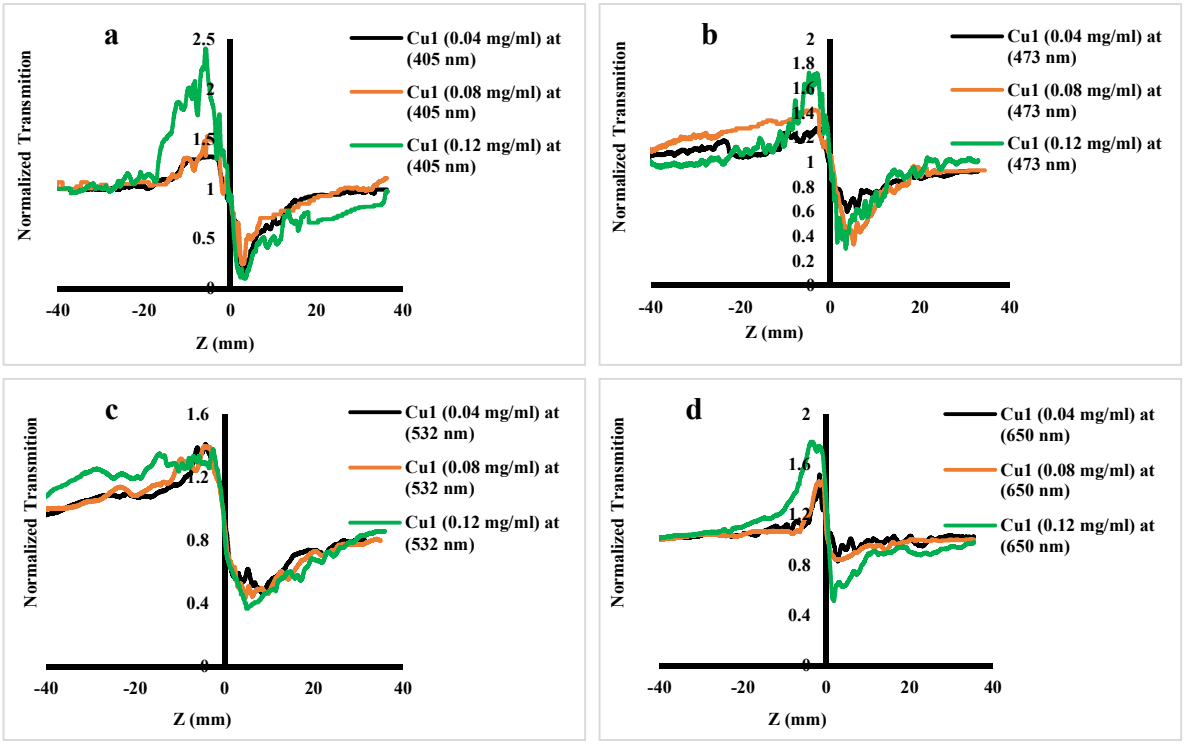

Fig (4.29): Z-scan closed aperture curves for spherical Cu1 suspension in three concentrations ((0.04, 0.08 and 0.12) mg/ml), with excitation wavelength (a) 405 nm, (b) 473 nm, (c) 532 nm, and (d) 650 nm and powers of (2, 4.8, 11, and 13.8 mW) respectively.

Table (4.5): The values of n_2 and $Re\chi^{(3)}$ at different concentrations and wavelengths for spherical Cu1

Cu1 Wavelength (405 nm), power (2 mW) and intensity (13.49 MW/m^2)				
Concentration (mg/ml)	Linear absorption coefficient α (m^{-1})	Linear refractive index n_o	Nonlinear Refractive index -n_2 (m^2/W)	Susceptibility $Re\chi^{(3)}$(esu)
0.04	10.55081067	1.358	1.38901×10^{-11}	6.49443×10^{-6}
0.08	17.59729977	1.358	1.55094×10^{-11}	7.25153×10^{-6}
0.12	29.06854277	1.358	2.80042×10^{-11}	1.31357×10^{-5}
Cu1 Wavelength (473 nm), power (4.8 mW) and intensity (4.98 MW/m^2)				
Concentration (mg/ml)	Linear absorption coefficient α (m^{-1})	Linear refractive index n_o	Nonlinear Refractive index -n_2 (m^2/W)	Susceptibility $Re\chi^{(3)}$(esu)
0.04	10.803373	1.358	2.60268×10^{-11}	1.22×10^{-5}
0.08	17.96078993	1.358	4.19359×10^{-11}	1.96×10^{-5}
0.12	29.9675572	1.358	5.51246×10^{-11}	2.58×10^{-5}
Cu1 Wavelength (532 nm), power (11 mW) and intensity (5.79 MW/m^2)				
Concentration (mg/ml)	Linear absorption coefficient α (m^{-1})	Linear refractive index n_o	Nonlinear Refractive index -n_2 (m^2/W)	Susceptibility $Re\chi^{(3)}$(esu)
0.04	10.7027319	1.358	3.48738×10^{-11}	1.63×10^{-5}
0.08	18.1119435	1.358	3.57677×10^{-11}	1.67×10^{-5}
0.12	30.05983073	1.358	3.76659×10^{-11}	1.76×10^{-5}
Cu1 Wavelength (650 nm), power (13.8 mW) and intensity (13.51 MW/m^2)				
Concentration (mg/ml)	Linear absorption coefficient α (m^{-1})	Linear refractive index n_o	Nonlinear Refractive index -n_2 (m^2/W)	Susceptibility $Re\chi^{(3)}$(esu)
0.04	10.2278533	1.358	1.07863×10^{-11}	5.04×10^{-6}
0.08	17.2773363	1.358	1.27831×10^{-11}	5.98×10^{-6}
0.12	28.62797887	1.358	2.42779×10^{-11}	1.14×10^{-5}

From observing the results listed in Table (4.5), we find that the highest values of the nonlinear refractive index and the nonlinear third order susceptibility of the Cu1 sample were recorded at wavelength (473 nm) and wavelength (532 nm) because they are located at the highest values of linear absorption for this sample, although its linear absorption curve appeared flat. The effect of changing the concentrations was noticeable at the wavelengths (473 and 405) nm, where the nonlinear optical properties values increased with increasing the concentration. The

effect of changing the concentration of the nonlinear optical properties was very slight at the wavelength (532 and 650) nm.

4.4.2.2 Nonlinear optical properties for Cu2

As for Cu1, from the Fig. (4.30 a, b, c and d) all the samples have negative refractive indices at all the wavelengths.

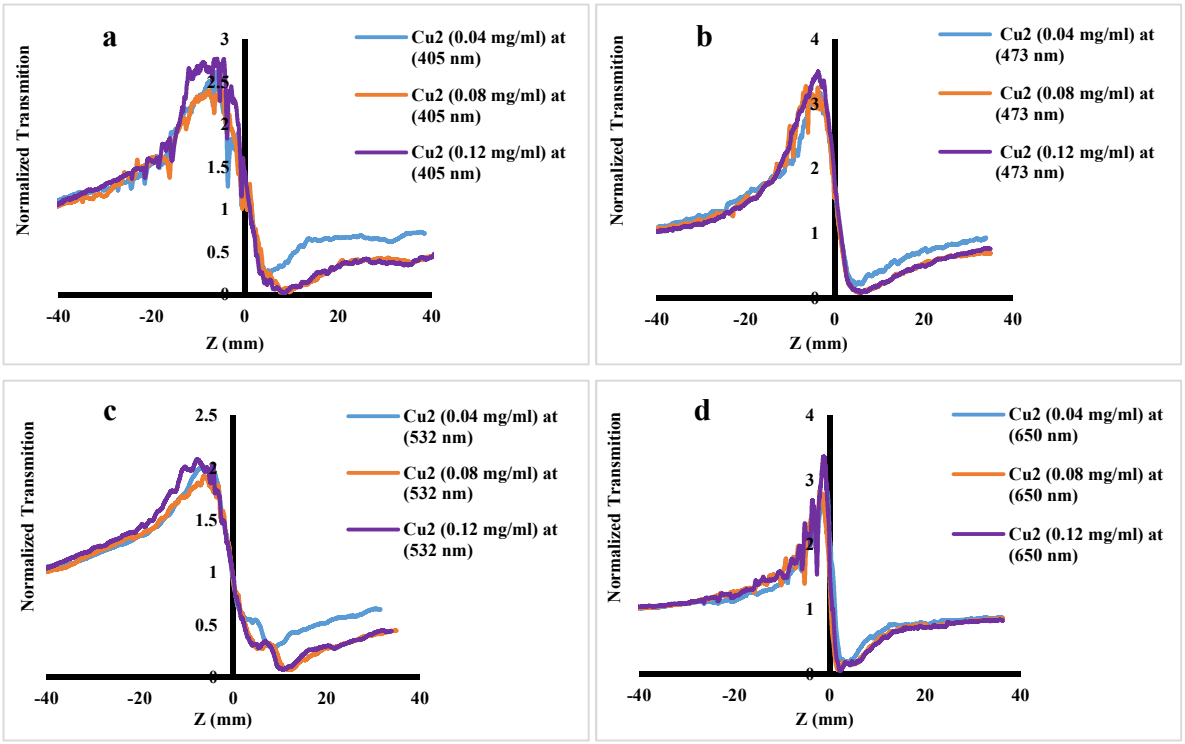

Fig (4.30): Z-scan closed aperture curves for spherical Cu2 suspension in three concentrations ((0.04, 0.08 and 0.12) mg/ml), with excitation wavelength (a) 405 nm, (b) 473 nm, (c) 532 nm, and (d) 650 nm and powers of (2, 4.8, 11, and 13.8 mW) respectively.

Table (4.6): The values of n_2 and $Re\chi^{(3)}$ at different concentrations and wavelengths for spherical Cu2

Cu2 Wavelength (405 nm), power (2 mW) and intensity (13.49 MW/m^2)				
Concentration (mg/ml)	Linear absorption coefficient α (m^{-1})	Linear refractive index n_o	Nonlinear Refractive index -n_2 (m^2/W)	Susceptibility $Re\chi^{(3)}$(esu)
0.04	48.17476813	1.358	2.90536×10^{-11}	1.35843×10^{-5}
0.08	72.0889666	1.358	2.99383×10^{-11}	1.39979×10^{-5}
0.12	85.83181203	1.358	3.45236×10^{-11}	1.61418×10^{-5}
Cu2 Wavelength (473 nm), power (4.8 mW) and intensity (4.98 MW/m^2)				
Concentration (mg/ml)	Linear absorption coefficient α (m^{-1})	Linear refractive index n_o	Nonlinear Refractive index -n_2 (m^2/W)	Susceptibility $Re\chi^{(3)}$(esu)
0.04	48.7858308	1.358	1.13795×10^{-10}	5.32×10^{-5}
0.08	72.2432676	1.358	1.23016×10^{-10}	5.75×10^{-5}
0.12	86.6252723	1.358	1.32163×10^{-10}	6.18×10^{-5}
Cu2 Wavelength (532 nm), power (11 mW) and intensity (5.79 MW/m^2)				
Concentration (mg/ml)	Linear absorption coefficient α (m^{-1})	Linear refractive index n_o	Nonlinear Refractive index -n_2 (m^2/W)	Susceptibility $Re\chi^{(3)}$(esu)
0.04	48.6331419	1.358	6.5518×10^{-11}	3.06×10^{-5}
0.08	71.64824917	1.358	7.06552×10^{-11}	3.30×10^{-5}
0.12	86.52632007	1.358	7.73128×10^{-11}	3.61×10^{-5}
Cu2 Wavelength (650 nm), power (13.8 mW) and intensity (13.51 MW/m^2)				
Concentration (mg/ml)	Linear absorption coefficient α (m^{-1})	Linear refractive index n_o	Nonlinear Refractive index -n_2 (m^2/W)	Susceptibility $Re\chi^{(3)}$(esu)
0.04	56.08825997	1.358	5.18867×10^{-11}	2.43×10^{-5}
0.08	84.38898253	1.358	5.50246×10^{-11}	2.57×10^{-5}
0.12	98.74534717	1.358	6.59321×10^{-11}	3.08×10^{-5}

From observing the results listed in Table (4.6), we find that the values of the linear absorption coefficient of the Cu2 sample seem to be stable at all wavelengths used at (0.12) mg/ml are very closed, except at the wavelength of (650 nm). At (650) nm some increase is recorded in this coefficient because this wavelength close to the top of the linear absorption spectrum of Cu2. The highest values of the nonlinear refractive index and third-order nonlinear optical susceptibility were recorded at the wavelength (473 nm), which is the highest values for all materials used in this thesis. The next highest value is at the wavelength (532 nm). However, it is seven times

lower than the values calculated at the wavelength (473 nm). The last two lowest values of the nonlinear refractive index were at (650 nm) and (405 nm) respectively.

In both samples Cu1 and Cu2, we notice that the values of the nonlinear refractive index and the third-order nonlinear susceptibility increase as the concentrations increases, however, despite the fact that the increase in concentrations is double, the increase in the nonlinear refractive index and the nonlinear susceptibility is small. The Cu2 sample showed much higher values than that of the Cu1 sample (the dominant size of the Cu2 (90-99) nm and the dominant size of the Cu1 particles being around (40-50) nm). This is due, according to the researchers' results in [147], to the fact that the nonlinear refractive index increases nonlinearly with the increase in the particle size. This increase can be attributed to the increase in the ratio between the linear absorption and the thermal diffusivity (α/D, since α is linear absorption and D is thermal diffusivity), which is the main factor that affect the thermal nonlinear refraction [140].

4.4.2.3 Nonlinear optical properties for Cu NWs D50

From Fig. (4.31), it is clear that all the samples have negative refractive indices at all the wavelengths. From the results recorded in Table (4.7), we notice that the values of the nonlinear refractive index and the nonlinear third-order susceptibility increase with the increasing concentrations.

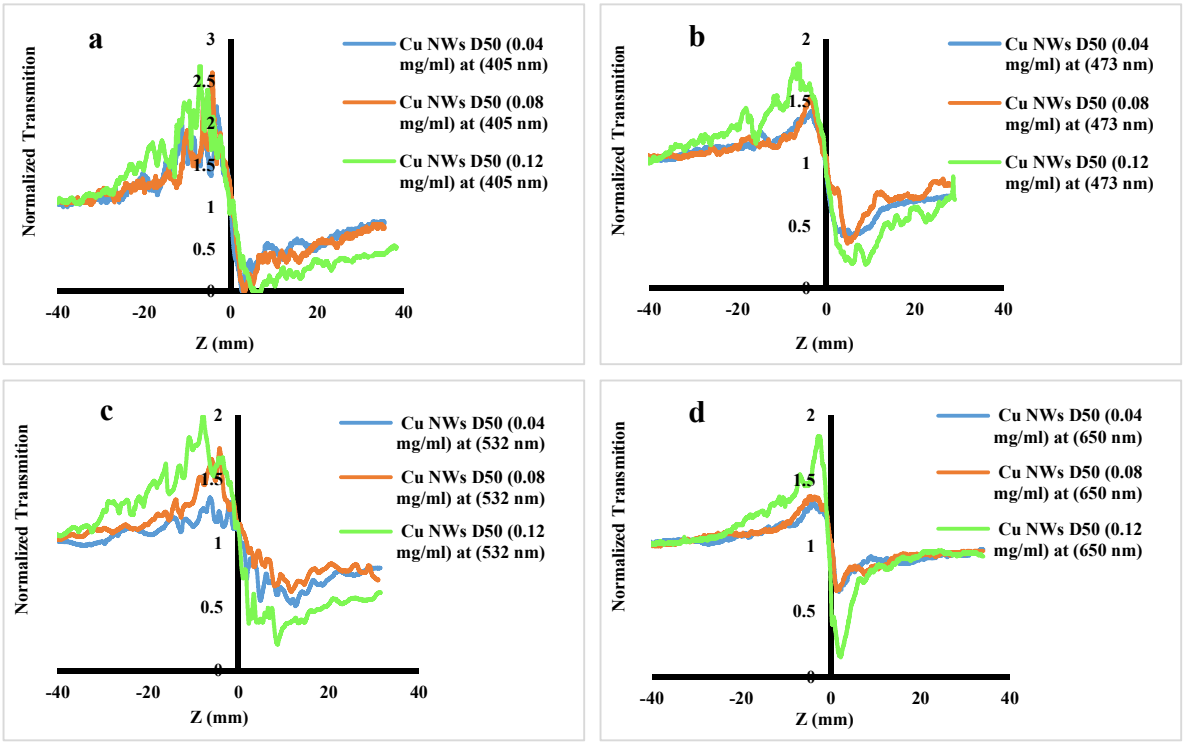

Fig (4.31): Z-scan closed aperture curves for Cu NWs D50 suspension in three concentrations ((0.04, 0.08 and 0.12) mg/ml), with excitation wavelength (a) 405 nm, (b) 473 nm, (c) 532 nm, and (d) 650 nm and powers of (2.2, 4.8, 13, and 13.8 mW) respectively.

The highest values were recorded at the wavelength (473 nm), followed by the wavelength (532 nm). Despite the different concentrations, the values of the linear absorption coefficient seem to be close to each other at all the values of the wavelengths used.

Table (4.7): The values of n_2 and $Re\chi^{(3)}$ at different concentrations and wavelengths for Cu NWs D50

Cu NWs D50 Wavelength (405 nm), power (2.2 mW) and intensity (14.83 MW/m^2)				
Concentration (mg/ml)	**Linear absorption coefficient α (m^{-1})**	**Linear refractive index n_o**	**Nonlinear Refractive index -n_2 (m^2/W)**	**Susceptibility $Re\chi^{(3)}$(esu)**
0.04	21.3398283	1.358	2.42832×10^{-11}	1.135×10^{-5}
0.08	27.30475183	1.358	2.87837×10^{-11}	1.345×10^{-5}
0.12	37.85801903	1.358	2.98170×10^{-11}	1.394×10^{-5}
Cu NWs D50 Wavelength (473 nm), power (4.8 mW) and intensity (4.98 MW/m^2)				
Concentration (mg/ml)	**Linear absorption coefficient α (m^{-1})**	**Linear refractive index n_o**	**Nonlinear Refractive index -n_2 (m^2/W)**	**Susceptibility $Re\chi^{(3)}$(esu)**
0.04	21.2668232	1.358	3.8388×10^{-11}	1.79×10^{-5}
0.08	26.70981017	1.358	4.4968×10^{-11}	2.10×10^{-5}
0.12	38.63896633	1.358	6.2503×10^{-11}	2.92×10^{-5}
Cu NWs D50 Wavelength (532 nm), power (13 mW) and intensity (6.84 MW/m^2)				
Concentration (mg/ml)	**Linear absorption coefficient α (m^{-1})**	**Linear refractive index n_o**	**Nonlinear Refractive index -n_2 (m^2/W)**	**Susceptibility $Re\chi^{(3)}$(esu)**
0.04	21.35172713	1.358	2.6732×10^{-11}	1.25×10^{-5}
0.08	26.3909982	1.358	3.5480×10^{-11}	1.66×10^{-5}
0.12	38.69876757	1.358	5.6793×10^{-11}	2.66×10^{-5}
Cu NWs D50 Wavelength (650 nm), power (13.8 mW) and intensity (13.51 MW/m^2)				
Concentration (mg/ml)	**Linear absorption coefficient α (m^{-1})**	**Linear refractive index n_o**	**Nonlinear Refractive index -n_2 (m^2/W)**	**Susceptibility $Re\chi^{(3)}$(esu)**
0.04	23.08404373	1.358	1.3075×10^{-11}	6.11×10^{-6}
0.08	28.31715063	1.358	1.3855×10^{-11}	6.48×10^{-6}
0.12	42.31724117	1.358	3.2648×10^{-11}	1.53×10^{-5}

4.4.3 Nonlinear optical properties for (Au) nanoparticles group

From Figs. (4.32, 33 and 34), it clear that all the samples (Au1, Au2 and Au3) have negative refractive indices at all the wavelengths. From the results recorded in Tables (4.8, 4.9 and 4.10), we notice that the values of the nonlinear refractive index and the nonlinear third-order susceptibility increase with increasing concentrations. The highest values were recorded at wavelength (473 nm), followed by wavelength (405 nm) for the sample (Au2).

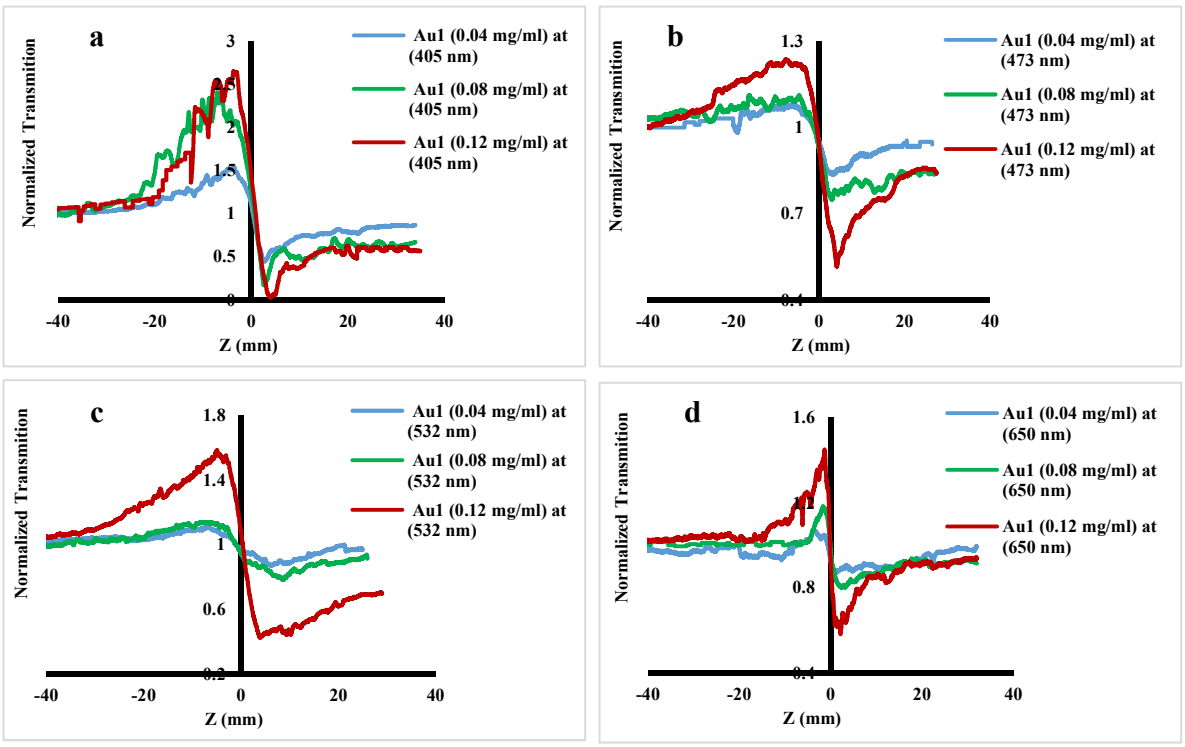

Fig (4.32): Z-scan closed aperture curves for Au1 suspension in three concentrations ((0.04, 0.08 and 0.12) mg/ml), with excitation wavelength (a) 405 nm, (b) 473 nm, (c) 532 nm, and (d) 650 nm and powers of (2.2, 2, 11, and 13.8 mW) respectively.

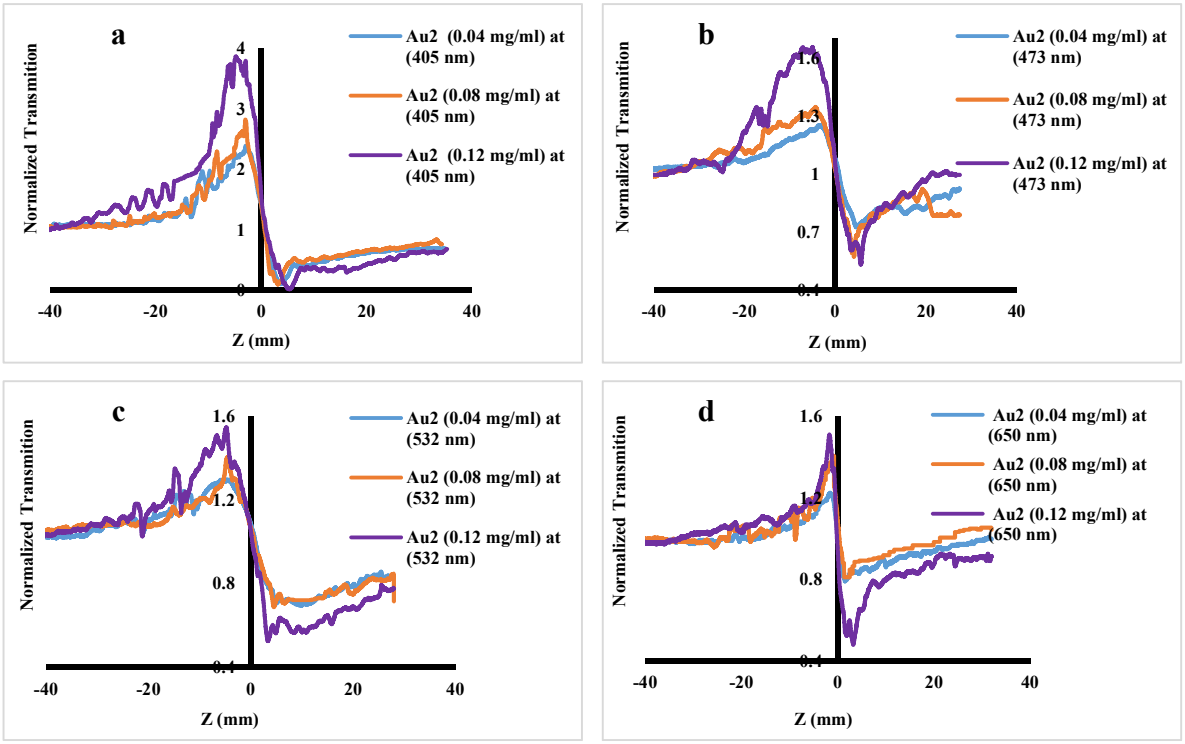

Fig (4.33): Z-scan closed aperture curves for Au2 suspension in three concentrations ((0.04, 0.08 and 0.12) mg/ml), with excitation wavelength (a) 405 nm, (b) 473 nm, (c) 532 nm, and (d) 650 nm and powers of (2.2, 2, 11, and 13.8 mW) respectively.

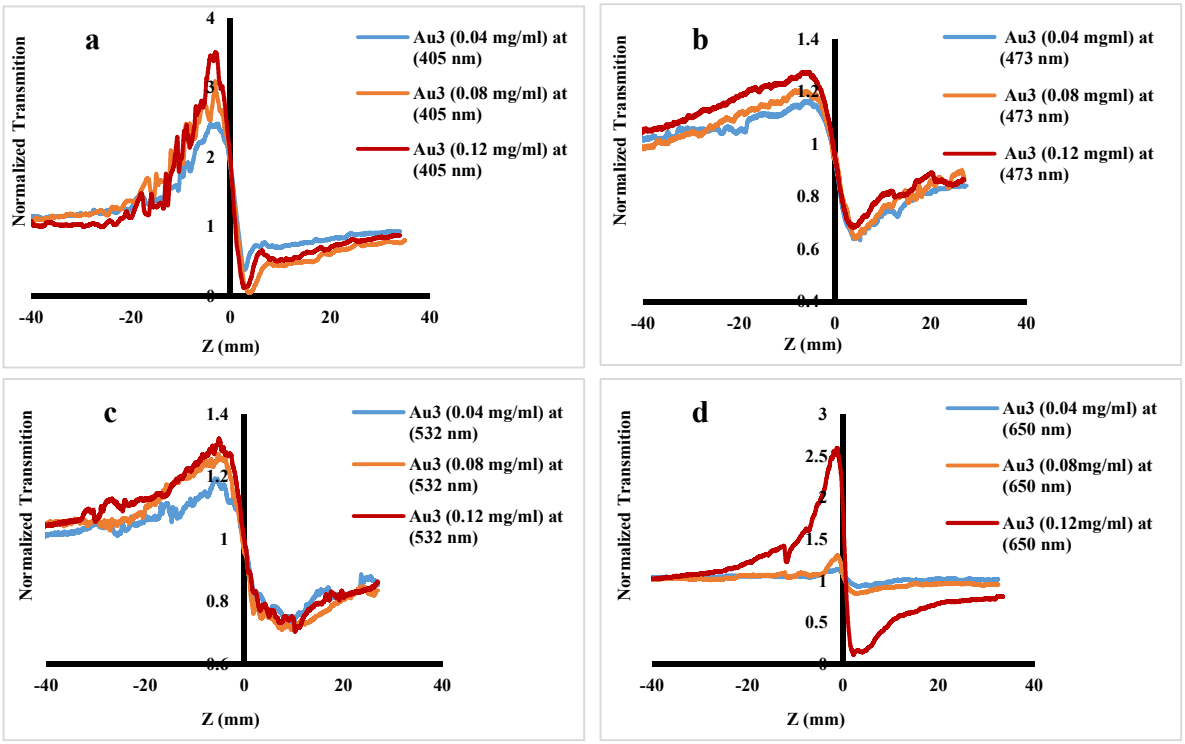

Fig (4.34): Z-scan closed aperture curves for Au3 suspension in three concentrations ((0.04, 0.08 and 0.12) mg/ml), with excitation wavelength (a) 405 nm, (b) 473 nm, (c) 532 nm, and (d) 650 nm and powers of (2.2, 2, 11, and 13.8 mW) respectively.

Table (4.8): The values of n_2 and $Re\chi^{(3)}$ at different concentrations and wavelengths for Au1

Au1 Wavelength (405 nm), power (2.2 mW) and intensity (14.84 MW/m^2)				
Concentration (mg/ml)	Linear absorption coefficient α (m^{-1})	Linear refractive index n_o	Nonlinear Refractive index -n_2 (m^2/W)	Susceptibility $Re\chi^{(3)}$(esu)
0.04	7.6445782	1.357	1.21749×0^{-11}	5.68408×10^{-6}
0.08	11.9703031	1.357	2.46451×0^{-11}	1.15060×10^{-5}
0.12	17.94420833	1.357	2.89471×0^{-11}	1.35145×10^{-5}
Au1 Wavelength (473 nm), power (2 mW) and intensity (2.07 MW/m^2)				
Concentration (mg/ml)	Linear absorption coefficient α (m^{-1})	Linear refractive index n_o	Nonlinear Refractive index -n_2 (m^2/W)	Susceptibility $Re\chi^{(3)}$(esu)
0.04	7.2887647	1.357	2.24573×0^{-11}	1.05×10^{-5}
0.08	12.05843123	1.357	3.32850×0^{-11}	1.55×10^{-5}
0.12	18.59296343	1.357	6.65056×0^{-11}	3.10×10^{-5}
Au1 Wavelength (532 nm), power (11 mW) and intensity (5.79 MW/m^2)				
Concentration (mg/ml)	Linear absorption coefficient α (m^{-1})	Linear refractive index n_o	Nonlinear Refractive index -n_2 (m^2/W)	Susceptibility $Re\chi^{(3)}$(esu)
0.04	7.700924933	1.357	8.92001×0^{-12}	4.16×10^{-6}
0.08	13.3097279	1.357	1.31963×0^{-11}	6.16×10^{-6}
0.12	20.522033	1.357	4.31816×0^{-11}	2.02×10^{-5}
Au1 Wavelength (650 nm), power (13.8 mW) and intensity (13.51 MW/m^2)				
Concentration (mg/ml)	Linear absorption coefficient α (m^{-1})	Linear refractive index n_o	Nonlinear Refractive index -n_2 (m^2/W)	Susceptibility $Re\chi^{(3)}$(esu)
0.04	6.315209833	1.357	4.1508×0^{-12}	1.94×10^{-6}
0.08	10.72860227	1.357	7.2769×0^{-12}	3.40×10^{-6}
0.12	15.10107807	1.357	1.6563×0^{-11}	7.73×10^{-6}

Table (4.9): The values of n_2 and $Re\chi^{(3)}$ at different concentrations and wavelengths for Au2

Au2 Wavelength (405 nm), power (2.2 mW) and intensity (14.84 MW/m^2)				
Concentration (mg/ml)	**Linear absorption coefficient α (m^{-1})**	**Linear refractive index n_o**	**Nonlinear Refractive index -n_2 (m^2/W)**	**Susceptibility $Re\chi^{(3)}$(esu)**
0.04	15.79988503	1.357	2.51671×10^{-11}	1.17497×10^{-5}
0.08	22.96244533	1.357	3.01435×10^{-11}	1.40731×10^{-5}
0.12	26.91001763	1.357	4.26584×10^{-11}	1.99159×10^{-5}
Au21 Wavelength (473 nm), power (2 mW) and intensity (2.07 MW/m^2)				
Concentration (mg/ml)	**Linear absorption coefficient α (m^{-1})**	**Linear refractive index n_o**	**Nonlinear Refractive index -n_2 (m^2/W)**	**Susceptibility $Re\chi^{(3)}$(esu)**
0.04	16.38231373	1.357	4.83056×10^{-11}	2.26×10^{-5}
0.08	23.6969488	1.357	7.15874×10^{-11}	3.34×10^{-5}
0.12	27.4278088	1.357	1.03968×10^{-10}	4.85×10^{-5}
Au2 Wavelength (532nm), power (11 mW) and intensity (5.79 MW/m^2)				
Concentration (mg/ml)	**Linear absorption coefficient α (m^{-1})**	**Linear refractive index n_o**	**Nonlinear Refractive index -n_2 (m^2/W)**	**Susceptibility $Re\chi^{(3)}$(esu)**
0.04	16.5290916	1.357	2.23783×10^{-11}	1.04×10^{-5}
0.08	23.98751063	1.357	2.66239×10^{-11}	1.24×10^{-5}
0.12	27.91044083	1.357	3.80557×10^{-11}	1.78×10^{-5}
Au2 Wavelength (650 nm), power (13.8 mW) and intensity (13.51 MW/m^2)				
Concentration (mg/ml)	**Linear absorption coefficient α (m^{-1})**	**Linear refractive index n_o**	**Nonlinear Refractive index -n_2 (m^2/W)**	**Susceptibility $Re\chi^{(3)}$(esu)**
0.04	15.22751277	1.357	8.28249×10^{-12}	3.87×10^{-6}
0.08	21.9696988	1.357	1.13709×10^{-11}	5.31×10^{-6}
0.12	26.3886952	1.357	1.97409×10^{-11}	9.22×10^{-6}

Table (4.10): The values of n_2 and $Re\chi^{(3)}$ at different concentrations and wavelengths for Au3

Au3 Wavelength (405 nm), power (2.2 mW) and intensity (14.84 MW/m^2)				
Concentration (mg/ml)	Linear absorption coefficient α (m^{-1})	Linear refractive index n_o	Nonlinear Refractive index -n_2 (m^2/W)	Susceptibility $Re\chi^{(3)}$(esu)
0.04	11.24132683	1.357	2.3063×10^{-11}	1.076×10^{-5}
0.08	18.8505156	1.357	3.3637×10^{-11}	1.570×10^{-5}
0.12	25.5022705	1.357	3.7561×10^{-11}	1.753×10^{-5}
Au3 Wavelength (473nm), power (2.2 mW) and intensity (2.28 MW/m^2)				
Concentration (mg/ml)	Linear absorption coefficient α (m^{-1})	Linear refractive index n_o	Nonlinear Refractive index -n_2 (m^2/W)	Susceptibility $Re\chi^{(3)}$(esu)
0.04	12.03448003	1.357	4.4515×10^{-11}	2.08×10^{-5}
0.08	20.16721747	1.357	4.7332×10^{-11}	2.21×10^{-5}
0.12	27.13056827	1.357	4.9486×10^{-11}	2.31×10^{-5}
Au3 Wavelength (532 nm), power (11 mW) and intensity (5.79 MW/m^2)				
Concentration (mg/ml)	Linear absorption coefficient α (m^{-1})	Linear refractive index n_o	Nonlinear Refractive index -n_2 (m^2/W)	Susceptibility $Re\chi^{(3)}$(esu)
0.04	13.17953163	1.357	1.72035×10^{-11}	8.03×10^{-6}
0.08	22.5675576	1.357	2.09314×10^{-11}	9.77×10^{-6}
0.12	29.82008843	1.357	2.30415×10^{-11}	1.08×10^{-5}
Au3 Wavelength (650 nm), power (13.8 mW) and intensity (13.51 MW/m^2)				
Concentration (mg/ml)	Linear absorption coefficient α (m^{-1})	Linear refractive index n_o	Nonlinear Refractive index -n_2 (m^2/W)	Susceptibility $Re\chi^{(3)}$(esu)
0.04	11.82145253	1.357	4.1091×10^{-12}	1.92×10^{-6}
0.08	20.6708068	1.357	8.8999×10^{-12}	4.16×10^{-6}
0.12	26.23961433	1.357	4.7580×10^{-11}	2.22×10^{-5}

4.4.4 Nonlinear optical properties for (Fe_2O_3) Nano fragments

From Fig. (4.35), it is clear that all the samples have negative refractive indices at all the wavelengths. From the results recorded in Table (4.11), we notice that the values of the nonlinear refractive index and the nonlinear third-order susceptibility the increase with increasing concentrations.

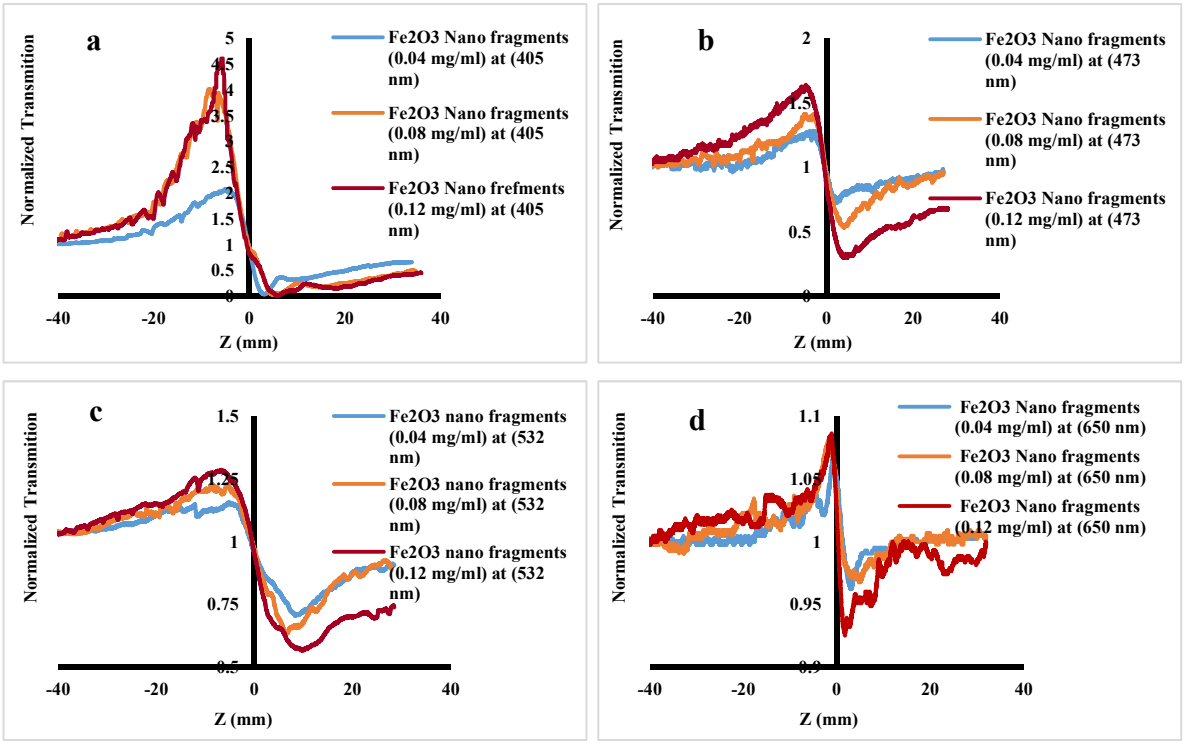

Fig (4.35): Z-scan closed aperture curves for Fe_2O_3 Nano fragments suspension in three concentrations ((0.04, 0.08 and 0.12) mg/ml), with excitation wavelength (a) 405 nm, (b) 473 nm, (c) 532 nm, and (d) 650 nm and powers of (2.2, 6, 13, and 13.8 mW) respectively.

The highest values of the nonlinear refractive indices and the nonlinear third-order susceptibilities were recorded at wavelength (405 nm), then it starts decreasing with increasing wavelength, that can be because that these wavelengths do not fall within the region of the linear absorption spectrum of (Fe2O3) Nano fragments. The highest values of the linear absorption coefficient were recorded at wavelength (405 nm) and these values decrease as the wavelength increase as well.

Table (4.11): The values of n_2 and $Re\chi^{(3)}$ at different concentrations and wavelengths for Fe_2O_3 Nano fragments

Fe_2O_3 Nano fragments Wavelength (405 nm), power (2.2 mW) and intensity (14.84 MW/m^2)				
Concentration (mg/ml)	Linear absorption coefficient α (m^{-1})	Linear refractive index n_o	Nonlinear Refractive index $-n_2$ (m^2/W)	Susceptibility $Re\chi^{(3)}$(esu)
0.04	21.78346287	1.359	2.25722×10^{-11}	1.0569×10^{-5}
0.08	40.47553207	1.359	4.44814×10^{-11}	2.0828×10^{-5}
0.12	49.64753663	1.359	5.16072×10^{-11}	2.4164×10^{-5}
Fe_2O_3 Nano fragments Wavelength (473 nm), power (6 mW) and intensity (6.22 MW/m^2)				
Concentration (mg/ml)	Linear absorption coefficient α (m^{-1})	Linear refractive index n_o	Nonlinear Refractive index $-n_2$ (m^2/W)	Susceptibility $Re\chi^{(3)}$(esu)
0.04	8.735355767	1.359	1.69553×10^{-11}	7.94×10^{-6}
0.08	13.07006237	1.359	2.69446×10^{-11}	1.26×10^{-5}
0.12	20.07003087	1.359	4.12158×10^{-11}	1.93×10^{-5}
Fe_2O_3 Nano fragments Wavelength (532 nm), power (13 mW) and intensity (6.84 MW/m^2)				
Concentration (mg/ml)	Linear absorption coefficient α (m^{-1})	Linear refractive index n_o	Nonlinear Refractive index $-n_2$ (m^2/W)	Susceptibility $Re\chi^{(3)}$(esu)
0.04	4.872143577	1.359	1.40477×10^{-11}	6.59×10^{-6}
0.08	4.871254331	1.359	1.8668×10^{-11}	8.75×10^{-6}
0.12	11.56697103	1.359	2.2351×10^{-11}	1.05×10^{-5}
Fe_2O_3 Nano fragments Wavelength (650 nm), power (13.8 mW) and intensity (13.51 MW/m^2)				
Concentration (mg/ml)	Linear absorption coefficient α (m^{-1})	Linear refractive index n_o	Nonlinear Refractive index $-n_2$ (m^2/W)	Susceptibility $Re\chi^{(3)}$(esu)
0.04	2.260778333	1.359	1.9467×10^{-12}	9.12×10^{-7}
0.08	2.235445333	1.359	2.1716×10^{-12}	1.02×10^{-6}
0.12	5.857526967	1.359	3.0512×10^{-12}	1.43×10^{-6}

4.4.5 Nonlinear optical properties for Mixtures group

4.4.5.1 Nonlinear optical properties for (Cu2+Ag NW D200)

From Figure (4.36), similar to the original materials of the mixture (Cu2 + Ag NW D200), it is clear that the mixtures have negative refractive indices at all wavelengths.

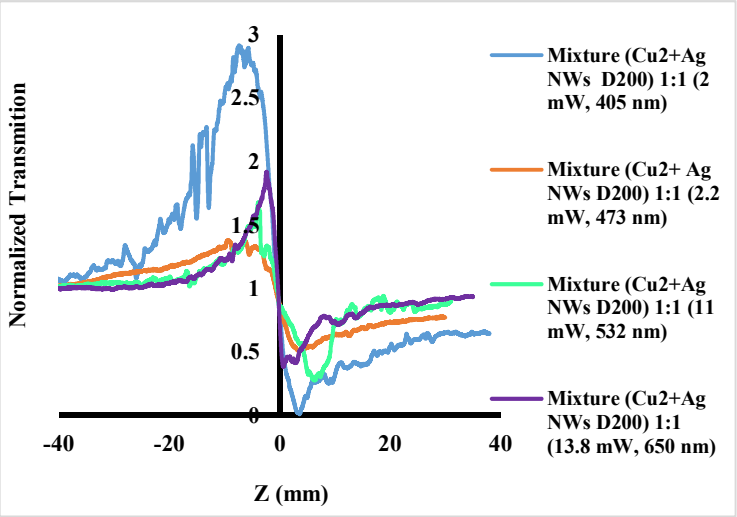

Fig (4.36): Z-scan closed aperture curves for Cu2+Ag NW D200 suspension with volume ratio (1:1) (0.12mg/ml), with CW laser wavelength (405 nm) with (2 mW), wave length (473 nm) with (2.2 mW), wave length (532 nm) with (11mW) and wave length (650 nm) with (13.8 mW)

From the results listed in Table (4.12), we note that the values of the nonlinear refractive index and the third-order nonlinear susceptibility are different from the values of their original materials. There is an improvement in the values of the nonlinear optical properties of Ag NWs D200. In addition, that the linear absorption coefficient of the mixture decreased by an average value of 56% in comparison to that of Ag NWs D200 and about 85% of that for Cu2. The highest values of the nonlinear refractive index and the third-order nonlinear susceptibility for the mixture were recorded at the wavelengths (473 nm) and (532 nm).

Table (4.12): The values of n_2 and $Re\chi^{(3)}$ at different wavelengths for Cu2+Ag NW D200

Material and Concentration (mg/ml)	Wavelength λ (nm)	Intensity (MW/m^2)	Linear absorption coefficient α (m^{-1})	Linear refractive index n_o	Nonlinear Refractive index $-n_2$ (m^2/W)	Susceptibility $Re\chi^{(3)}$ (esu)
Mixture of (Cu2 + Ag NWs D200) (0.12)	405	13.49	14.91955049	1.358	3.51699×10^{-11}	1.644×10^{-5}
	473	2.28	14.79920594	1.358	7.32736×10^{-11}	3.43×10^{-5}
	532	5.79	14.18885977	1.358	5.20102×10^{-11}	2.43×10^{-5}
	650	13.51	13.5175822	1.358	2.90940×10^{-11}	1.36×10^{-5}
Cu2 (0.12)	405	13.49	85.83181203	1.358	3.45236×10^{-11}	1.61×10^{-5}
	473	4.98	86.6252723	1.358	1.32163×10^{-10}	6.18×10^{-5}
	532	5.79	86.52632007	1.358	7.73128×10^{-11}	3.61×10^{-5}
	650	13.51	98.74534717	1.358	6.59321×10^{-11}	3.08×10^{-5}
Ag NWs D200 (0.12)	405	14.84	109.9425332	1.357	2.83396×0^{-11}	1.32×10^{-5}
	473	9.03	103.0887284	1.357	3.7441×0^{-11}	1.75×10^{-5}
	532	8.21	93.98880773	1.357	3.17805×0^{-11}	1.49×10^{-5}
	650	13.32	84.53330387	1.357	1.43215×0^{-11}	6.69×10^{-6}

4.4.5.2 Nonlinear optical properties for mixture of (Ag NPs + Cu NWs D50)

From Figure (4.37), such as that of the original materials of the mixture (Ag NPs + Cu NWs D50), it is clear that the mixture have a negative refractive indices at all wavelengths.

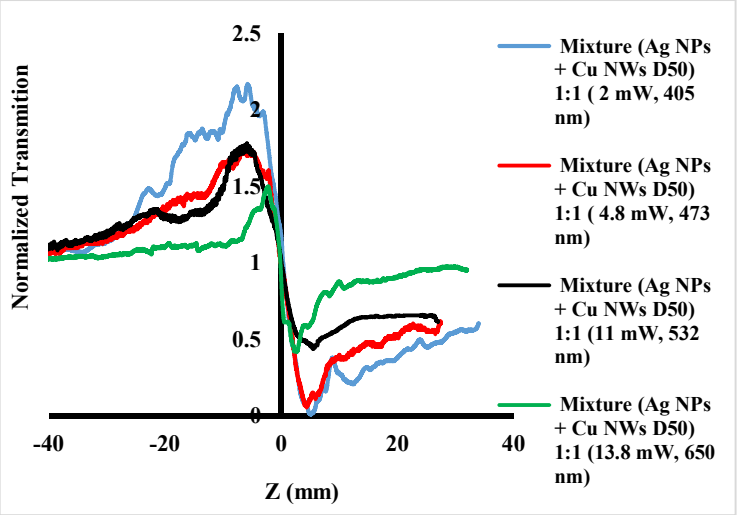

Fig (4.37): Z-scan closed aperture curves for Ag NPs + Cu NWs D50 suspension with volume ratio (1:1) (0.12mg/ml), with CW laser wavelength (405 nm) with (2 mW), wave length (473 nm) with (4.8 mW), wave length (532 nm) with (11mW) and wave length (650 nm) with (13.8 mW)

From the results listed in Table (4.13), we note that the values of the nonlinear refractive index and the third-order nonlinear susceptibility are different from the values of their original materials. The values of the nonlinear refractive index and the third-order nonlinear susceptibility of mixture are clearly different from those of the original material especially the values of linear absorption coefficient. They are less than the values of the raw material and they decrease as the wavelength increases, an opposite case in comparison with the raw material.

Table (4.13): The values of n_2 and $Re\chi^{(3)}$ at different wavelengths for Ag NPs + Cu NWs D50

Material and Concentration (mg/ml)	Wavelength λ (nm)	Intensity (MW/m^2)	Linear absorption coefficient α (m^{-1})	Linear refractive index n_o	Nonlinear Refractive index $-n_2$ (m^2/W)	Susceptibility $Re\chi^{(3)}$ (esu)
Mixture of (Ag NPs + Cu NW) (0.12) (1:1)	405	13.49	36.08655143	1.362	2.6423×0^{-11}	1.24×10^{-5}
	473	4.98	31.42197847	1.362	6.5538×0^{-11}	3.08×10^{-5}
	532	5.79	22.6928408	1.362	4.9953×0^{-11}	2.35×10^{-5}
	650	13.51	18.28866037	1.362	2.0570×0^{-11}	9.67×10^{-6}
Cu NW (0.12)	405	14.83	37.85801903	1.358	2.9817×10^{-11}	1.39×10^{-5}
	473	4.98	38.63896633	1.358	6.2503×10^{-11}	2.92×10^{-5}
	532	6.84	38.69876757	1.358	5.6069×10^{-11}	2.62×10^{-5}
	650	13.51	42.31724117	1.358	5.6069×10^{-11}	2.62×10^{-5}
Ag NPs (0.12)	405	13.49	64.4653457	1.357	4.31252×0^{-11}	2.01×10^{-5}
	473	4.98	65.97580663	1.357	1.2371×10^{-10}	5.77×10^{-5}
	532	5.79	57.98462693	1.357	9.5475×10^{-11}	4.46×10^{-5}
	650	13.51	39.55786333	1.357	2.2507×10^{-11}	1.05×10^{-5}

4.4.5.3 Nonlinear optical properties mixture of spherical (Ag NPs + Fe_2O_3 Nano fragments) (1:3)

In this mixture, two different methods were used to prepare the mixtures. The first method was done by using ultrasonic waves for mixing, while the second was done by using a pulsed laser with a wavelength of (532 nm). From the observation of Fig. (4.38), it is clear that it has negative refractive indices at all wavelengths such as its original materials.

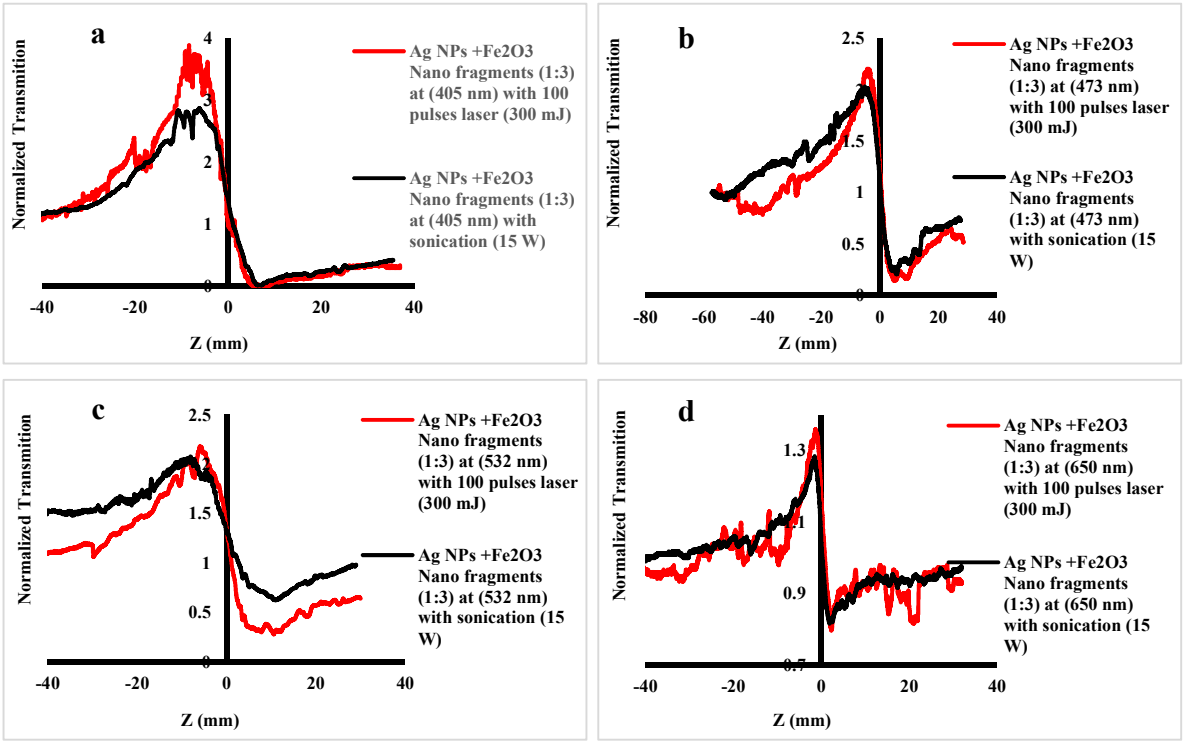

Fig (4.38): Z-scan closed aperture curves for Ag NPs + Fe2O3 Nano fragments suspension with volume ratio (1:3) with two methods of mixing (laser pulses and sonication), with excitation wavelength (a) 405 nm, (b) 473 nm, (c) 532 nm, and (d) 650 nm and powers of (2.2, 4.8, 11, and 13.8 mW) respectively.

From observing the results in Table (4.14), we find that the values of the nonlinear refractive index and the third-order nonlinear susceptibility of the pulsed laser mixture are better than those in the case of using the ultrasonic method. The reason for this is that, the energy of the laser wave is much higher than the energy of the ultrasound waves, and thus the adhesions caused by the pulsed laser wave are different from those caused by the Ultrasound.

From comparing the values of the nonlinear properties and the linear absorption coefficient of the mixtures with the values of the materials constituting the mixture, we find, that the values of the nonlinear properties of the Ag NPs differ from those of the mixture as they are larger. This may be due to the shape difference.

As for the comparison with Fe_2O_3 Nano fragments, we find that there is also a difference in the values. The linear and the nonlinear coefficient of the mixtures are much better those of Fe_2O_3 Nano fragments, especially with regard to expanding the linear absorption spectrum of Fe_2O_3 Nano fragments to be doubled at the wavelength of (650 nm).

Table (4.14): The values of n_2 and $Re\chi^{(3)}$ at different wavelengths for Ag NPs + Fe2O3 Nano fragments

Material and Concentration (mg/ml)	Wavelength λ (nm)	Intensity (MW/m^2)	Linear absorption coefficient α (m^{-1})	Linear refractive index n_o	Nonlinear Refractive index $-n_2$ (m^2/W)	Susceptibility $Re\chi^{(3)}$(esu)
Mixture of (Ag NPs + Fe_2O_3 NPs) (0.12 mg/ml) (1:3) With sonication	405	14.84	54.99686827	1.363	3.2181×0^{-11}	1.51×10^{-5}
	473	4.98	29.39656673	1.363	7.0443×10^{-11}	3.32×10^{-5}
	532	5.79	15.6113461	1.363	5.3905×10^{-11}	2.54×10^{-5}
	650	13.51	6.352979033	1.363	8.8784×10^{-12}	4.18×10^{-6}
Mixture of (Ag NPs + Fe_2O_3 NPs) (0.12 mg/ml) (1:3) With laser pulses	405	14.84	57.64240113	1.363	4.3783×10^{-11}	2.06×10^{-5}
	473	4.98	38.6887879	1.363	7.9840×10^{-11}	3.76×10^{-5}
	532	5.79	24.92460133	1.363	7.0777×10^{-11}	3.33×10^{-5}
	650	13.51	12.11378	1.363	1.0696×10^{-11}	5.04×10^{-6}
Ag NPs (0.12 mg/ml)	405	13.49	64.4653457	1.357	4.31252×0^{-11}	2.01×10^{-5}
	473	4.98	65.97580663	1.357	1.2371×10^{-10}	5.77×10^{-5}
	532	5.79	57.98462693	1.357	9.5475×10^{-11}	4.46×10^{-5}
	650	13.51	39.55786333	1.357	2.2507×10^{-11}	1.05×10^{-5}
Fe2O3 Nano fragments (0.12 mg/ml)	405	14.84	49.64753663	1.357	4.31252×0^{-11}	2.01×10^{-5}
	473	6.22	20.07003087	1.359	4.1216×10^{-11}	1.93×10^{-5}
	532	6.84	11.56697103	1.359	2.2351×10^{-11}	1.05×10^{-5}
	650	13.51	5.857526967	1.359	3.0512×10^{-12}	1.43×10^{-6}

4.4.5.4 Nonlinear optical properties mixture of spherical (Cu1+Fe_2O_3 Nano fragments) (1:3)

As for the previous mixture in the paragraph (4.4.5.3). From the observation of Fig. (4.39), it is clear that the mixtures have negative refractive indices at all wavelengths such as its original materials.

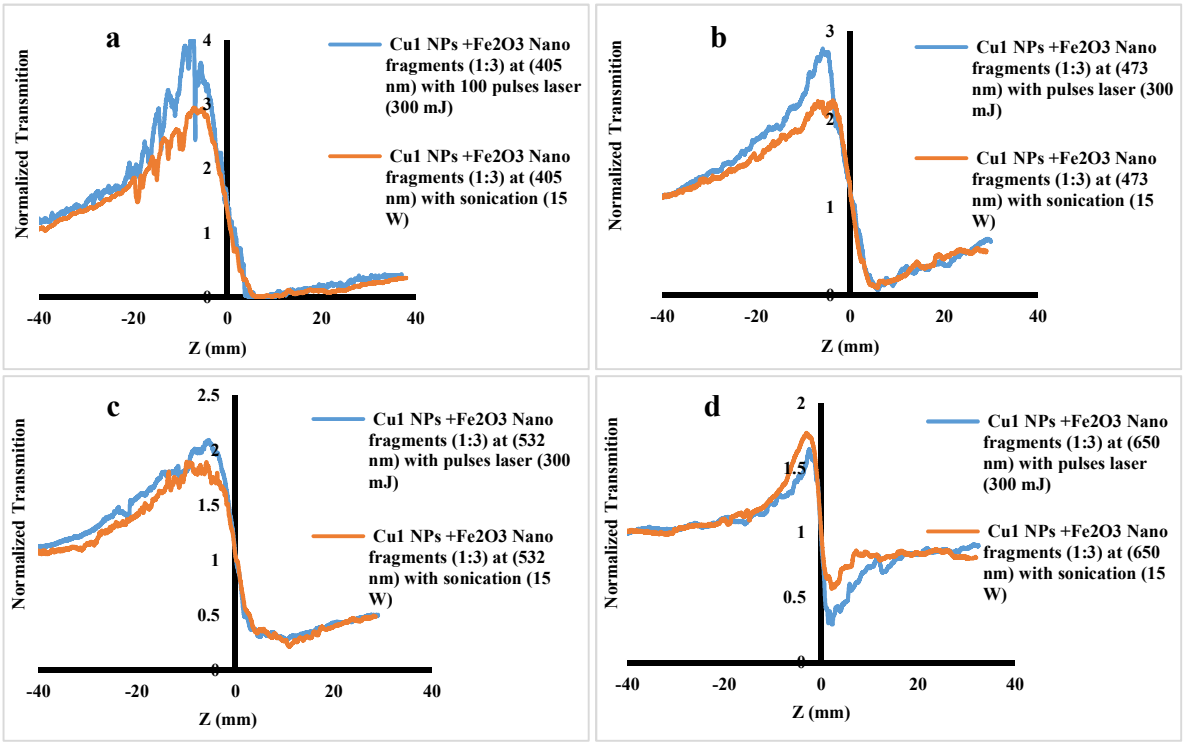

Fig (4.39): Z-scan closed aperture curves for Cu1+Fe2O3 Nano fragments suspension in volume ratio (1:3) with two methods of mixing (laser pulses and sonication), with excitation wavelength (a) 405 nm, (b) 473 nm, (c) 532 nm, and (d) 650 nm and powers of (2.2, 4.8, 11, and 13.8 mW) respectively.

From observing the results in Table (4.15), we find that the values of the nonlinear refractive index and the nonlinear third-order susceptibility of the mixture that treated with laser are better than those with the ultrasonic method. The reason

for this can also be attributed to the higher energy of laser in comparison with the direct ultrasonic waves which can lead to different structures.

From comparing the values of the nonlinear properties and the linear absorption coefficient of the mixtures with the values of the materials constituting the mixture, we find that the valuesof the nonlinear properties of the Cu1 are different from those of the mixture as they are smaller. This may be due to the shape or structure differences. As for the comparison with Fe_2O_3 Nano fragments, we find that there is also a difference in the optical values, where the mixture have much better properties than Fe_2O_3 Nano fragments, especially with regard to expanding the linear absorption spectrum of Fe_2O_3 Nano fragments to multi times at the wavelengths of (473, 532 and 650) nm.

Table (4.15): The values of n_2 and $Re\chi^{(3)}$ at different wavelengths for Cu1 + Fe2O3 Nano fragments

Material and Concentration (mg/ml)	Wavelength λ (nm)	Intensity (MW/m^2)	Linear absorption coefficient α (m^{-1})	Linear refractive index n_o	Nonlinear Refractive index $-n_2$ (m^2/W)	Susceptibility $Re\chi^{(3)}$(esu)
Mixture of (Cu1 NPs + Fe_2O_3 NPs) (0.12) (1:3) With sonication	405	14.84	72.5723663	1.361	3.3380×0^{-11}	1.56×10^{-5}
	473	4.98	52.50064657	1.361	8.3247×10^{-11}	3.91×10^{-5}
	532	5.79	43.2648489	1.361	6.3195×10^{-11}	2.97×10^{-5}
	650	13.51	35.75300027	1.361	2.3106×10^{-11}	1.09×10^{-5}
Cu1 NPs + Fe_2O_3 NPs (0.12) (1:3) With pulses	405	14.84	74.92242427	1.361	4.5844×10^{-11}	2.15×10^{-5}
	473	4.98	50.65617387	1.361	1.0682×10^{-10}	5.02×10^{-5}
	532	5.79	38.893064	1.361	6.8107×10^{-11}	3.20×10^{-5}
	650	13.51	31.57635623	1.361	2.5911×10^{-11}	1.22×10^{-5}
Cu1 NPs (0.12 mg/ml)	405	13.49	29.06854277	1.358	2.8004×10^{-11}	1.31×10^{-5}
	473	4.98	29.9675572	1.358	5.5124×10^{-11}	2.58×10^{-5}
	532	5.79	30.05983073	1.358	3.7665×10^{-11}	1.76×10^{-5}
	650	13.51	28.62797887	1.358	2.4278×10^{-11}	1.14×10^{-5}
Fe2O3 Nano fragments (0.12 mg/ml)	405	14.84	49.64753663	1.357	4.3125×0^{-11}	2.01×10^{-5}
	473	6.22	20.07003087	1.359	4.1216×10^{-11}	1.93×10^{-5}
	532	6.84	11.56697103	1.359	2.2351×10^{-11}	1.05×10^{-5}
	650	13.51	5.857526967	1.359	3.0512×10^{-12}	1.43×10^{-6}

4.5 Optical Limiting Response

The optical limiting effects was studied for all samples (Ag group, Cu group, Au group, Fe2O3 Nano fragments and mixtures) as a suspensions in absolute ethanol media at three concentrations (0.04, 0.08 and 0.12) mg/ml by two wavelengths (405 and 532) nm. Threshold power (P_{th}) and limiting power (P_L) in (mW) unit are tabulated in tables for all samples.

4.5.1 Characteristics Optical Limiting of Ag Nano group

4.5.1.1 Characteristics Optical Limiting of Ag NPs

From the Fig. (4.40 a and b), the result shows that observed the limiting power (P_L) and threshold power (P_{th}) are decreased with increasing the concentrations and wavelength.

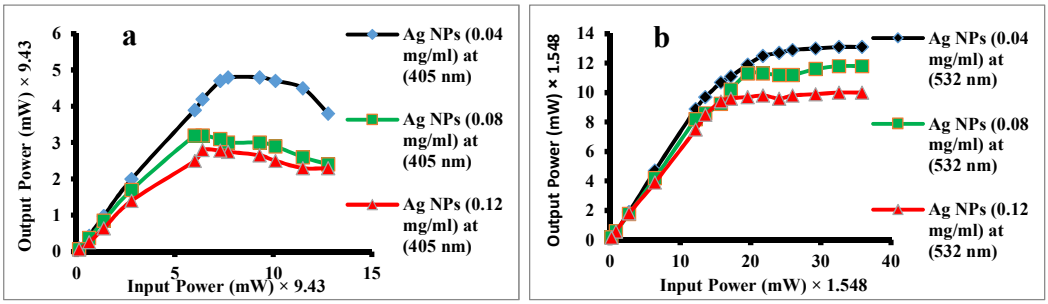

Fig. (4.40): The optical limiting curves of Ag at three different concentrations by two wavelengths, a: (405 nm), b: (532 nm).

Table (4.16): Threshold and limiting power for suspension of Ag NPs at three different concentrations by two wavelengths

Wavelength (nm)	Transmittance %	Concentration (mg/ml)	P_{th} (mW)	P_L (mW)
405 nm	65	0.04	44.321	45.264
	60.7	0.08	30.176	31.119
	43.7	0.12	26.404	23.57
532 nm	72.9	0.04	19.35	20.2788
	63.2	0.08	17.4924	18.266
	59.5	0.12	14.5512	15.48

By observing the data in the Table (4.16), we can clearly notice that the (P_L) and the (P_{th}) decrease with increasing wavelength, and that transmittance decreases with increasing concentration and increases slightly with increasing wavelength.

4.5.1.2 Characteristics Optical Limiting of Ag NWs

In Fig. (4.41), the result shows that the limiting power (P_L) and threshold power (P_{th}) are decreased with increasing the concentrations. In addition, it can be seen that the shape of the optical limiter curve shows a clearer behavior of the optical limiter with increasing concentration.

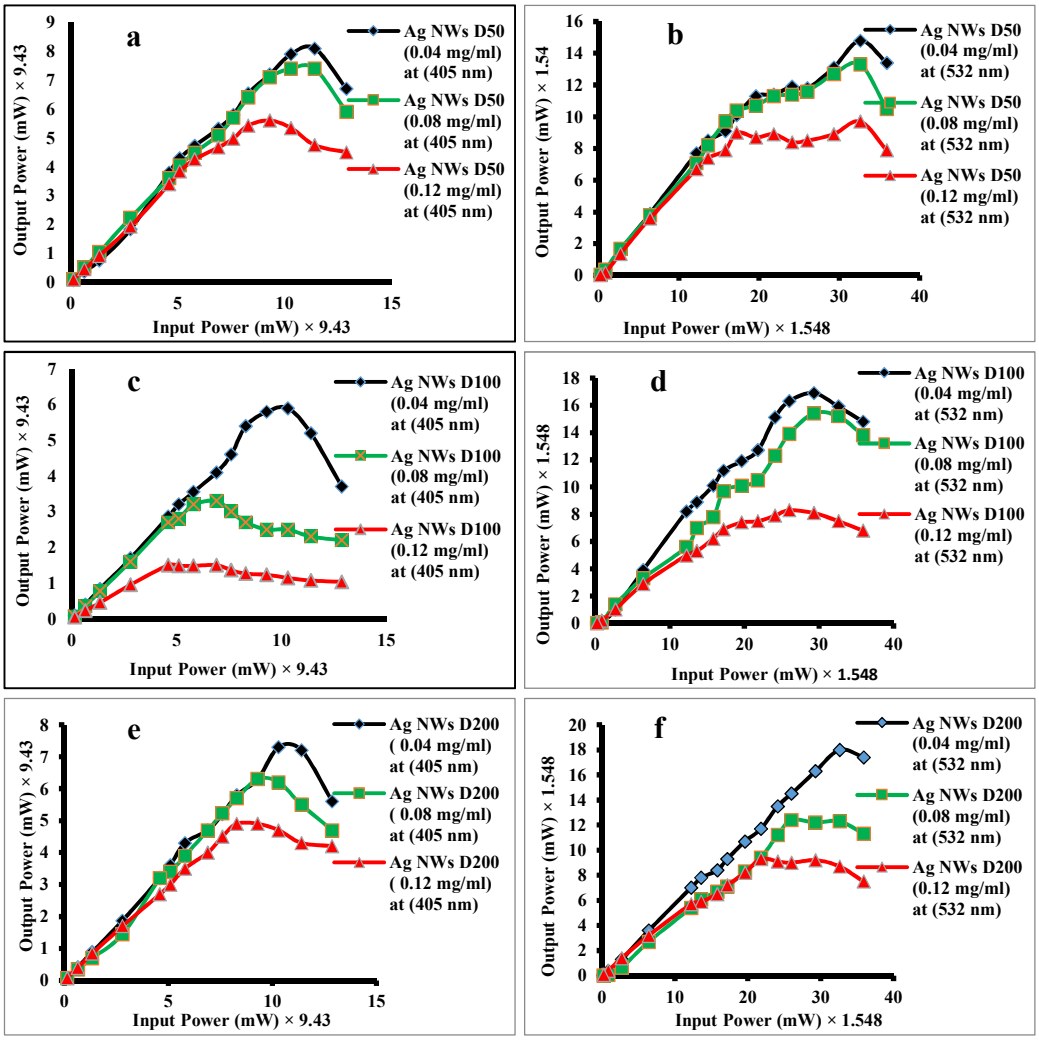

Fig. (4.41): The optical limiting curves at three concentrations, a & b: Ag NWs D50 (405 and 532) nm, c & d: Ag NWs D100 (405 and 532) nm and e & f: Ag NWs D200 (405 and 532) nm

Table (4.17): Threshold and limiting power for suspension of three sizes of Ag NWs at three different concentrations by two wavelengths

Ag NWs Diameters (nm)	Wavelength (nm)	Transmittance %	Concentration (mg/ml)	P_{th} (mW)	P_L (mW)
Ag NWs D50	405 nm	69.87	0.04	74.497	76.383
		68.67	0.08	66.953	69.78
		59.21	0.12	46.9614	52.808
	532 nm	55.76	0.04	17.4924	22.910
		61.4	0.08	17.4924	22.136
		54.9	0.12	13.932	15.0156
Ag NWs D100	405 nm	62.2	0.04	50.922	55.637
		46.47	0.08	28.29	25.46
		34	0.12	14.145	14.164
	532 nm	67.21	0.04	25.2324	24.613
		51.4	0.08	23.8392	23.529
		45	0.12	12.8484	12.538
Ag NWs D200	405 nm	68.74	0.04	68.839	67.896
		68.67	0.08	59.409	58.466
		57.97	0.12	46.207	44.321
	532 nm	56	0.04	27.864	26.9352
		47.69	0.08	19.1952	19.0404
		42.6	0.12	14.3964	14.2416

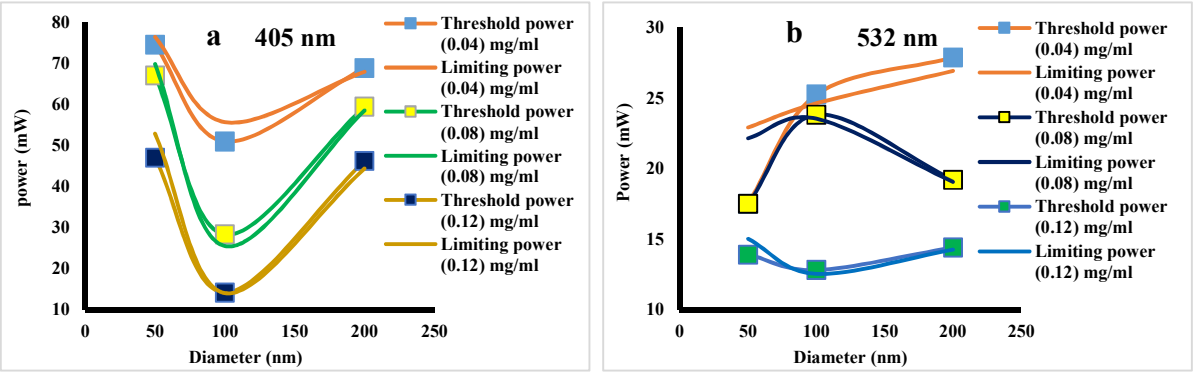

Fig. (4.42): Threshold and limiting power behavior at three different concentrations according to diameter change of Ag NWs, a: at 405 nm, b: at 532 nm

From the data in Table (4.17), for each diameter the (P_L) and (P_{th}) are decreased with increasing the wavelengths. In addition, with increasing of concentrations, the transmittance was decreased with increasing of concentrations and it increased with increasing the wavelengths.

From Fig. (4.42 a) we can notice that the values of (P_L) and (P_{th}) decrease and then increase with Increasing the diameter of the wire for all concentrations at wavelength (405 nm). However, for the wavelength (532 nm) as in Fig. (4.42 b), the behavior was random, where at the concentration (0.04 mg/ml), the (P_L) and (P_{th}) increased with the increase of the diameter. In the concentration (0.08 mg/ml), they increased and then decreased with increasing the diameter. In the concentration (0.12 mg/ml) they were decreasing and then increasing with the increase in the diameter.

4.5.2 Optical Limiting of Au group

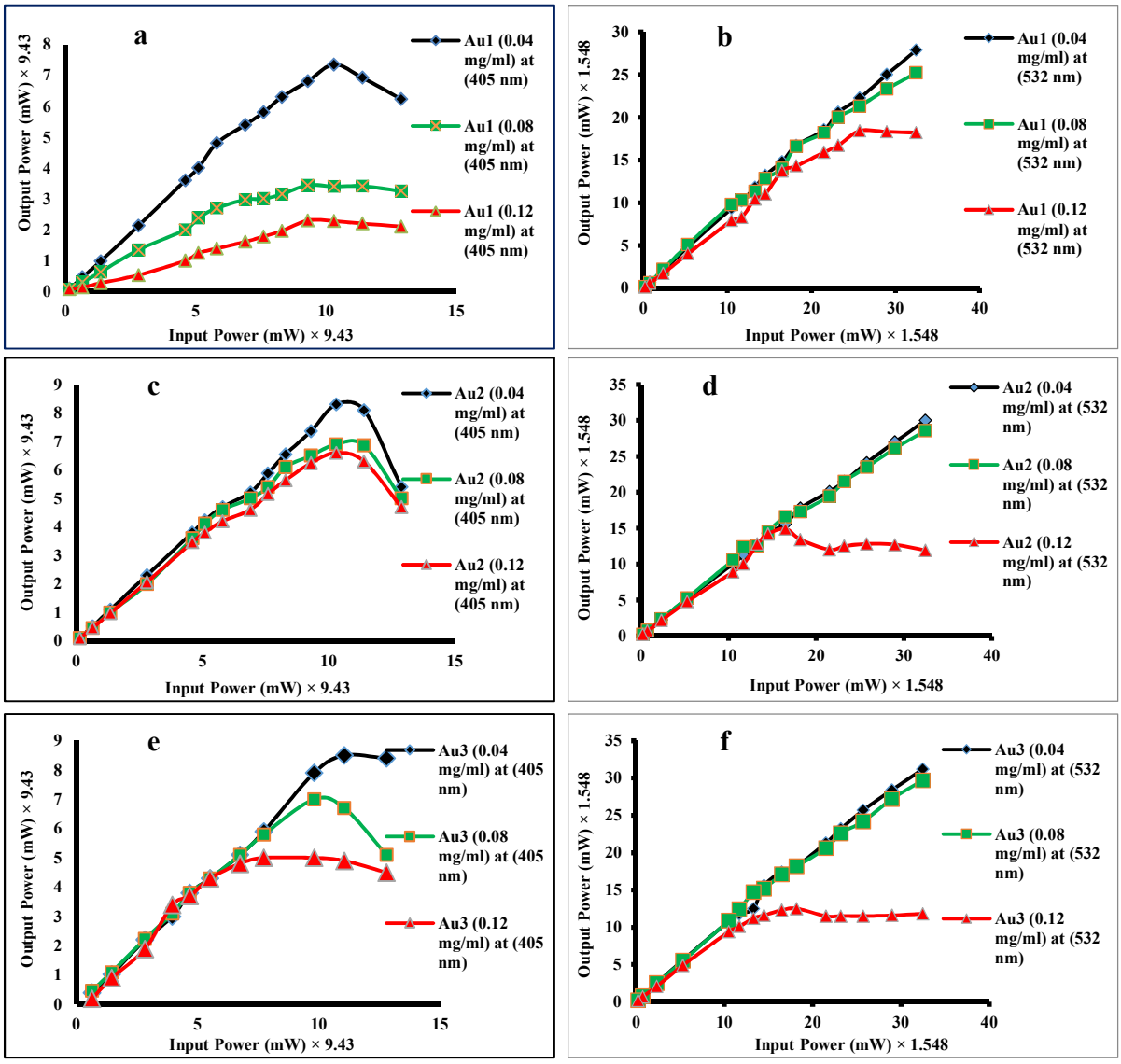

Fig. (4.43): The optical limiting curves at three concentrations, a & b: Au1 at (405 and 532) nm, c & d: Au2 at (405 and 532) nm and e & f: Au3 at (405 and 532) nm

From Fig. (4.43), the result show that the limiting power (P_L) and threshold power (P_{th}) are decreased with increasing the concentrations.

From the data of (P_L) and (P_{th}) in the Table (4.18), we can observed that the behavior of increasing and decreasing of (P_L) and (P_{th}) are not linearly with the change of particle sizes. For each size, the transmittance values decreased very slightly with increasing the wavelengths except (Au2) they were increased very slightly.

Table (4.18): Threshold and limiting power for suspension of three sizes of spherical Au NPs group at three different concentrations at two wavelengths

Au size (nm)	Wavelength (nm)	Transmittance %	Concentration (mg/ml)	P_{th} (mW)	P_L (mW)
Au 1	405 nm	78.2	0.04	69.3105	65.2556
		43.47	0.08	32.4392	32.1563
		21.73	0.12	21.689	20.746
	532 nm	89.68	0.04	-	-
		84.84	0.08	-	-
		75.23	0.12	28.4832	28.1736
Au 2	405 nm	80.58	0.04	78.269	76.383
		87.2	0.08	65.067	64.6898
		75.2	0.12	62.238	59.409
	532 nm	93.6	0.04	-	-
		92.6	0.08	-	-
		96.2	0.12	23.065	19.6596
Au 3	405 nm	80.6	0.04	80.155	79.212
		75.03	0.08	66.01	63.181
		79.05	0.12	45.264	42.435
	532 nm	97.9	0.04	-	-
		93.8	0.08	-	-
		92.4	0.12	19.35	17.802

From Fig. (4.44) we can notice that the values of (P_L) and (P_{th}) increase with increasing the particle sizes for the concentrations (0.04 and 0.08) mg/ml at wavelength (405 nm). For the concentration (0.12 mg/ml), the behavior was

changed, where the (P_L) and (P_{th}) increased and then decrease with the increase of the particle sizes. At wavelength (532 nm), (P_L) and (P_{th}) were decrease with the increase of particle sizes for the concentration (0.12 mg/ml). There was no optical limiting at the concentrations (0.04 and 0.08) mg/ml for all particle sizes at the wavelength (532 nm).

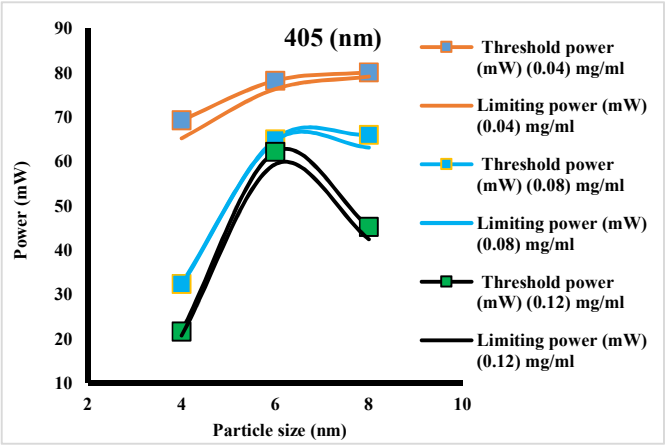

Fig. (4.44): Threshold and limiting power behavior at three different concentrations at (405 nm) wavelength according to particle sizes of Au NPs

4.5.3 Optical Limiting of Cu group

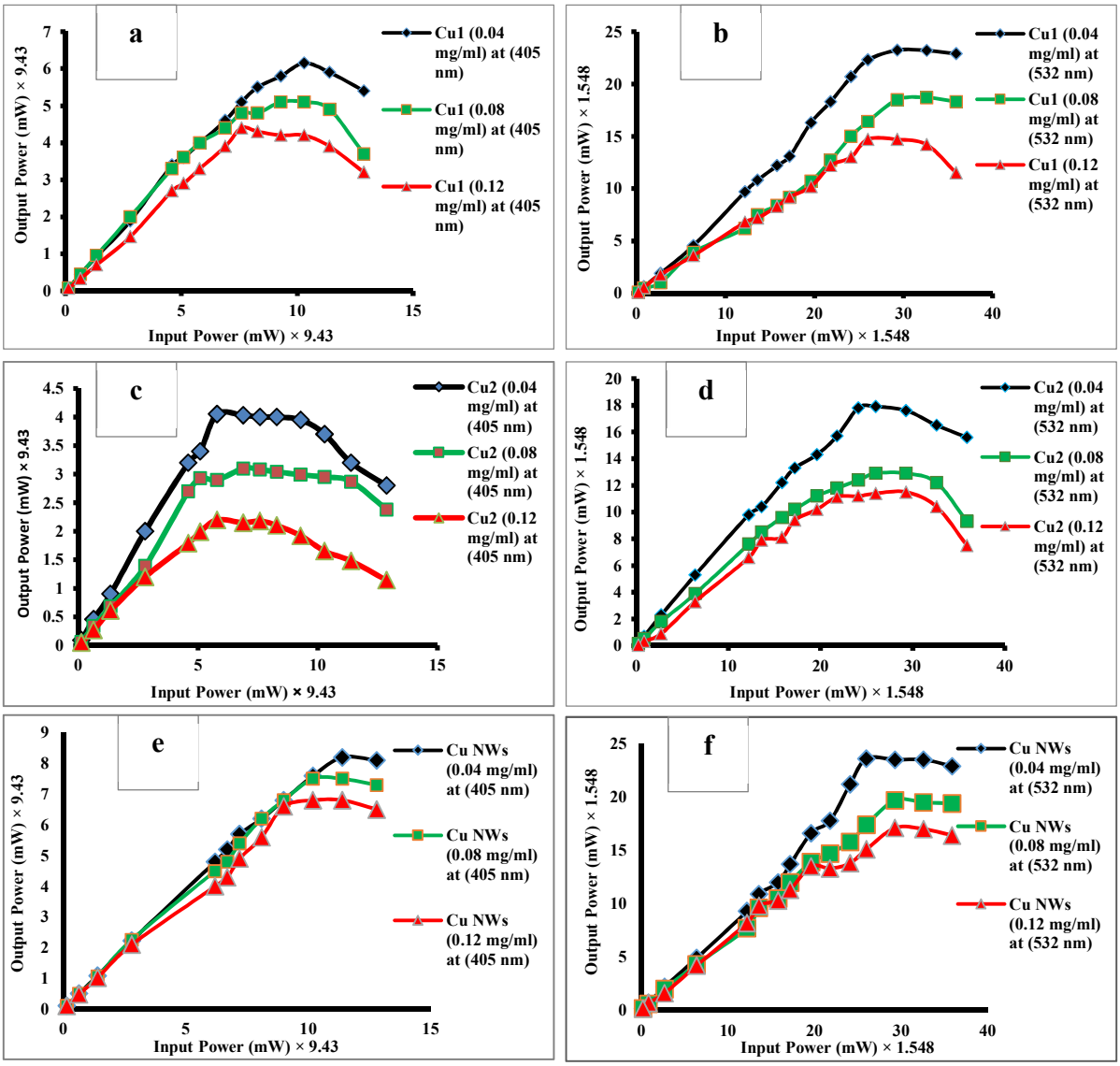

Fig. (4.45): The optical limiting curves at three concentrations, a & b: Cu1 at (405 and 532) nm, c & d: Cu2 at (405 and 532) nm and e & f: Cu NWs D50 at (405 and 532) nm

Table (4.19): Threshold and limiting power for suspension of three sizes of Cu group at three different concentrations by two wavelengths

Cu size & shapes (nm)	Wavelength (nm)	Transmittance %	Concentration (mg/ml)	P_{th} (mW)	P_L (mW)
Cu 1	405 nm	73.8	0.04	57.9945	55.637
		70.58	0.08	48.093	46.207
		57.89	0.12	41.492	39.606
	532 nm	77.21	0.04	35.96004	35.4492
		62.2	0.08	28.638	28.3284
		52.2	0.12	22.78656	21.9816
Cu 2	405 nm	69.5	0.04	38.1915	34.891
		58.69	0.08	29.233	27.0641
		38.9	0.12	20.746	15.5595
	532 nm	73.8	0.04	27.5544	25.542
		60.7	0.08	19.1952	18.8856
		53.2	0.12	17.22924	16.1
Cu NWs	405 nm	74.5	0.04	77.326	76.383
		73.5	0.08	70.725	68.839
		69.1	0.12	62.238	61.295
	532 nm	87.9	0.04	36.5328	35.4492
		67.2	0.08	30.4956	30.0312
		58.3	0.12	26.4708	25.3872

From the Fig. (4.45) and the data in Table (4.19) for (Cu1 and Cu2), the result show that the limiting power (P_L) and threshold power (P_{th}) are decreased with increasing the concentrations and they decrease with increase of wavelengths and particle size. For Cu NWs D50, the values of (P_L) and (P_{th}) are higher than those for (Cu1 and Cu2) which may be due to the shape effect and they decrease with increase of wavelength. The transmittance values for (Cu1, Cu2 and Cu NWs) seemed constant with increasing of the wavelengths

4.5.4 Optical Limiting of Fe_2O_3 Nano fragments

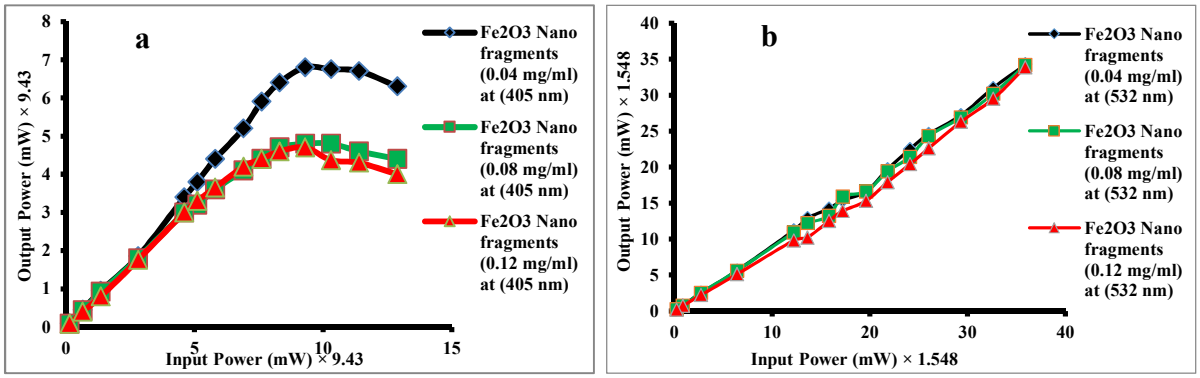

Fig. (4.46): Threshold and limiting power at three different concentrations by two wavelengths, a: (405 nm), b: (532 nm), for suspension of Fe2O3 Nano fragments

Table (4.20): Threshold and limiting power for suspension of three sizes of Fe2O3 Nano fragments at three different concentrations by two wavelengths

Wavelength (nm)	Transmittance %	Concentration (mg/ml)	P_{th} (mW)	P_L (mW)
405 nm	77.1	0.04	64.124	63.181
	65.2	0.08	45.264	43.378
	62.8	0.12	43.378	40.549
532 nm	94.6	0.04	-	-
	93.4	0.08	-	-
	90	0.12	-	-

From the Fig. (4.46) and the data in Table (4.20) for (Fe_2O_3 Nano fragments), the result shown observed the limiting power (P_L) and threshold power (P_{th}) are decreased with increasing the concentrations at the wavelength (405 nm) and there was no optical limiting at the wavelength (532 nm), because of the high values of transmittance at this wavelengths. This means that the values of the absorbed intensity are not sufficient to cause the thermal change that leads to the occurrence of optical limitation.

4.5.5 Optical Limiting for Mixtures

4.5.5.1 Optical Limiting for Cu2+Ag NWs D200

From the Fig. (4.47 a and b), we can see a new behavior for this mixture at wavelengths (405 nm) and (532 nm) to be a two-stage optical limiter or it can be used as a two-stage optical switch. The values of (P_L) and (P_{th}) for the mixture appeared with completely different values as they were more than the values of the materials that made it up.

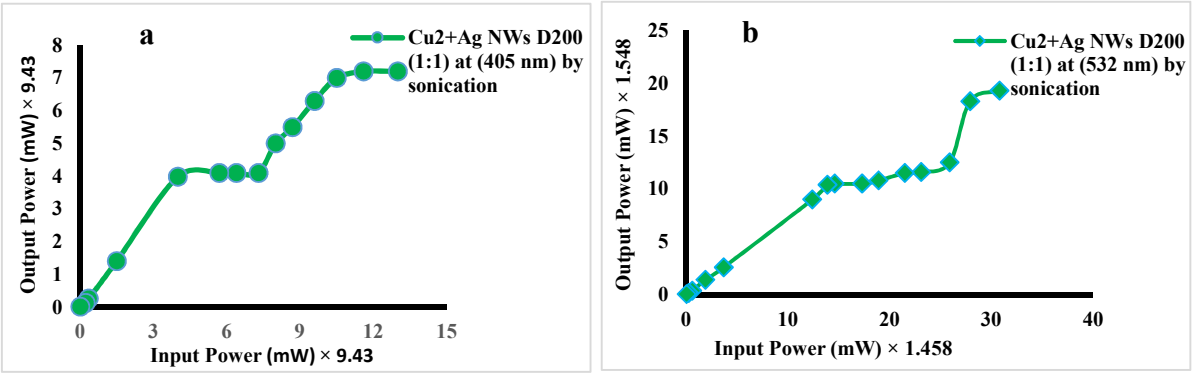

Fig. (4.47): Threshold and limiting power by two wavelengths, a: (405 nm), b: (532 nm), for suspension of mixture (Cu2 + Ag NWs D200)

Table (4.21): Threshold and limiting power for suspension of mixture (Cu2 + Ag NWs D200) by two wavelengths

Material	Wavelength (nm)	Transmittance %	Concentration (mg/ml)	P_{th} (mW)	P_L (mW)
Mixture	405 nm	93 & 70	0.12	37.53 & 66.01	38.663 & 67.896
	532 nm	73.6 & 65.6	0.12	16.1 & 28.328	16.254 & 30.65
Cu2	405 nm	38.9	0.12	20.746	15.559
	532 nm	53.2	0.12	17.229	16.1
Ag NWs D200	405 nm	57.97	0.12	46.207	44.321
	532 nm	42.6	0.12	14.396	14.246

From the Fig. (4.47) and the data in Table (4.21) for the mixture (Cu2 + Ag NWs D200) prepared by ultrasonic mixing, the result shown observed the limiting power (P_L) and threshold power (P_{th}) are decreased with increasing of wavelength. The transmittance values of the mixture became higher than those of the materials before mixing and increased with increasing wavelength.

4.5.5.2 Optical Limiting for Ag NPs + Cu NWs D50

From the Fig. (4.48 a), we can see a new behavior for this mixture at wavelength (405 nm) to be a two-stage optical limiter or it can be used as a two-stage optical switch. For wavelength (532 nm), this behavior is not as pronounced as at wavelength (405 nm) as it is present as in Fig. (4.48 b). The values of (P_L) and (P_{th}) for the mixture appeared with values completely different from the values of the materials that made it up.

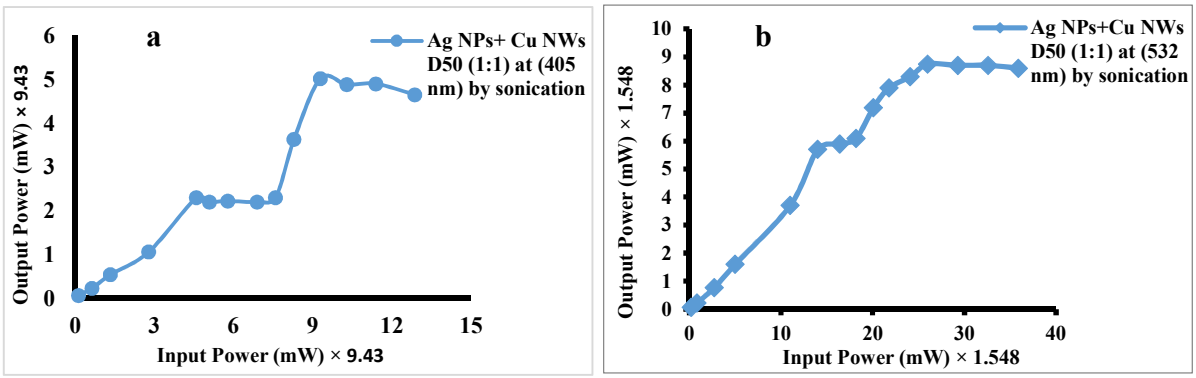

Fig. (4.48): Threshold and limiting power by two wavelengths, a: (405 nm), b: (532 nm), for suspension of mixture (Ag NPs + Cu NWs D50)

Table (4.22): Threshold and limiting power for suspension of mixture (Ag NPs + Cu NWs D50) by two wavelengths

Material	Wavelength (nm)	Transmittance %	Concentration (mg/ml)	P_{th} (mW)	P_L (mW)
Mixture	405 nm	50 & 48.6	0.12	21.69 & 47.3386	21.69 & 46.207
	532 nm	40.7	0.12	8.82 & 13.53	9.443 & 13.313
Ag NPs	405 nm	43.7	0.12	26.404	23.57
	532 nm	59.5	0.12	14.5512	15.48
Cu NWs	405 nm	69.1	0.12	62.238	61.295
	532 nm	58.3	0.12	26.4708	25.3872

From the Fig. (4.48) and the data in Table (4.22) for the mixture (Ag NPs + Cu NWs D50) prepared by ultrasonic mixing, the result shown observed the limiting power (P_L) and threshold power (P_{th}) of mixture are decreased with increasing of wavelength. The transmittance values of the mixture became as average at the wavelength (405 nm) of the materials before mixing and decreased with increasing

wavelength. For the wavelength (532 nm) the transmittance values of the mixture became less than the value of the materials before mixing.

4.5.5.3 Optical Limiting for Ag NPs + Fe_2O_3 Nano fragments

From the Fig. (4.49 a) for the ultrasonic method of preparation, we can see a new behavior for this mixture at wavelength (405 nm) compared to the material it is made of in Fig. (4.46) and Fig. (4.40). Two regions for (P_L) and (P_{th}), appeared and they lead to be a two-stage optical limiter or it can be used as a two-stage optical switch. For the pulse laser method of preparation this behavior not appear. The mixture seemed to be one substance in its behavior, especially since we have indicated the formation of a new structure, which is the core-shell. At the wavelength (532 nm), this behavior is not appeared as at wavelength (405 nm) and the behavior for both methods similarly. The values of (P_L) and (P_{th}) appeared for the pulsed laser method at a wavelength of (405 nm), higher than the first region of the optical limiter curve using ultrasonic and less than the second region of it. For a wavelength of (532 nm), the values of the (P_L) and (P_{th}) of the laser pulse method are less than the ultrasonic method.

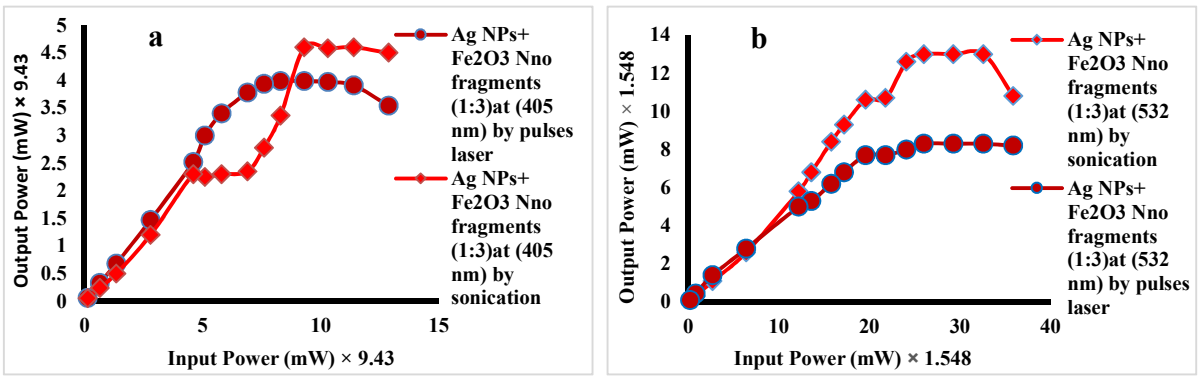

Fig. (4.49): Threshold and limiting power by two wavelengths, a: (405 nm), b: (532 nm), for suspension of mixture (Ag NPs + Fe2O3 Nano fragments) and two methods of preparation

From the Fig. (4.49) and the data in Table (4.23) for the mixture (Ag NPs + Fe2O3 Nano fragments) prepared by two methods of mixing (ultrasonic and pulse laser), the result shown observed the limiting power (P_L) and threshold power (P_{th}) are decreased with increasing of wavelength. The transmittance values of the mixture became different according to the preparation method, as its values were lower for the ultrasonic preparation method than for the laser pulse method at the wavelength (405 nm) and opposite of that at the wavelength (532 nm) due to the change in wavelengths, size and shape.

Table (4.23): Threshold and limiting power for suspension of mixture (Ag NPs + Fe2O3 Nano fragments) by two wavelengths and two methods of preparation

Method of mixing (1:3) Ag NPs + Fe2O3 Nano fragments	Wavelength (nm)	Transmittance %	P_{th} (mW)	P_L (mW)
Sonication	405 nm	50 & 40	21.689 & 43.378	21.689 & 42.435
	532 nm	54.08	20.124	16.7184
Pulse Laser	405 nm	54.78	37.6257	34.891
	532 nm	40.9	11.9196	12.6936

4.5.5.4 Optical Limiting for Cu1 + Fe_2O_3 Nano fragments

From the Fig. (4.50 a) for the ultrasonic method of preparation, we can see a new behavior for this mixture at wavelength (405 nm) compared to the material it is made of in Fig. (4.46) and Figs. (4.45 a & b). Two regions for (P_L) and (P_{th}), appeared and they lead to be a two-stage optical limiter or it can be used as a two-stage optical switch. For the pulse laser method of preparation this behavior not

appear. The mixture seemed to be one substance in its behavior, especially since we have indicated that may be the formation of a new structure, which is the core-shell.

At the wavelength (532 nm), this behavior is not appeared as at wavelength (405 nm) and the behavior for both methods similarly. The values of (P_L) and (P_{th}) appeared for the pulsed laser method at a wavelength of (405 nm), higher than the first region of the optical limiter curve using ultrasonic and less than the second region of it. For a wavelength of (532 nm), the values of the (P_L) and (P_{th}) of the laser pulse method are higher than the ultrasonic method.

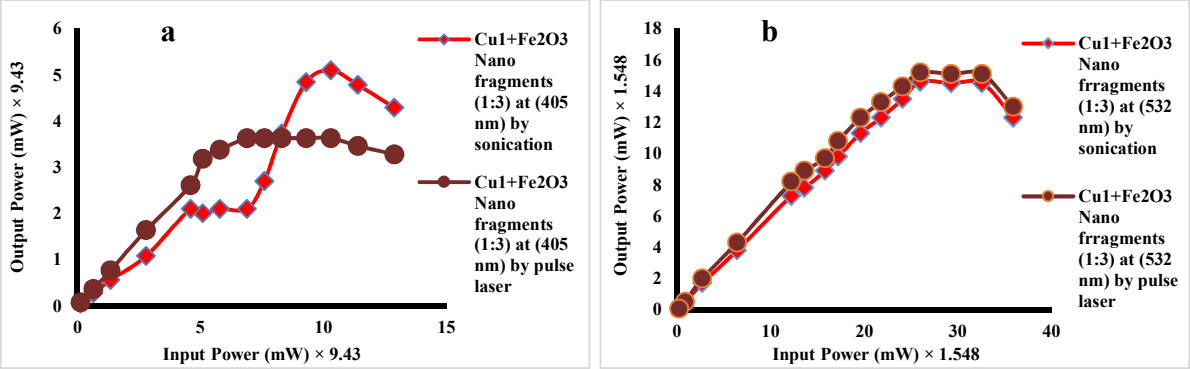

Fig. (4.50): Threshold and limiting power by two wavelengths, a: (405 nm), b: (532 nm), for suspension of mixture (Cu1 + Fe2O3 Nano fragments) and two methods of preparation

Table (4.24): Threshold and limiting power for suspension of mixture (Cu1 + Fe2O3 Nano fragments) by two wavelengths and two methods of preparation

Method of mixing (1:3) Cu1 + Fe2O3 Nano fragments	Wavelength (nm)	Transmittance %	P_{th} (mW)	P_L (mW)
Sonication	405 nm	41.48 & 45	21.68 & 44.46	21.68 & 43.37
	532 nm	57.6	22.6008	22.44
Pulse Laser	405 nm	56.7	34.2309	30.9304
	532 nm	67.18	23.5296	23.065

From the Fig. (4.50) and the data in Table (4.24) for the mixture (Cu1+ Fe2O3 Nano fragments) prepared by two methods of mixing (ultrasonic and pulse laser), the result shown observed the limiting power (P_L) and threshold power (P_{th}) are increased with increasing of wavelength for sonication method and opposite for pulse laser method. The transmittance values of the mixture were not affected much by the method of preparation, so the difference between its values was slight, as the values for the method of preparation with laser pulses were slightly higher than for the method of ultrasonic preparation.

4.6 Conclusions

1- Approximately all prepared samples show a good optical transmittance, which is one of the important criterion for chosen material as optical limiting.

2- The nonlinear properties measurements showed that all prepared samples have a negative n2 due to heat effects, and they also have only $Re^{\chi(3)}$at all wavelengths used. The results of the nonlinear measurements showed that there was not nonlinear absorption for all samples at all wavelengths used.

3- The results confirmed that, all prepared samples except the Fe2O3 Nano fragments showed a good absorption bandwidth within the visible region of the electromagnetic spectrum, which gives a good indication that they can work as an optical limiter within this region.

4- Ultrasound mixing process of Cu2 +Ag NWs D200 and Ag NPs +Cu NWs D50 showed a decrease in absorbance as well as an increase in the bandwidth of the absorption region than the materials from which they were mixed. All that lead to improve the optical limiter properties by decreasing the values of Pth and PL and producing a two-stage optical limiter.

5- Pulsed Laser and Ultrasonic Mixing Processes for Ag NPs+Fe2O3 Nano Fragments and Cu1+ Fe2O3 Nano fragments leads to increasing the bandwidth of the linear absorption region of Fe2O3 Nano fragments, generated a new shape of the material and different values of the linear absorbance and transmittance of the mix-

tures compared to the materials from which they were mixed. all these led to improving the properties of optical limiter.

6- The highest values of the n_2 and the $Re^{\chi(3)}$ of Cu2 nanoparticles suspension in absolute ethanol for the three concentrations used were recorded at the wavelength of (473 nm) and the intensity of (4.98 Mw/m2) and their values were (1.13795×10^{-10}, 1.23016×10^{-10} and 1.32163×10^{-10}) m2/W and (5.32×10^{-5}, 5.75×10^{-5} and 6.18×10^{-5}) esu respectively.

7- The lowest values of the n2 and the $Re^{\chi(3)}$ were recorded for the suspension of Fe2O3 Nano fragments in absolute ethanol with a concentration of (0.04 mg/ml) at a wavelength of (405 nm) and an intensity of (13.5 Mw/m2) and their values were (1.94×10^{-12} m2/W) and (9.12×10^{-7} esu) respectively.

8- The results of OL measurements showed a decrease in P_{th} and P_L values with increasing concentration for all samples.

9- All samples showed optical limiting at wavelength (405 nm).

10- At the wavelength of (532 nm), the suspensions of Au NPs did not show the behavior of optical limiting in all sizes at the concentrations (0.04 and 0.08) mg/ml. This means that these concentrations are critical concentrations of the optical limiter. The behavior of the optical limiter of the Fe_2O_3 Nano fragments did not appear for the same wavelength and for all concentrations, but for all other samples the behavior of the optical limiting is clear at this wavelength.

11- The results of the OL measurements for the prepared suspensions mixtures which were mixed by the ultrasonic method showed a dual behavior of the optical limiter at the wavelength (405 nm), as two visible regions of the optical limiter appeared, making it a candidate to work as a two-stage optical switch. At the wavelength 532 nm, the behavior of the optical limiter was not clear for two regions of work, but seemed as one region. For the prepared suspensions of the mixtures that were mixed by the pulsed laser method showed a clear behavior of the OL at the two wavelengths used in one region of work.

4.7 Suggestion for future work

1- Expanding the circle of study of the effect of the shape of nanoparticles on the properties of the optical limiting using multiple different shapes of the same nanomaterial.

2- Study the effect of diameter on the optical limiter for nanowires and rods for the materials that used in this study and compering between them.

3- Preparing more mixtures from these used materials in this study and studying their morphological, structural and optical properties, and studying the effect of mixing ratios and methods of mixing on the properties of the optical limiter.

4- Study the effect of the host using different types of hosts and study their effect on the properties of the optical limiter of the same materials that were used in this study. Orientation towards making the host from a solid material using different types of polymers or glass and studying the effect of the type of polymer or glass and the thickness of the prepared films or foils on the properties of the optical limiter of the same materials that were used in this study.

References

References

[1] Li, C. (2017). Nonlinear optics. *Principles and Applications*.

[2] Baldwin, G. C. (2012). *An introduction to nonlinear optics*. Springer Science & Business Media.

[3] Franken, P. A., Hill, A. E., Peters, C. E., & Weinreich, G. (1961). Generation of optical harmonics. *Physical Review Letters*, *7*(4), 118.

[4] Rentzepis, P. M., & Pao, Y. H. (1964). Laser-induced optical second harmonic generation in organic crystals. *Applied Physics Letters*, *5*(8), 156-158.

[5] Boyd, R. W. (2020). Nonlinear optics. Academic press.

[6] Zhang, Y., Hu, X., Yang, H., & Gong, Q. (2011). Multi-component nanocomposite for all-optical switching applications. *Applied Physics Letters*, *99*(14), 141113.

[7] Huang, T., Hao, Z., Gong, H., Liu, Z., Xiao, S., Li, S., ... & Qin, J. (2008). Third-order nonlinear optical properties of a new copper coordination compound: A promising candidate for all-optical switching. *Chemical Physics Letters*, *451*(4-6), 213-217.

[8] Zyss, J., & Ledoux, I. (1994). Nonlinear optics in multipolar media: theory and experiments. *Chemical reviews*, *94*(1), 77-105.

[9] Eisenthal, K. B. (2006). Second harmonic spectroscopy of aqueous nano-and microparticle interfaces. *Chemical reviews*, *106*(4), 1462-1477.

[10] Simon, H. J., Mitchell, D. E., & Watson, J. G. (1974). Optical second-harmonic generation with surface plasmons in silver films. *Physical Review Letters*, *33*(26), 1531.

[11] Kumar, C. S. (Ed.). (2013). *UV-VIS and photoluminescence spectroscopy for nanomaterials characterization* (pp. 5-7). Berlin: Springer.

[12] Hagan, D. J., Van Stryland, E. W., Wu, Y. Y., Wei, T. H., Sheik-Bahae, M., Said, A., ... & Soileau, M. J. (1989, August). Passive broadband high dynamic range semiconductor limiters. In *Materials for Optical Switches, Isolators, and Limiters* (Vol. 1105, pp. 103-113). SPIE.

[13] Pan, M., Yang, J., Liu, K., Yin, Z., Ma, T., Liu, S., ... & Wang, S. (2020). Noble metal nanostructured materials for chemical and biosensing systems. *Nanomaterials*, *10*(2), 209.

[14] Souza, R. F., Alencar, M. A., da Silva, E. C., Meneghetti, M. R., & Hickmann, J. M. (2008). Nonlinear optical properties of Au nanoparticles colloidal system: local and nonlocal responses. *Applied Physics Letters*, *92*(20), 201902.

[15] Richardson, H. H., Hickman, Z. N., Govorov, A. O., Thomas, A. C., Zhang, W., & Kordesch, M. E. (2006). Thermooptical properties of gold nanoparticles embedded in ice: characterization of heat generation and melting. *Nano letters*, *6*(4), 783-788.

[16] Skupin, S., Bang, O., Edmundson, D., & Krolikowski, W. (2006). Stability of two-dimensional spatial solitons in nonlocal nonlinear media. *Physical Review E*, *73*(6), 066603.

[17] Ashkarran, A. A., Estakhri, S., Nezhad, M. R. H., & Eshghi, S. (2013). Controlling the geometry of silver nanostructures for biological applications. *Physics Procedia*, *40*, 76-83.

[18] Meng, X. K., Tang, S. C., & Vongehr, S. (2010). A review on diverse silver nanostructures. *Journal of Materials Science & Technology*, *26*(6), 487-522.

[19] Wiley, B., Sun, Y., & Xia, Y. (2007). Synthesis of silver nanostructures with controlled shapes and properties. *Accounts of chemical research*, *40*(10), 1067-1076.

[20] Zhang, P., Wyman, I., Hu, J., Lin, S., Zhong, Z., Tu, Y., ... & Wei, Y. (2017). Silver nanowires: Synthesis technologies, growth mechanism and multifunctional applications. *Materials Science and Engineering: B*, *223*, 1-23.

[21] Dong, H., Chen, Y. C., & Feldmann, C. (2015). Polyol synthesis of nanoparticles: status and options regarding metals, oxides, chalcogenides, and non-metal elements. *Green chemistry*, *17*(8), 4107-4132.

[22] Songping, W., Li, J., Jing, N., Zhenou, Z., & Song, L. (2007). Preparation of ultra fine copper–nickel bimetallic powders for conductive thick film. *Intermetallics*, *15*(10), 1316-1321.

[23] Jeong, S., Woo, K., Kim, D., Lim, S., Kim, J. S., Shin, H., ... & Moon, J. (2008). Controlling the thickness of the surface oxide layer on Cu nanoparticles for the fabrication of conductive structures by ink-jet printing. *Advanced functional materials*, *18*(5), 679-686.

[24] Stewart, I. E., Rathmell, A. R., Yan, L., Ye, S., Flowers, P. F., You, W., & Wiley, B. J. (2014). Solution-processed copper–nickel nanowire anodes for organic solar cells. *Nanoscale*, *6*(11), 5980-5988.

[25] Stortini, A. M., Moretto, L. M., Mardegan, A., Ongaro, M., & Ugo, P. (2015). Arrays of copper nanowire electrodes: Preparation, characterization and application as nitrate sensor. *Sensors and Actuators B: Chemical*, *207*, 186-192.

[26] Ai, X., Fei, H., Yang, Y., Han, L., Nie, R., Zhang, Y., ... & Yu, J. (1994). Polar enhancement of the nonlinear optical properties of Fe2O3 microcrystallites. *Journal of luminescence*, *60*, 364-367.

[27] Yu, B., Zhu, C., & Gan, F. (2000). Large nonlinear optical properties of Fe2O3 nanoparticles. *Physica E: Low-dimensional Systems and Nanostructures*, *8*(4), 360-364.

[28] Sun, Y. P., Riggs, J. E., Rollins, H. W., & Guduru, R. (1999). Strong optical limiting of silver-containing nanocrystalline particles in stable suspensions. *The Journal of Physical Chemistry B*, *103*(1), 77-82.

[29] Ganeev, R. A., Ryasnyansky, A. I., Kamalov, S. R., Kodirov, M. K., & Usmanov, T. (2001). Nonlinear susceptibilities, absorption coefficients and refractive indices of colloidal metals. *Journal of Physics D: Applied Physics*, *34*(11), 1602.

[30] Tom, R. T., Nair, A. S., Singh, N., Aslam, M., Nagendra, C. L., Philip, R., ... & Pradeep, T. (2003). Freely dispersible Au@ TiO2, Au@ ZrO2, Ag@ TiO2, and Ag@ ZrO2 core− shell nanoparticles: one-step synthesis, characterization, spectroscopy, and optical limiting properties. *Langmuir*, *19*(8), 3439-3445.

[31] Stepanov, A. L., Ganeev, R. A., Ryasnyansky, A. I., & Usmanov, T. (2003). Non-linear optical properties of metal nanoparticles implanted in silicate glass. *Nuclear Instruments and Methods in Physics Research Section B: Beam Interactions with Materials and Atoms*, *206*, 624-628.

[32] Kiran, P. P., Shivakiran Bhaktha, B. N., Rao, D. N., & De, G. (2004). Nonlinear optical properties and surface-plasmon enhanced optical limiting in Ag–Cu nanoclusters co-doped in SiO 2 Sol-Gel films. *Journal of applied physics*, *96*(11), 6717-6723.

[33] Pan, H., Chen, W., Feng, Y. P., Ji, W., & Lin, J. (2006). Optical limiting properties of metal nanowires. *Applied physics letters*, *88*(22), 223106.

[34] Gao, Y., Chang, Q., Ye, H., Jiao, W., Li, Y., Wang, Y., ... & Zhu, D. (2007). Size effect of optical limiting in gold nanoparticles. *Chemical Physics*, *336*(2-3), 99-102.

[35] Sreeja, R., Aneesh, P. M., Aravind, A., Reshmi, R., Philip, R., & Jayaraj, M. K. (2008). Size-dependent optical nonlinearity of Au nanocrystals. *Journal of The Electrochemical Society*, *156*(10), K167.

[36] Yang, Q., Seo, J., Kim, W. J., Jung, S., Tabibi, B., Vazquez, J., ... & Temple, D. (2009, February). Optical properties of morphology-controlled gold nanoparticles. In *Photonics and Optoelectronics Meetings (POEM) 2008: Laser Technology and Applications* (Vol. 7276, p. 727617). International Society for Optics and Photonics.

[37] Anvari, J. Z., Karimzadeh, R., & Mansour, N. (2010). Thermo-optic properties and nonlinear responses of copper nanoparticles in polysiloxane oil. *Journal of Optics*, *12*(3), 035212.

[38] Han, Y. P., Luo, M. H., Wang, Q. W., Wang, J. X., & Gao, X. L. (2011). Synthesis of silver nanowires and investigation of their optical limiting properties. In *Advanced Materials Research* (Vol. 295, pp. 152-155). Trans Tech Publications Ltd.

[39] Eslamifara, M., & Mansour, N. (2012). Optical limiting properties of colloids enhanced by gold nanoparticles based on thermal nonlinear refraction. *Int. J. Opt. Photonics*, *6*(1), 49.

[40] Aleali, H., Sarkhosh, L., Karimzadeh, R., & Mansour, N. (2012). Threshold-tunable optical limiters of Au nanoparticles in castor oil. *Journal of Nonlinear Optical Physics & Materials*, *21*(02), 1250024.

[41] Muller, O., Dengler, S., Ritt, G., & Eberle, B. (2013). Size and shape effects on the nonlinear optical behavior of silver nanoparticles for power limiters. *Applied Optics*, *52*(2), 139-149.

[42] Rashidian, M., & Dorranian, D. (2015). INVESTIGATION OF OPTICAL LIMITING IN NANOMETALS. *Reviews On Advanced Materials Science*, *40*(2).

[43] Gao, Y. C., & He, C. Y. (2015, May). Solvent-dependent optical limiting response of platinum nanoparticles stabilized by [60] fullerene derivative. In Third International Symposium on Laser Interaction with Matter (Vol. 9543, p. 95432C). International Society for Optics and Photonics.

[44] Tamgadge, Y. S., Sunatkari, A. L., Talwatkar, S. S., Pahurkar, V. G., & Muley, G. G. (2016). Passive optical limiting studies of nanostructured Cu doped ZnO–PVA composite thin films. *Optical Materials*, *51*, 175-184.

[45] Bi, M., Shao, Y., Wang, Y., Zhang, J., Niu, H., Gao, Y., ... & Li, C. (2017). Liquid crystalline elastomer doped with silver nanoparticles: Fabrication and nonlinear absorption properties. *Molecular Crystals and Liquid Crystals*, *652*(1), 41-50.

[46] DEHGHANipoor, M. A. S. O. U. D., & Khanzadeh, M. (2018). Enhancement of nonlinear absroption and optical limiting properties of graphene oxide in mixed with Fe2O3 nanoparticles.

[47] John, J., Mathew, R. M., Rejeena, I., Jayakrishnan, R., Mathew, S., Thomas, V., & Mujeeb, A. (2019). Nonlinear optical limiting and dual beam mode matched thermal lensing of nano fluids containing green synthesized copper nanoparticles. *Journal of Molecular Liquids*, *279*, 63-66.

[48] Zhang, H., Li, Y., Li, D., & Li, C. (2020). Preparation of silver nanoparticles with different sizes and their optical-limiting property. *Journal of Nanophotonics*, *14*(4), 040502.

[49] Tian, P. (2021). The nonlinear optical absorption and optical limiting properties of noble metal-doped ZnO films. *AIP Advances*, *11*(11), 115315.

[50] Aboud, L. H., Mahdi, Z. F., & Al-Zahra, W. J. A. (2014). Linear and Nonlinear Optical Properties of the Dye Laser (Acridine Dye). *Academic Research International*, *5*(4), 135.

[51] Hemerik, M. (2001). *Design of a mid-infrared cavity ring down spectrometer*. Technische Universiteit Eindhoven.

[52] Andreasen, J., Sebbah, P., & Vanneste, C. (2011). Nonlinear effects in random lasers. *JOSA B*, *28*(12), 2947-2955.

[53] Fowles, G. R. (1989). *Introduction to modern optics*. Courier Corporation.

[54] Nelson, J. A. (2003). *The physics of solar cells*. World Scientific Publishing Company.

[55] Straughan, B. P., & Walker, S. (1976). Molecular Quantum Numbers of Diatomic Molecules. In *Spectroscopy* (pp. 1-25). Springer, Dordrecht.

[56] Parikh, V. M. (1974). *Absorption spectroscopy of organic molecules*. Reading, Mass.: Addison-Wesley Publishing Company.

[57] Jackson, J. D. (1962). : Classical electrodynamics. John Wiley and Sons, Inc., New York-London-Sydney, 641 p.

[58] Hollas, J. M. (2004). *Modern spectroscopy*. John Wiley & Sons.

[59] László, P. (2003). *Investigation of nonlinear optical properties of LiNbO3 by Z-scan method* (Doctoral dissertation, Ph. D. thesis, University of Szeged).

[60] Davies, M. (1963). Infra-red spectroscopy and molecular structure.

[61] Qi, S., Zhang, C., Yang, X., Chen, K., Zhang, L., Liu, Y., ... & Tian, J. (2007). Effective indexes of refraction and limiting properties of ethyl red. *Optik*, *118*(9), 425-429.

[62] Li, Q. S., Liu, C. L., Zang, L. Y., Gong, Q. H., Yu, X. L., & Cao, C. B. (2008). Broadband optical limiting in the suspensions of lead sulfide nanoparticles. *Laser Physics*, *18*(4), 434-437.

[63] Menzel, R. (2013). *Photonics: linear and nonlinear interactions of laser light and matter*. Springer Science & Business Media.

[64] Marciu, D. (1999). *Optical limiting and degenerate four-wave mixing in novel fullerenes* (Doctoral dissertation, Virginia Polytechnic Institute and State University).

[65] Neethling, P. H. (2005). *Determining non-linear optical properties using the Z-scan technique* (Doctoral dissertation, Stellenbosch: University of Stellenbosch).

[66] Boyd, R. W. (2020). *Nonlinear optics*. Academic press.

[67] Steinmann, C. M. (1999). *Development and characterisation of a tunable laser source in the vacuum ultraviolet* (Doctoral dissertation, Stellenbosch: Stellenbosch University).

[68] Milonni, P. W., & Eberly, J. H. (1988). Lasers john wiley and sons. *New York*.

[69] He, G., & Liu, S. H. (1999). *Physics of nonlinear optics*. World Scientific.

[70] Vinitha, G., & Ramalingam, A. (2008). Spectral characteristics and nonlinear studies of methyl violet 2B dye in liquid and solid media. *Laser physics*, *18*(1), 37-42.

[71] Sadigh, M. K., Zakerhamidi, M. S., Rezaei, B., & Milanchian, K. (2017). Environment effects on the nonlinear absorption properties of Methylene blue under different power of excitation beam. *Journal of Molecular Liquids*, *229*, 548-554.

[72] Irimpan, L. (2019). Spectral and nonlinear optical characterization of ZnO nanocomposites.

[73] Marburger, J. H. (1975). Self-focusing: theory. *Progress in quantum electronics*, *4*, 35-110.

[74] Ghatak, A. (2012). *Contemporary optics*. Springer Science & Business Media.

[75] Jaffar, A. F. (2020). The Effects of Initial Laser Intensity on the Nonlinear Optical Properties of The Laser Dye DQOCI Doped Films Using Z-Scan Technique. *Iraqi Journal of Science*, 2551-2561.

[76] Jaffar, A. F. (2017). Nonlinear optical characteristics of Nile blue films doped with the polymers PMMA, PVC and their blend by using z-scan technique. *Iraqi Journal of Science*, 1839-1848.

[77] Veselago, V. G. (1968). Reviews of topical problems: the electrodynamics of substances with simultaneously negative values of ε and μ. *Sov. Phys.-Usp*, *10*(4), 509-514.

[78] Smith, D. R., Padilla, W. J., Vier, D. C., Nemat-Nasser, S. C., & Schultz, S. (2000). Composite medium with simultaneously negative permeability and permittivity. *Physical review letters*, *84*(18), 4184.

[79] Shelby, R. A., Smith, D. R., & Schultz, S. (2001). Experimental verification of a negative index of refraction. *science*, *292*(5514), 77-79.

[80] Pendry, J. B. (2000). Negative refraction makes a perfect lens. *Physical review letters*, *85*(18), 3966.

[81] Shen, Y. R. (1975). Self-focusing: experimental. *Progress in quantum electronics*, *4*, 1-34.

[82] Marburger, J. H. (1975). Self-focusing: theory. *Progress in quantum electronics*, *4*, 35-110.

[83] Wen, S., Wu, J., Tang, K., Su, W., Fu, X., & Fan, D. (2005, January). Self-focusing and self-defocusing of the optical beam propagation in a nonlinear negative-refractive-index material. In *High-Power Lasers and Applications III* (Vol. 5627, pp. 71-75). International Society for Optics and Photonics.

[84] Sheik-Bahae, M., & Hasselbeck, M. P. (2000). Third-order optical nonlinearities. *Handbook of Optics*, *4*, 16-1.

[85] Sutherland, R. L. (2003). *Handbook of nonlinear optics*. CRC press.

[86] Göppert-Mayer, M. (1931). Über elementarakte mit zwei quantensprüngen. *Annalen der Physik*, *401*(3), 273-294.

[87] He, G. S., Tan, L. S., Zheng, Q., & Prasad, P. N. (2008). Multiphoton absorbing materials: molecular designs, characterizations, and applications. *Chemical reviews*, *108*(4), 1245-1330.

[88] Maruo, S., Nakamura, O., & Kawata, S. (1997). Three-dimensional microfabrication with two-photon-absorbed photopolymerization. *Optics letters*, *22*(2), 132-134.

[89] Parthenopoulos, D. A., & Rentzepis, P. M. (1989). Three-dimensional optical storage memory. *Science*, *245*(4920), 843-845.

[90] Yanik, M. F., Cinar, H., Cinar, H. N., Gibby, A., Chisholm, A. D., Jin, Y., & Ben-Yakar, A. (2006). Nerve regeneration in Caenorhabditis elegans after femtosecond laser axotomy. *IEEE Journal of selected topics in quantum electronics*, *12*(6), 1283-1291.

[91] Li, X. C., Moratti, S. C., Wise, D. L., Wnek, G. E., Trantolo, D. J., Cooper, T. M., & Gresser, J. D. (1998). Photonic Polymer Systems.

[92] Irimpan, L., Deepthy, A., Krishnan, B., Nampoori, V. P. N., & Radhakrishnan, P. (2008). Nonlinear optical characteristics of self-assembled films of ZnO. *Applied Physics B*, *90*(3), 547-556.

[93] Laud, B. B. (1986). Lasers and nonlinear optics.

[94] Blau, W., Byrne, H., Dennis, W. M., & Kelly, J. M. (1985). Reverse saturable absorption in tetraphenylporphyrins. *Optics Communications*, *56*(1), 25-29.

[95] Tutt, L. W., & Boggess, T. F. (1993). A review of optical limiting mechanisms and devices using organics, fullerenes, semiconductors and other materials. *Progress in quantum electronics*, *17*(4), 299-338.

[96] Boggess, T., Bohnert, K., Mansour, K., Moss, S., Boyd, I., & Smirl, A. (1986). Simultaneous measurement of the two-photon coefficient and free-carrier cross section above the bandgap of crystalline silicon. *IEEE journal of quantum electronics*, *22*(2), 360-368.

[97] Malacara-Hernández, D., Malacara-Hernández, Z., & Malacara, Z. (2003). *Handbook of optical design*. CRC Press.

[98] Wang1a, J., Chen1b, Y., Li1a, R., Dong1a, H., Zhang1a, L., Lotya, M., ... & Blau, W. J. (2011). Nonlinear optical properties of graphene and carbon nanotube composites. *Carbon Nanotubes: Synthesis, Characterization, Applications*, 397.

[99] Saleh, B. E., & Teich, M. C. (1991). Fundamentals of photonics. *NASA STI/Recon Technical Report A*, *92*, 35987.

[100] Long, D. A., & Long, D. A. (2002). *The Raman effect: a unified treatment of the theory of Raman scattering by molecules* (Vol. 8, pp. 31-48). Chichester: Wiley.

[101] Berne, B. J., & Pecora, R. (2000). *Dynamic light scattering: with applications to chemistry, biology, and physics*. Courier Corporation.

[102] Damzen, M. J., Vlad, V., Mocofanescu, A., & Babin, V. (2003). *Stimulated Brillouin scattering: fundamentals and applications*. CRC press.

[103] Shen, Y. R. (2002). The Principles of Nonlinear Optics. 3rd edn, 576.

[104] Sutherland, R. L. (2003). *Handbook of nonlinear optics*. CRC press.

[105] Boyd, R. W. (2003). Nonlinear Optics, Acad.

[106] Levenson, M. D., & Kano, S. S. (1982). Introduction to Nonlinear Laser Spectroscopy Academic Press. *New York*.

[107] He, G., & Liu, S. H. (1999). *Physics of nonlinear optics*. World Scientific.

[108] Sheik-Bahae, M., Said, A. A., & Van Stryland, E. W. (1989). High-sensitivity, single-beam n 2 measurements. *Optics letters*, *14*(17), 955-957.

[109] De Araújo, C. B., Gomes, A. S., & Boudebs, G. (2016). Techniques for nonlinear optical characterization of materials: a review. *Reports on Progress in Physics*, *79*(3), 036401.

[110] Chapple, P. B., Staromlynska, J., Hermann, J. A., Mckay, T. J., & McDuff, R. G. (1997). Single-beam Z-scan: measurement techniques and analysis. *Journal of Nonlinear Optical Physics & Materials*, *6*(03), 251-293.

[111] Pálfalvi, L., Tóth, B. C., Almási, G., Fülöp, J. A., & Hebling, J. (2009). A general Z-scan theory. *Applied Physics B*, *97*(3), 679-685.

[112] Neethling, P. H. (2005). *Determining non-linear optical properties using the Z-scan technique* (Doctoral dissertation, Stellenbosch: University of Stellenbosch).

[113] Yunus, E. S. W. M. M. (2010). Single beam Z-scan measurements of nonlinear refraction and nonlinear absorption coefficients in silver nano-fluid. *Am. J. Engg. & Applied Sci*, *3*(1), 98-101.

[114] Gomez, S. L., Cuppo, F. L. S., & Figueiredo Neto, A. M. (2003). Nonlinear optical properties of liquid crystals probed by Z-scan technique. *Brazilian Journal of Physics*, *33*(4), 813-820.

[115] Sheik-Bahae, M., & Hasselbeck, M. P. (2000). Third-order optical nonlinearities. *Handbook of Optics*, *4*, 16-1.

[116] Dhinaa, A. N., & Palanisamy, P. K. (2010). Z-Scan technique: To measure the total protein and albumin in blood. *J. Biomed. Sci. Eng*, *3*(03), 285-290.

[117] Van Stryland, E. W., & Sheik-Bahae, M. (1998). Z-scan measurements of optical nonlinearities. *Characterization techniques and tabulations for organic nonlinear materials*, *18*(3), 655-692.

[118] Ali, A. A., Sindhu, V., & Srinivasan, A. G. (2013). Third order nonlinear optical studies of bromocresol purple in liquid and solid media. *Optik*, *124*(21), 4836-4840.

[119] Abrinaei, F. (2017). Nonlinear optical response of Mg/MgO structures prepared by laser ablation method. *Journal of the European Optical Society-Rapid Publications*, *13*(1), 1-10.

[120] Sheik-Bahae, M., Said, A. A., & Van Stryland, E. W. (1989). High-sensitivity, single-beam n 2 measurements. *Optics letters*, *14*(17), 955-957.

[121] Sheik-Bahae, M., Said, A. A., Wei, T. H., Hagan, D. J., & Van Stryland, E. W. (1990). Sensitive measurement of optical nonlinearities using a single beam. *IEEE journal of quantum electronics*, *26*(4), 760-769.

[122] Patil, P. S., Maidur, S. R., Rao, S. V., & Dharmaprakash, S. M. (2016). Crystalline perfection, third-order nonlinear optical properties and optical limiting studies of 3, 4-Dimethoxy-4′-methoxychalcone single crystal. *Optics & Laser Technology*, *81*, 70-76.

[123] Van Stryland, E. W., Soileau, M. J., Ross, S., & Hagan, D. J. (1999). Passive Optical Limiting: Where are we?. *NONLINEAR OPTICS-READING-*, *21*, 29-29.

[124] Khoo, I. C., Michael, R. R., & Finn, G. M. (1988). Self-phase modulation and optical limiting of a low-power CO2 laser with a nematic liquid-crystal film. *Applied physics letters*, *52*(25), 2108-2110.

[125] Lide, D. R. (Ed.). (2004). *CRC handbook of chemistry and physics* (Vol. 85). CRC press.

[126] Turro, N. J. (1991). *Modern molecular photochemistry*. University science books.

[127] Sakthisabarimoorthi, A., Jose, M., Martin Britto Dhas, S. A., & Jerome Das, S. (2017). Fabrication of Cu@ Ag core–shell nanoparticles for nonlinear optical

applications. *Journal of Materials Science: Materials in Electronics*, *28*(6), 4545-4552.

[128] Mostafa, A. M., & Mwafy, E. A. (2020). Synthesis of ZnO and Au@ ZnO core/shell nano-catalysts by pulsed laser ablation in different liquid media. *Journal of Materials Research and Technology*, *9*(3), 3241-3248.

[129] Holec, D., Dumitraschkewitz, P., Vollath, D., & Fischer, F. D. (2020). Surface energy of Au nanoparticles depending on their size and shape. *Nanomaterials*, *10*(3), 484.

[130] Peng, S., McMahon, J. M., Schatz, G. C., Gray, S. K., & Sun, Y. (2010). Reversing the size-dependence of surface plasmon resonances. *Proceedings of the National Academy of Sciences*, *107*(33), 14530-14534.

[131] Shafiqa, A. R., Aziz, A. A., & Mehrdel, B. (2018, August). Nanoparticle optical properties: size dependence of a single gold spherical nanoparticle. In *Journal of Physics: Conference Series* (Vol. 1083, No. 1, p. 012040). IOP Publishing.

[132] Cuando-Espitia, N., Hernández-Cordero, J., García-Segundo, C., & Quispe-Siccha, R. (2011, June). Effects of scatterer size and concentration on the spectral features of dye-based random lasers. In *Integrated Photonics Research, Silicon and Nanophotonics* (p. IMD5). Optical Society of America.

[133] Liu, P., Wang, H., Li, X., Rui, M., & Zeng, H. (2015). Localized surface plasmon resonance of Cu nanoparticles by laser ablation in liquid media. *Rsc Advances*, *5*(97), 79738-79745.

[134] Ramyadevi, J., Jeyasubramanian, K., Marikani, A., Rajakumar, G., Rahuman, A. A., Santhoshkumar, T., ... & Marimuthu, S. (2011). Copper nanoparticles synthesized by polyol process used to control hematophagous parasites. *Parasitology research*, *109*(5), 1403-1415.

[135] Duan, J. L., Cornelius, T. W., Liu, J., Karim, S., Yao, H. J., Picht, O., ... & Neumann, R. (2009). Surface plasmon resonances of Cu nanowire arrays. *The Journal of Physical Chemistry C*, *113*(31), 13583-13587.

[136] Lotey, G. S., Kumar, S., & Verma, N. K. (2012). Fabrication and electrical characterization of highly ordered copper nanowires. *Applied Nanoscience*, *2*(1), 7-13.

[137] Mirzaei, A., Janghorban, K., Hashemi, B., Bonavita, A., Bonyani, M., Leonardi, S. G., & Neri, G. (2015). Synthesis, characterization and gas sensing properties of Ag@ α-Fe2O3 core–shell nanocomposites. *Nanomaterials*, *5*(2), 737-749.

[138] Qu, S., Gao, Y., Jiang, X., Zeng, H., Song, Y., Qiu, J., ... & Hirao, K. (2003). Nonlinear absorption and optical limiting in gold-precipitated glasses induced by a femtosecond laser. *Optics communications*, *224*(4-6), 321-327.

[139] Zhao, Y., Fitzgerald, M. L., Tao, Y., Pan, Z., Sauti, G., Xu, D., ... & Li, D. (2020). Electrical and thermal transport through silver nanowires and their contacts: effects of elastic stiffening. *Nano Letters*, *20*(10), 7389-7396.

[140] Shahriari, E., & Yunus, W. M. M. (2010). Effect of particle size on nonlinear refraction and absorption of Ag nanoparticles. *Dig. J. Nanomater. Biostruct*, *5*(4), 939-946.

Appendix

r_a (mm)	1
w_a (mm) at (405, 473 & 532) nm	5
w_a (mm) at (650) nm	13
L (mm)	10
f (cm)	8.5
S	0.076883654

λ (nm)	ω_0^2 (m^2)
405	8.9×10^{-10}
473	13.9×10^{-10}
532	18.7×10^{-10}
650	6.17×10^{-10}

Ag NPs					
λ (nm)	I_o (MW/m^2)	Concentration (mg/ml)	L_{eff} (m)	ΔT	A
405	13.48980506	0.04	0.000981057	2.022727273	0.166613667
		0.08	0.0009757	2.695473251	0.214518667
		0.12	0.000968449	3.476635514	0.279919
473	4.982735847	0.04	0.00098015	2.125307125	0.174700667
		0.08	0.000975062	2.200902935	0.220245
		0.12	0.000967726	3.151898734	0.286477667
532	5.792389222	0.04	0.000982078	1.655976676	0.157524
		0.08	0.00097799	2.430976431	0.194003333
		0.12	0.00097156	2.52407932	0.251778667
650	13.5175822	0.04	0.000987953	0.625570776	0.105472667
		0.08	0.000985002	1.046683047	0.131565
		0.12	0.000980479	1.166666667	0.171766667

Ag NW D50					
λ (nm)	I_o (MW/m^2)	Concentration (mg/ml)	L_{eff} (m)	ΔT	A
405	14.83878556	0.04	0.000970887	0.611336032	0.257853333
		0.08	0.00095869	0.898305085	0.368983333
		0.12	0.000935239	0.955017301	0.58808
473	9.031208724	0.04	0.000972396	0.348571429	0.24424
		0.08	0.000959978	0.696428571	0.357156667
		0.12	0.000939328	1.696035242	0.54935
532	8.214661079	0.04	0.000974112	0.323333333	0.22879
		0.08	0.000962821	0.56741573	0.33113
		0.12	0.000943319	0.664031621	0.51176
650	13.32167522	0.04	0.000978408	0.238410596	0.19026
		0.08	0.000968589	0.375	0.278653333
		0.12	0.000952967	0.622377622	0.42178

Ag NW D100					
λ (nm)	I_o (MW/m^2)	Concentration (mg/ml)	L_{eff} (m)	ΔT	A
405	14.83878556	0.04	0.000985896	1.73245614	0.123645
		0.08	0.000974654	2.507614213	0.223910111
		0.12	0.000967232	2.845679012	0.290962111
473	9.031208724	0.04	0.000989568	1.965299685	0.091234778
		0.08	0.000981389	2.151202749	0.163659333
		0.12	0.00097624	2.28	0.209678
532	8.214661079	0.04	0.000992584	1.196428571	0.064725333
		0.08	0.000986723	1.591304348	0.116329556
		0.12	0.000983326	1.933333333	0.146434556
650	13.32167522	0.04	0.000994822	0.596059113	0.045121222
		0.08	0.000990437	0.830769231	0.083584111
		0.12	0.000988331	0.942105263	0.102137556

Ag NW D200					
λ (nm)	I_o (MW/m^2)	Concentration (mg/ml)	L_{eff} (m)	ΔT	A
405	14.83878556	0.04	0.000993716	1.397129187	0.054799889
		0.08	0.000989783	1.59798995	0.089334889
		0.12	0.000981898	2.548022599	0.159129444
473	9.031208724	0.04	0.000994089	1.205278592	0.051533
		0.08	0.00099047	1.501992032	0.083295111
		0.12	0.000983014	1.756272401	0.149209333
532	8.214661079	0.04	0.00099457	0.963768116	0.047325889
		0.08	0.00099131	0.976377953	0.075908667
		0.12	0.000984498	1.207407407	0.136038222
650	13.32167522	0.04	0.000995146	0.308411215	0.042286778
		0.08	0.00099225	0.355769231	0.067649333
		0.12	0.000986043	0.735751295	0.122352444

Au1					
λ (nm)	I_o (MW/m^2)	Concentration (mg/ml)	L_{eff} (m)	ΔT	A
405	14.83878556	0.04	0.000996187	1.110576923	0.033194
		0.08	0.000994039	2.243243243	0.051977
		0.12	0.000991081	2.626984127	0.077916667
473	2.076139936	0.04	0.000996364	0.245454545	0.031649
		0.08	0.000993995	0.362934363	0.052359667
		0.12	0.000990761	0.722807018	0.080733667
532	5.792389222	0.04	0.000996159	0.241791045	0.033438667
		0.08	0.000993375	0.356707317	0.057793
		0.12	0.000989809	1.163043478	0.08911
650	13.5175822	0.04	0.000996849	0.21875	0.027421667
		0.08	0.000994655	0.382653061	0.046585333
		0.12	0.000992487	0.869109948	0.065571333

Au2					
λ (nm)	I_o (MW/m^2)	Concentration (mg/ml)	L_{eff} (m)	ΔT	A
405	14.83878556	0.04	0.000992141	2.286384977	0.068605667
		0.08	0.000988606	2.728723404	0.099706667
		0.12	0.000986665	3.854054054	0.116847667
473	2.076139936	0.04	0.000991853	0.525581395	0.071134667
		0.08	0.000988245	0.776061776	0.102896
		0.12	0.000986411	1.125	0.119096
532	5.792389222	0.04	0.000991781	0.603932584	0.071772
		0.08	0.000988102	0.715846995	0.104157667
		0.12	0.000986174	1.021220159	0.121191667
650	13.5175822	0.04	0.000992425	0.434554974	0.066120333
		0.08	0.000989095	0.594594595	0.095396
		0.12	0.000986921	1.03	0.114584

Au3					
λ (nm)	I_o (MW/m^2)	Concentration (mg/ml)	L_{eff} (m)	ΔT	A
405	14.83878556	0.04	0.0009944	2.1	0.048811667
		0.08	0.000990634	3.051282	0.081852
		0.12	0.000987357	3.395973	0.110735
473	2.28375393	0.04	0.000994007	0.533936652	0.052255667
		0.08	0.000989984	0.565420561	0.087569333
		0.12	0.000986557	0.589108911	0.117805333
532	5.792389222	0.04	0.000993439	0.465053763	0.057227667
		0.08	0.000988801	0.563186813	0.097992
		0.12	0.000985237	0.617728532	0.129483667
650	13.5175822	0.04	0.000994112	0.215962441	0.051330667
		0.08	0.000989735	0.465686275	0.089756
		0.12	0.000986994	2.482758621	0.113936667

Cu1					
λ (nm)	I_o (MW/m^2)	Concentration (mg/ml)	L_{eff} (m)	ΔT	A
405	13.48980506	0.04	0.000994743	1.15018315	0.045813333
		0.08	0.000991253	1.279761905	0.076410333
		0.12	0.000985606	2.305	0.126220333
473	4.982735847	0.04	0.000994618	0.681528662	0.04691
		0.08	0.000991073	1.094202899	0.077988667
		0.12	0.000985165	1.429752066	0.130124
532	5.792389222	0.04	0.000994668	0.943894389	0.046473
		0.08	0.000990998	0.964516129	0.078645
		0.12	0.00098512	1.009677419	0.130524667
650	13.5175822	0.04	0.000994903	0.567335244	0.044411
		0.08	0.000991411	0.67	0.075021
		0.12	0.000985822	1.265306122	0.124307333

Cu2					
λ (nm)	I_o (MW/m^2)	Concentration (mg/ml)	L_{eff} (m)	ΔT	A
405	13.48980506	0.04	0.000976295	2.36119403	0.209182667
		0.08	0.000964806	2.404458599	0.313022
		0.12	0.000958286	2.75399361	0.372695667
473	4.982735847	0.04	0.000975999	2.971698113	0.211836
		0.08	0.000964733	3.2	0.313692
		0.12	0.000957911	3.429752066	0.376141
532	5.792389222	0.04	0.000976073	1.74015748	0.211173
		0.08	0.000965016	1.855345912	0.311108333
		0.12	0.000957958	2.012738854	0.375711333
650	13.5175822	0.04	0.000972473	2.667597765	0.243544333
		0.08	0.000958968	2.789634146	0.366430667
		0.12	0.000952213	3.319078947	0.428768333

Cu NW D50					
λ (nm)	I_o (MW/m^2)	Concentration (mg/ml)	L_{eff} (m)	ΔT	A
405	14.83878556	0.04	0.000989406	2.2	0.092661
		0.08	0.000986471	2.6	0.118561667
		0.12	0.000981308	2.679245283	0.164385667
473	4.982735847	0.04	0.000989442	1	0.092344
		0.08	0.000986763	1.168224299	0.115978333
		0.12	0.000980927	1.614173228	0.167776667
532	6.845550899	0.04	0.0009894	0.850574713	0.092712667
		0.08	0.00098692	1.126086957	0.114594
		0.12	0.000980898	1.791519435	0.168036333
650	13.5175822	0.04	0.000988546	0.683333333	0.100234667
		0.08	0.000985974	0.722222222	0.122957667
		0.12	0.000979137	1.69	0.183748333

Fe_2O_3 Nano fragments					
λ (nm)	I_o (MW/m^2)	Concentration (mg/ml)	L_{eff} (m)	ΔT	A
405	14.83878556	0.04	0.000989187	2.044534413	0.094587333
		0.08	0.000980033	3.991735537	0.175751333
		0.12	0.000975582	4.610169492	0.215577667
473	6.228419809	0.04	0.000995645	0.555555556	0.037930333
		0.08	0.000993493	0.880952381	0.056752333
		0.12	0.000990032	1.342857143	0.087147333
532	6.845550899	0.04	0.000997569	0.451388889	0.021146333
		0.08	0.000997569	0.599250936	0.021146333
		0.12	0.000994239	0.717391304	0.050225667
650	13.5175822	0.04	0.00099887	0.102803738	0.009816667
		0.08	0.000998883	0.114678899	0.009706667
		0.12	0.000997077	0.160839161	0.025434333

Cu2 + Ag NW D200 (1:1)				
λ (nm)	I_o (MW/m^2)	L_{eff} (m)	ΔT	A
405	13.48980506	0.000992577	2.905940594	0.064783111
473	2.28375393	0.000992637	0.877659574	0.064260556
532	5.792389222	0.000992939	1.405263158	0.061610333
650	13.5175822	0.000997588	1.534412955	0.062936667

Ag NPs + Cu NW D50 (1:1)				
λ (nm)	I_o (MW/m^2)	L_{eff} (m)	ΔT	A
405	13.48980506	0.000982172	2.160337553	0.156693667
473	4.982735847	0.000984452	1.698630137	0.136439333
532	5.792389222	0.000988739	1.343971631	0.098536
650	13.5175822	0.000990911	1.077625571	0.079412333

Ag NPs + Fe2O3 Nano fragments (1:3) with sonication				
λ (nm)	I_o (MW/m^2)	L_{eff} (m)	ΔT	A
405	14.83878556	0.000972999	2.867256637	0.238805333
473	4.982735847	0.000985445	1.827586207	0.127644667
532	5.792389222	0.000992235	1.455445545	0.067787
650	13.5175822	0.00099683	0.467889908	0.027585667

Ag NPs + Fe2O3 Nano fragments (1:3) with pulses laser				
λ (nm)	I_o (MW/m^2)	L_{eff} (m)	ΔT	A
405	14.83878556	0.000971725	3.895833333	0.250292667
473	4.982735847	0.000980903	2.06185567	0.167993
532	5.792389222	0.000987641	1.90212766	0.108226667
650	13.5175822	0.000993967	0.562091503	0.0526

Cu1 + Fe2O3 Nano fragments (1:3) with sonication				
λ (nm)	I_o (MW/m^2)	L_{eff} (m)	ΔT	A
405	14.83878556	0.000964576	2.948275862	0.315121
473	4.982735847	0.000974203	2.135135135	0.227966333
532	5.792389222	0.000978676	1.685618729	0.187863
650	13.5175822	0.000982335	1.2	0.155245333

Cu1 + Fe2O3 Nano fragments (1:3) with pulses laser				
λ (nm)	I_o (MW/m^2)	L_{eff} (m)	ΔT	A
405	14.83878556	0.000964576	4.044444444	0.325325333
473	4.982735847	0.000975094	2.742268041	0.219957333
532	5.792389222	0.000980803	1.817708333	0.16888
650	13.5175822	0.000984377	1.348484848	0.137109667

Republic of Iraq
Ministry of Higher Education
And Scientific Research
University of Kerbala
Dean Office

جمهورية العراق
وزارة التعليم العالي والبحث العلمي
جامعة كربلاء كلية العلوم
مكتب العميد

No : 73 / 5 / م
date : 2021 / 6 / 28

العدد : 73 / 5 / م
التاريخ : 2021 / 6 / 28

Subject: Paper Publishing Acceptance

Dear Hayder AL-Aaraji

We are delighted to inform you that your manuscript entitled "**Third Order Nonlinear Susceptibility of Cu Nanoparticles, Ag Nano-wires, and Their Mixture at Different Wavelengths**" has been accepted in the 9th International Conference of Applied Science andTechnology (ICAST2021) Conference Proceeding.

The accepted manuscripts will be published in the AIPconference proceedings which is Scopus indexed and has an impact factor.

Once your article is uploaded online, a notification email will be sent to you.

If you have any enquiry, please, do not hesitate to contact us.

Yours Sincerely,

Karbala University
Dean Office
Science College

Jasim Alawadi

Assist. Prof. Dr. Jasim Hanoon Hashim Al-Awadi
Chairman of ICAST 2021
Dean of the Faculty of Science, University of Kerbala, Karbala, Iraq.
Phone: +9647831556219
E-mail: jasem.h@uokerbala.edu.iq

SECOND INTERNATIONAL SCIENTIFIC CONFERENCE (SISC2021)
24 – 25 May 2021 | College of Science, Al-Nahrain University
Baghdad – Iraq

Acceptance Letter

Dear (s): Hayder H. Al-Aaraji , Qussay Mohamad Salman

On behalf of the Second International Scientific Conference SISC2021, it is a great pleasure to inform you that after a peer-review assessment, your manuscript entitled:

"Wavelengths Effect on Nonlinear Refraction of Copper Nanoparticles Suspension"

has been **accepted** and considered for publication in the AIP Conference Proceedings Scopus Indexed.

Your participation is much appreciated.

With best regards,

Nasreen Raheem

Prof. Dr. Nasreen R. Jber
General Chair

جمهورية العراق
وزارة التعليم العالي والبحث العلمي
جامعة بابل
كلية العلوم للبنات

دراسة الخواص المورفولوجية والبصرية

(الخطية واللاخطية) للجسيمات النانوية كمحدد بصري

أطروحة

مقدمة الى قسم فيزياء الليزر في كلية العلوم للبنات - جامعة بابل
كجزء من متطلبات نيل درجة الدكتوراه في فيزياء الليزر وتطبيقاته

من قبل

حيدر حسين حمّود الأعرجي

(بكالوريوس علوم فيزياء - جامعة بابل ١٩٩٤ م)

(ماجستير كهروبصريات - الجامعة التكنولوجية ٢٠٠٢ م)

بإشراف

الأستاذ المساعد الدكتور

قصي محمد سلمان

١٤٤٣ هـ

٢٠٢٢ م

الخلاصة:

تهدف هذه الدراسة الى دراسة الخواص المورفولوجية والبصرية الخطية واللاخطية لجسيمات نانوية معدنية وأحد اكاسيد المعادن لتوضيفها كمحدد بصري بالإضافة الى عمل خلطات من هذه المواد لاثراء الخواص البصرية وخواص المحدد البصري. ان المواد التي تم استخدامها في هذه الدراسة هي (جسيمات الفضة النانوية الكروية واسلاك الفضة النانوية وجسيمات الذهب النانوية الكروية وجسيمات النحاس النانوية الكروية واسلاك النحاس النانوية وجسيمات أوكسيد الحديد النانوية).

تم دراسة الخواص المورفولوجية لغرض تحديد شكل وحجم الجسيمات قيد الدراسة لجميع المواد وكذلك الخواص المورفولوجية للخلطات المحضرة من خلال تحليل الصور المستحصلة من المجهر الالكتروني الماسح. أظهرت النتائج ان جسيمات (Ag NPs) كروية وبحجم سائد مقداره (٧٠) نانومتر. وان (Ag NWs) ذات ثلاثة اقطار (٥٠، ١٠٠، ٢٠٠) نانومتر وبطول واحد لجميعها مقداره يتراوح (٥-٥٠) مايكرومتر. كانت نتائج (Au NPS) انها جسيمات كروية وبثلاثة حجوم سائدة هي(٤،٦،٨) نانومتر. اما (Cu NPs) فانها كانت كروية ايضاً وبحجمين سائدين الأول (٥٠) نانومتر والثاني (٩٠-٩٩) نانومتر. اما اسلاك النحاس النانوية فكانت بقطر (٥٠) نانومتر وبطول مقداره (٥٠) مايكرومتر. كانت نتائج (Fe_2O_3) انها جسيمات نانوية بشكل شضايا وبحجم سائد مقداره (٦٥) نانومتر. اما نتائج الخلطات والتي كانت أربعة خلطات الأولى (Ag NWs D200+Cu2) بنسبة (١:١) لمعلقها في الايثانول المطلق وبتركيز (٠,١٢) مليغرام/ مليلتر وتم استخدام الموجات فوق الصوتية لاجراء عملية الخلط واظهرت نتائج صور المجهر الالكتروني الماسح حدوث تلاصق سطحي بين جسيمات النحاس الناوية الكروية واسلاك الفضة النانوية كان له الأثر في اظهار نتائج مغايرة للخواص البصرية الخطية واللاخطية وخواص المحدد البصري لمكونات مواد هذه الخلطة منفردة. اما الخلطة الثانية فكانت (Cu NWs D50+Ag NPs) وبنفس النسب الحجمية للخلطة الأولى واظهر النتائج ايضاً حدوث التصاق سطحي بين المادتين. الخلطة الثالثة كانت (Fe_2O_3 Nano fragments + Ag NPs) بنسبة (١:٣) لمعلقها في الايثانول المطلق بتركيز (٠,١٢) مليغرام/ مليلتر. تمت عملية الخلط بطريقتين مختلفتين الأولى باستخدام الليزر البنضي والثانية باستخدام الموجات فوق الصوتية واظهرت النتائج حدوث تركيب جديد بينها وهو تركيب لب-غلاف. اما الخلطة الرابعة (Fe_2O_3 Nano fragments + Cu1) فكانت بنفس النسب الحجمية للخلطة الثالثة وبنفس طريقتي الخلط للخلطة الثالثة وكانت النتائج كما للخلطة الثالثة ايضاً.

تم دراسة خواص الامتصاص البصري لمعلقات جميع المواد والخلطات في الايثانول المطلق بثلاثة تراكيز (٠,٠٤ و ٠,٠٨ و ٠,١٢) مليغرام/ مليلتر . حيث تم حساب معامل الامتصاص الخطي ,والنفاذية الخطية لجميع المعلقات ولجميع التراكيز وتحديد عرض نطاق وقمة الامتصاص لكل مادة واظهرت النتائج معدلات امتصاص خطية منخفضة لجميع عينات المواد النانوية. وكذلك تم قياس معامل الانكسار الخطي لجميع معلقات المواد والخلطات.

تم دراسة الخواص البصرية اللاخطية لجميع المواد والخلطات بجميع التراكيز باستخدام تقنية المسح على المحور الثالث وباستخدام أربعة اطوال موجية (٤٠٥ و ٤٧٣ و ٥٣٢ و ٦٥٠) نانومتر من ليزر اشباه الموصلات المستمر. اظهرت النتائج لجميع المواد ان لها معامل انكسار لاخطي سالب ناتج من عملية إعادة التبئير الذاتي. ان معامل الانكسار اللاخطي يزداد بزيادة التركيز لكل مادة. أظهرت نتائج معامل الانكسار اللاخطي للخلطات قيم مغايرة لقيم المواد الموكونة منها. أظهرت النتائج عدم وجود امتصاص لاخطي لجميع

معلقات المواد والخلطات. بالاعتماد على على نتائج معامل الانكسار الخطي واللاخطي تم حساب الجزء الحقيقي لقابلية المرتبة الثالثة اللاخطية لجميع معلقات المواد والخلطات. تم تسجيل اعلى قيم (n_2) و ($Re\ \chi^{(3)}$) لل (Cu2) عند الطول الموجي (٤٧٣) نانومتر وشدة (٤,٩٨) ميكاواط/م^{٢} وكانت قيمها (١,١٣٧٩٥×١٠$^{-١٠}$، ١,٢٣٠١٦ ×١٠$^{-١٠}$ و ١,٣٢١٦٣ ×١٠$^{-١٠}$) م^{٢}/ واط و ٥,٣٢ ×١٠$^{-٥}$، ٥,٧٥×١٠$^{-٥}$ و ٦,١٨ ×١٠$^{-٥}$) (وحدة شحنة كهروستاتيكية) على الترتيب. تم تسجيل اقل قيم (n_2) و ($Re\ \chi^{(3)}$) للشضايا النانوية ل (Fe_2O_3) للتركيز (٠,٠٤ مليغرام/مليلتر)عند الطول الموجي (٤٠٥) نانومتر وشدة (١٣,٥) ميكاواط/م^{٢} وكانت قيمها (١,٩٤×١٠$^{-١٢}$) م^{٢}/ واط و (٩,١٢×١٠$^{-٧}$) (وحدة شحنة كهروستاتيكية) على الترتيب.

تم دراسة خواص المحدد البصري لجميع معلقات المواد والخلطات باستخدام طولين موجيين (٤٠٥ و ٥٣٢) نانومتر. أظهرت النتائج ان ان لجميع المواد خواص تحديد بصري عند الطولين الموجيين المستخدمين ما عدى جسيمات الذهب النانوية الكروية حيث لم تظهر لها خواص تحديد بصري عند الطول الموجي (٥٣٢) نانومتر للتركيزين (٠,٠٤ و ٠,٠٨) مليغرام/ مليلتر وكذلك شظايا أوكسيد الحديد النانوية لنفس الطول الموجي ولجميع التراكيز. أظهرت النتائج ان قيم قدرة العتبة وقدرة التحديد لجميع المواد تنخفظ بزيادة التركيز وزيادة الطول الموجي. أظهرت نتائج المحدد البصري للخلطات المخلوطة بطريقة الموجات فوق الصوتية ظهور محدد بصري بمرحلتين عند الطول الموجي (٤٠٥) نانومتر.